Politecnico di Milano

Scuola di Ingegneria Industriale e dell'Informazione
Corso di Laurea Magistrale in Ingegneria Nucleare

Tesi di Laurea Magistrale

Uncertainty quantification of CFD simulation for turbulent mixing

Relatore interno:
Prof. Marco Enrico Ricotti

Relatore esterno:
Dr. Arnoldo Badillo, Paul Scherrer Institut

Autore:
Antonio Buccio
Matr. 799433

Anno Accademico 2013-2014

Uncertainty quantification of CFD simulation for turbulent mixing

Antonio Buccio

Abstract

Physical modeling, large scale simulations and experiments have long been recognized as critical for understanding and advancing science and technology. In the field of computational modeling, Uncertainty Quantification can be broadly defined as a tool for identifying, quantifying and reducing uncertainties associated with models, numerical algorithms, experiments and predicted outcomes. In the experimental field, the quantification of measurement uncertainties is well understood and is addressed by classical statistical methods. However, the systematic quantification of uncertainties and the analysis of how they propagate through complex models, is a new area of research in the field of Computational Fluid Dynamics (CFD). One large-scale application, where Uncertainty Quantification might find an important and useful role, is in the design and safety demonstration of Nuclear Reactors. In the design of Nuclear Reactors, knowing the uncertainties related to predictive models is a key point to define the degree of reliability of numerical simulations. In nuclear reactor models, the main sources of uncertainties are: initial and boundary conditions, input parameters, model and geometrical uncertainties. The resulting numerical models are computationally expensive and require the development of models reproducing the system response to determine uncertainties for the quantities of interest. In the present work, Stochastic Computational Fluid Dynamics–based on generalized Polynomial Chaos Expansion (PCE)–is used to simulate the GEneral MIxing eXperiment(GEMIX), carried out at the Paul Scherrer Institute, where uncertainty, arising from boundary conditions and models input parameters, are propagated through the hydrodynamic model. To quantify the uncertainty in the CFD simulations–using the non-intrusive Polynomial Chaos Expansion–seven stochastic variables have been introduced to handle uncertain boundary conditions and the phenomenological coefficients in the $k - \varepsilon$ turbulence model. Two random variables were used to describe the inlet conditions and five to describe the turbulence model. The PCE approximates the response of the system in terms of a series of orthogonal polynomials. The orthogonality property of the polynomial basis is then applied to derive suitable expressions for relevant statistical moments (mean and standard deviation) for concentration, turbulence kinetic energy and velocity. From the standard deviation fields, uncertainty bands were computed. Mean PCE values for velocity, turbulence kinetic energy and concentration were compared with experimental measurements at several locations inside the mixing section. The numerical results show good agreement with experiments, which are well bounded by the uncertainty bands obtained from the PCE analysis. From the sensitivity analysis–based on the Sobol decomposition–was determined that the inlet conditions introduce the highest uncertainty to the CFD results.

Key words: Uncertainty Quantification, Polynomial Chaos Expansion, Stochastic Computational Fluid Dynamics, Sensitivity Analysis, Turbulence modelling.

Sommario

Modelli fisici, simulazioni su grandi scale ed esperimenti sono da sempre ritenuti come un punto critico per la comprensione e il progresso scientifico e tecnologico. Nel campo della modellistica computazionale, Uncertainty Quantification puó essere definita come uno strumento per identificare, quantificare e ridurre le incertezze associate a modelli, algoritmi numerici, esperimenti e risultati attesi. In ambito sperimentale, la stima delle incertezze é un problema largamente affrontato e compreso tramite l'uso dei metodi statistici classici. Tuttavia, la sistematica quantificazione delle incertezze e l'analisi di come propagano all'interno id modelli complessi é una nuova area di ricerca nel campo della Fluidodinamica Computazionale. Un'applicazione su grande scala, nella quale Uncertainty Quantification puó svolgere un ruolo importante e utile, é rappresentata dal design e dalle problematiche legate alla sicurezza dei Reattori Nucleari. Nella concezione dei Reattori Nucleari, la conoscenza dell'incertezze legate ai modelli predittivi é un punto chiave al fine di definire il grado di affidabilitá delle simulazioni numeriche. Nei modelli riguardanti i reattori nucleari, le principali fonti di incertezza sono: condizioni iniziali e al contorno, parametri d'ingresso, incertezze legate ai modelli matematici ed alle geometrie dei componenti. I modelli numerici ottenuti sono dispendiosi da un punto di vista computazionale ed inoltre necessitano lo sviluppo di modelli capaci di riprodurre la risposta del sistema per determinare le incertezze legate alle variabili d'interesse. Nel presente lavoro, Fluidodinamica Computazionale Stocastica, basata sul generalized Polynomial Chaos Expansion (PCE), é usata per simulare il GEneral MIxing eXperiment (GEMIX), realizzato nell'istituto Paul Scherrer, nel quale le incertezze, derivanti dalle condizioni al contorno e dai parametri d'ingresso del modello, sono propagate attraverso il modello idrodinamico. Per quantificare l'incertezza legata alla simulazione fluidodinamica, usando il metodo non intrusivo del Polynomial Chaos Expansion, sette variabili stocastiche sono state introdotte al fine di maneggiare le incerte condizioni al contorno e i fenomenologici coefficienti presenti nel modello di turbolenza $k - \varepsilon$. Due variabili casuali sono state usate per descrivere le condizioni di ingresso e cinque per descrivere il modello di turbolenza. PCE approssima la risposta del sistema tramite una serie di polinomi ortogonali. L'ortogonalitá della base di polinomi é stata applicata per derivare un'adatta espressione per i momenti statistici (valore medio e deviazione standard) per la concentrazione, l'energia cinetica turbolenta e la velocitá. Tramite il campo di deviazione standard calcolato sono state generate bande di incertezza. I valori medi ottenuti tramite PCE per velocitá, energia cinetica turbolenta e concentrazione sono stati confrontati con le misure sperimentali per differenti posizioni all'interno della mixing section. I risultati numerici concordano con i risultati sperimentali, i quali risultano ben confinati all'interno delle barre d'incertezza valutate tramite Polynomial Chaos Expansion. Tramite un'analisi di sensitivitá–basata sulla decomposizione di Sobol–si é individuato che le condizioni all'ingresso dell'esperimento introducono l'incertezza piú grande all'interno della simulazione CFD.

Parole chiave: Uncertainty Quantification, Polynomial Chaos Expansion, Fluidodinamica Computazionale Stocastica, Sensitivity Analysis, Modello di turbolenza.

Contents

List of Figures

List of Tables

Chapter 1

Introduction

The synthesis of modeling, large scale simulations and experiments has long been recognized as critical for understanding and advancing of the state of science and technology. In the context of predictive science, uncertainty quantification can be broadly defined as the science of identifying, quantifying and reducing uncertainties associated with models, numerical algorithms, experiments and predicted outcomes or quantities of interest. Aspects of this field, such as the quantification of measurement uncertainties and numerical errors are well understood and are addressed by classical statistics and numerical analysis theory. However, the systematic quantification of uncertainties and errors in models, simulations and experiments and the analysis of how they are propagated through complex models to affect predicted outcomes is more recent and it is at the beginning of its developing.

One large-scale application, where the Uncertainty Quantification finds an important and useful role is the Nuclear Reactor design field. In the Nuclear Reactor design field the model predictions with quantified uncertainties are critical for understanding and predicting scientific phenomena and making design decision based upon these predictions. In nuclear reactor models four main sources of uncertainties are identifies: input uncertainties, model errors, numerical errors and uncertainties in measurements. Especially for the thermal-hydraulics correlations a quantification of the uncertainty is sought, indeed these relations are based on conservation of mass, momentum, energy and species concentration in combination with phenomenological closure relations and source terms. The resulting coupled systems are highly nonlinear and numerically difficult to resolve and verify for small gridsize.

In addition to numerical errors, the thermal-hydraulic correlations exhibit varying degrees of uncertainty in the phenomenological models used to characterize complex or poorly understood physics and nonphysical parameters in these models, which must be estimated using model calibration techniques before they can be propagated through the models. Finally the harsh environment inside a nuclear reactor limits the number and type of measurements that can be obtained for model calibration and validation and experimental design.

A substantial challenge associated with uncertainty quantification for nuclear reactor designs is the necessity for propagating uncertainties through several linked simulation codes for all of the coupled subsytems. The resulting models and simulation codes are computationally intensive and require the development of surrogate models to construct uncertainties for the quantity of interest.

1.1 Scope of this work

The problem of turbulent mixing is well known and it's one of the more crucial aspect inside nuclear projects, several papers[16],[7] and also an European poject[20] have shown how the turbulent mixing between two fluid stream at different temperatures

and/or density, can provoke, especially in the T-jucnction, component failure due to thermal fatigue. Thermal fatigue is a mechanism which results in significant degradation of the mechanical properties of a material exposed to cyclic thermal stresses, which superimposes on mechanical loads. Therefore the turbulent mixing play a key role in the management of aging in nuclear power plants and a perfect knowledge and prediction of the temperature profile is necessary to assure the nuclear safety and plant operation.

The present work applies Stochastic Computational Fluid Dynamics based on generalized Polynomial Chaos Expansion to simulate the GEneral MIxing eXperiment(GEMIX) carried out at the Paul Scherrer Institute and to quantify the uncertainty propagating inside the numerical model. Computational Fluid Dynamics is not exempted from uncertain results, even for laminar flows. The equations solved in numerical simulations are based on conservations laws but they are not free of assumptions which inevitably introduce a certain level of uncertainty in the results. An other source of uncertainty comes from the measurement the physical properties, also from the uncertainty coming from the boundary conditions can translate into important deviation from the experimental observations. A better agreement with experiments cannot always be achieved by improving the discretization schemes, mesh quality or linear solve in the numerical solution of the model. By accepting that some boundary conditions or model parameters follow a stochastic process with a given probability distribution, a way to quantify the level of uncertainty introduced by these random parameter can be opened.

Therefore the objective of this work is to evaluate the uncertainty introduced by the boundary conditions, unknown from the experiment, and by the $k - \varepsilon$, which is the turbulence model used to performed the numerical simulations.

1.2 Outline of the thesis

In the chapter 2 and 3 the fundamental conservation law and the Reynolds Averaged Navier Stokes equations are derived in order to build the basis to derive the turbulence model $k-\varepsilon$. Chapter4 describes some important aspects of the turbulence phenomenon as well as the turbulence model employed. The turbulence mixing and the GEMIX facility are presented in Chapter5.

The Uncertainty Quantification and the Polynomial Chaos Expansions are explained in Chapter6, this method is applied to the $k - \varepsilon$ model to evaluate the uncertainty in the numerical simulations. The chapter 7 explains all the steps realized to quantify the uncertainty inside the simulations.

Finally in the Chapter8 the PCE results, the comparison with the experimental results and the global sensitivity analysis are presented.

Chapter 2

Conservation law

The aim of this chapter is to derive the fundamental laws of conservation, that is:

1. **Mass conservation.**
2. **Momentum conservation.**
3. **Energy conservation.**

These conservations laws are the basis to describe any phenomena, including turbulence, indeed they are the basis on which turbulence models are derived.

All the conservation laws are derived, as much as possible, in a general way, using as reference system that being in Fig. 2.1. Inside the universe volume, the total volume of the reference system, called V a control volume with whatever shape, denoted cv, is considered. The control volume is crossed by a fluid with density ρ and velocity $\mathbf{u}$, furthermore the control volume moves, warping, inside the whole space as much as its boundaries that move with a velocity $\mathbf{v_{cv}}$.

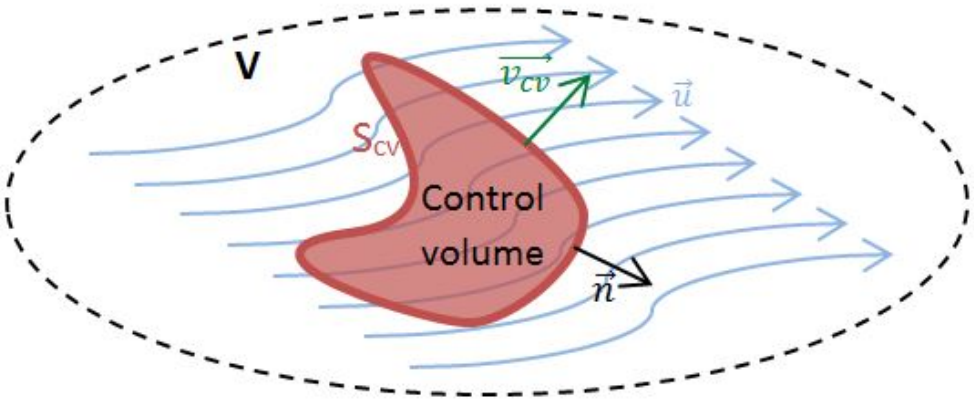

Fig. 2.1: Reference system.

2.1 Mass conservation

The first conservation law derived is the *Mass Conservation*. The mass conservation law states that the rate of increase of mass in the control volume is equal to the net rate of flow of mass into fluid element, this can be expressed with the following relation:

$$\frac{dm_{cv}}{dt} = -\int_{S_{cv}} \mathbf{J} \cdot \mathbf{dA} \tag{2.1}$$

The mass is defined as following:

$$m_{cv} = \int_{V_{cv}} \rho dV_{cv}. \tag{2.2}$$

so the Eq. (2.1) can be expressed:

$$\frac{d}{dt}\int_{V_{cv}} \rho dV_{cv} = -\int_{S_{cv}} \mathbf{J}\cdot\mathbf{dA} \tag{2.3}$$

In Eq. (2.3) right hand side the terms $\mathbf{J}$ indicates the fluxes entering in the control volume, it's the sum of many terms: advection, diffusive.... The total flux $\mathbf{J}$ can be split into two parts, the advection part equals to $\rho\mathbf{u}$, called $\mathbf{C}$ and the others flux describing different phenomena,$\mathbf{J}_i$:

$$\mathbf{J} = \mathbf{C} + \sum_i \mathbf{J_i} \tag{2.4}$$

The fact that the control volume is moving and that its boundaries changing in time and in the space, obligates to pay attention to the volume integral in the Eq. 2.3 since it's not a fixed volume. This problem can be dropped carrying the integration on the entire volume of the universe, the whole volume surrounding the system which doesn't change in time and space. Introducing a step function defined everywhere in the space:

$$\phi(\mathbf{x}(t)) = \begin{cases} 1, & \mathbf{x} \in V_{cv} \\ 0, & \mathbf{x} \notin V_{cv} \end{cases} \tag{2.5}$$

it's possible change the integration volume thanks to the following definition valid for any quantity of any nature(scalar,vector,tensor):

$$\int_{V_{cv}} F dV_{cv} := \int_V \phi F dV \tag{2.6}$$

Using the above definition Eq. (2.3) becomes:

$$m = \int_{V_{cv}} \rho(t) dV_{cv} = \int_V \phi\left(\mathbf{x}(t)\right)\rho(t) dV \tag{2.7}$$

The property F, representing either the mass or the momentum or the energy, is a function of its density f and of the step function ϕ. Fundamental is to know its rate of change in time:

$$\frac{dF}{dt} = \int_V \left[\left(\frac{\delta F}{\delta f}\right)\frac{\partial f}{\partial t} + \left(\frac{\delta F}{\delta \phi}\right)\frac{\partial \phi}{\partial t}\right] dV \tag{2.8}$$

So for the mass case F, the density f and the respective derivatives are:

$$\begin{cases} F = m \\ f = \rho \end{cases} \quad \Rightarrow \quad \begin{cases} \frac{\delta m}{\delta \rho} = \phi \\ \frac{\delta m}{\delta \phi} = \rho \end{cases}$$

Combining the definition in Eq. (2.6) and Eq. (2.8) the mass time derivative being in Eq. (2.1) becomes:

$$\begin{aligned} \frac{dm}{dt} = & \\ &= \int_V \frac{\partial \phi}{\partial t}\rho dV + \int_V \phi\frac{\partial \rho}{\partial t} dV = \\ &= \underbrace{-\int_V \nabla\phi\frac{d\mathbf{x}}{dt}\rho dV}_{=(*)} + \int_V \phi\frac{\partial \rho}{\partial t} dV \end{aligned} \tag{2.9}$$

The **(*)** integral is negative because the surface normal is outgoing. Applying the integration by part rule, mention just below, at **(*)** the integral becomes:

$$\int_\Omega \nabla u \cdot \mathbf{v} d\Omega = \int_{\partial\Omega} u\mathbf{v} \cdot \mathbf{d\Gamma} - \int_\Omega u(\nabla \cdot \mathbf{v}) d\Omega$$

$$\textbf{(*)} = \int_V \nabla\phi \cdot \mathbf{v_c} \mathbf{v} \rho dV = \underbrace{\int_{\partial V} \phi\rho\mathbf{v_{cv}} \cdot \mathbf{dA}}_{=0} - \int_V \phi\nabla \cdot (\rho\mathbf{v_{cv}}) dV \tag{2.10}$$

The first integral being in the Eq. (2.10) RHS vanish because the integration surface is the whole surface of the reference system that contains the system studied. So in this space the step function ϕ is equal to zero.
Therefore the finally expression for the rate of mass change is:

$$\frac{dm}{dt} = \frac{d}{dt}\int_V \phi(\mathbf{x}(t))\rho(t)dV = \int_{V_{cv}} \frac{\partial\rho}{\partial t} dV + \int_V \phi\nabla \cdot (\rho\mathbf{v_{cv}}) dV \tag{2.11}$$

where the presence of the step function ϕ in the second integral in the Eq. (2.9) RHS allows to evaluate the inegral only inside the control volume since outside the integral argument vanishes. Replacing Eq. (2.11) into Eq. (2.1) it's possible write the integral form for the mass conservation:

$$\int_{V_{cv}} \frac{\partial\rho}{\partial t} dV + \int_{\partial V_{cv}} \rho\mathbf{v_{cv}} \cdot \mathbf{dA} = -\int_{S_{cv}} \mathbf{J} \cdot \mathbf{dA} \tag{2.12}$$

Using the divergence theorem one can write the differential form for the mass conservation:

$$\int_V \nabla \cdot \mathbf{F} dV = \oint_{\partial V} \mathbf{F} \cdot \mathbf{dA} \tag{2.13}$$

$$\frac{\partial\rho}{\partial t} + \nabla \cdot \mathbf{J} = -\nabla \cdot (\rho\mathbf{v_{cv}}) \tag{2.14}$$

The Eq. (2.14) is the mass conservation express in a differential way and it's composed by:

- The first term is the net mass variation inside the control volume.
- The second term is the mass flux, it is composed by many elements and it have to be evaluated according to the problem.
- The third term is due to the moving boundary and it is really important when there is a phase change.

2.2 Momentum conservation

Starting from the second Newton's law is possible to derive the second conservation law, the *Momenutm Conservation*. The reference system used is the same as used in Sec. 2.1. The second Newton's law states:

$$\frac{d\mathbf{P}}{dt} = -\vec{\Psi} + \sum_i \mathbf{F_i} \tag{2.15}$$

where $\mathbf{P}$ is the fluid total momentum, $\mathbf{F}$ is the sum of the forces acting on the control volume and $\vec{\Psi}$ is the momentum fluxes across the control volume. The Eq. (2.15) is analyzed taking one hand at time starting from the left hand side.

The total momentum can be written using the momentum per unit of volume $\mathbf{p}$:

$$\mathbf{P}(\mathbf{x}(t), t) = \int_{V_{cv}} \mathbf{p}(\mathbf{x}(t), t) dV_{cv} \tag{2.16}$$

As in the Sec. 2.1 the control volume moves and warps so the integration volume in Eq. (2.16) has to be changed in order to permit its computation. Finally the step function defined in the previous section is introduced:

$$\mathbf{P} = \int_{V_{cv}} \mathbf{p} dV_{cv} = \int_V \phi \mathbf{p} dV \tag{2.17}$$

Using Eq. (2.8) one can write the total momentum time rate as:

$$\begin{cases} F = \mathbf{P} \\ f = \mathbf{p} \end{cases} \Rightarrow \begin{cases} \frac{\delta \mathbf{P}}{\delta \mathbf{p}} = \phi \\ \frac{\delta \mathbf{P}}{\delta \phi} = \mathbf{p} \end{cases}$$

$$\frac{d\mathbf{P}}{dt} = \underbrace{\int_V \mathbf{p} \frac{\partial \phi}{\partial t} dV}_{=(*)} + \int_V \phi \frac{\partial \mathbf{p}}{\partial t} dV \tag{2.18}$$

The term (*****) is solved through the integration by part rule:

$$\begin{aligned} (*) &= \int_V \mathbf{p} \frac{\partial \phi}{\partial t} dV = -\int_V \nabla \phi \cdot \mathbf{v_{cv}} \mathbf{p} dV = \\ &= -\underbrace{\int_{\partial V} \phi \mathbf{v_{cv}} \mathbf{p} \cdot \mathbf{dA}}_{=0} + \int_V \phi \nabla \cdot (\mathbf{v_{cv}} \mathbf{p}) dV = \\ &= \int_V \phi \nabla \cdot (\mathbf{v_{cv}} \mathbf{p}) dV = \int_{V_{cv}} \nabla \cdot (\mathbf{v_{cv}} \mathbf{p}) dV \end{aligned} \tag{2.19}$$

Finally Eq. (2.18) becomes:

$$\begin{aligned} \frac{d\mathbf{P}}{dt} = \frac{d}{dt} \int_V \phi \mathbf{p} dV &= \int_{V_{cv}} \nabla \cdot (\mathbf{v_{cv}} \mathbf{p}) dV + \int_V \phi \frac{\partial \mathbf{p}}{\partial t} dV = \\ &= \int_{V_{cv}} \nabla \cdot (\mathbf{v_{cv}} \mathbf{p}) dV + \int_{V_{cv}} \frac{\partial \mathbf{p}}{\partial t} dV \end{aligned} \tag{2.20}$$

The Eq. (2.15) right hand side is the force term and it's composed by the sum of the body forces $\mathbf{F}_i$ and the forces due to the momentum fluxes $\vec{\Psi}$. The latter is the summation of the momentum convection and momentum diffusion that generates a force acting on the surface of control volume. $\vec{\Psi}$ can be expressed as following:

$$\vec{\Psi} = \int_{S_{cv}} \mathbf{up} \cdot \mathbf{dS} + \int_{S_{cv}} \underline{\underline{\sigma}} \cdot \mathbf{dS} \tag{2.21}$$

where the first integral is the momentum carried by the fluid while the second integral is the stress tensor generated by the momentum diffusion. Applying the divergence theorem to the Eq. (2.21) one gets:

$$\vec{\Psi} = \int_{V_{cv}} \nabla \cdot (\mathbf{up}) dV + \int_{V_{cv}} \nabla \cdot \underline{\underline{\sigma}} dV \tag{2.22}$$

The stress tensor is a symmetric tensor and it can be decomposed into two tensor, a symmetric tensor and the stress deviator tensor, according this relation:

$$\sigma_{ij} = p\delta_{ij} - \tau_{ij} \tag{2.23}$$

where p is hydrostatic pressure defined as one-third of $\underline{\underline{\sigma}}$ trace:

$$p := \frac{1}{3} Tr\left(\underline{\underline{\sigma}}\right) = \frac{\sigma_{11} + \sigma_{22} + \sigma_{33}}{3}$$

About the body forces it's possible to introduce the total boyd force per unit of volume:

$$\sum_i \mathbf{F}_i = \sum_i \int_{V_{cv}} \mathbf{f}_i dV = \int_{V_{cv}} \sum_i \mathbf{f}_i dV = \int_{V_{cv}} \mathbf{f} dV \tag{2.24}$$

where $\mathbf{f}_i$ is the i-th body force per unity of volume and $\mathbf{f}$ is the total body force per unity of volume. That being so the Eq. (2.15) RHS can be rewritten:

$$-\vec{\Psi} + \sum_i \mathbf{F_i} = -\int_{V_{cv}} \nabla \cdot (\mathbf{up}) dV - \int_{V_{cv}} \nabla p dV + \int_{V_{cv}} \nabla \cdot \underline{\underline{\tau}} dV + \int_{V_{cv}} \mathbf{f} dV \tag{2.25}$$

Finally the second Newton's law becomes:

$$\int_{V_{cv}} \left[\nabla \cdot (\mathbf{v_{cv}p}) + \frac{\partial \mathbf{p}}{\partial t} \right] dV = -\int_{V_{cv}} \left[\nabla \cdot (\mathbf{up}) - \nabla \cdot \underline{\underline{\sigma}} + \mathbf{f} dV \right] \tag{2.26}$$

The Eq. (2.26) is the integral form of the momentum conservation, applying the divergence theorem the differential form can be computed:

$$\frac{\partial \mathbf{p}}{\partial t} + \nabla \cdot (\mathbf{up}) = -\nabla \cdot (\mathbf{v_{cv}p}) - \nabla p + \nabla \cdot \underline{\underline{\tau}} + \mathbf{f} \tag{2.27}$$

The equation (2.27) is the differential form for the momentum conservation law and it's composed by:

- The LHS represents the rate of increase momentum inside the control volume.
- The first term in the RHS is the variation of momentum due to the boundaries moving, it's important in the phase change phenomena.
- The others terms in the RHS represent the forces that act on the control volume.

2.3 Energy conservation

The third and last conservation law derived is the *Energy conservation*. Starting from the first thermodynamic law it's possible to compute a conservation law for the total energy from which other equation ca be derived. In this section the energy conservation law is derived, after an equation for kinetic energy, internal energy, enthalpy and temperature is equally computed.
The system and hypotheses are the same used in the previous two section to derive the mass and momentum conservation laws.

2.3.1 Total energy conservation

The first thermodynamic law states the variation of the total system energy is equals to the sum of the energy fluxes across the control volume and the work done by the forces acting in the system:

$$\frac{dE}{dt} = \dot{\Phi} + \dot{W} \tag{2.28}$$

where E is the total energy of the system, that is the sum of kinetic and internal energy, while $\dot{\Phi}$ is the energy flux and $\dot{W}$ is the work done by the forces acting on the system. The Eq. (2.28) can be split into two components, internal energy and kinetic energy:

$$E = E_{int} + E_{kin} \quad \Rightarrow \quad \frac{dE}{dt} = \frac{dE_{int}}{dt} + \frac{dE_{kin}}{dt} \tag{2.29}$$

where the kinetic energy is defined:

$$E_{kin} = \frac{\mathbf{P} \cdot \mathbf{P}}{2m} = \frac{\mathbf{P} \cdot \mathbf{P}}{2m} \frac{V^2}{V^2} = \frac{\mathbf{p} \cdot \mathbf{p}}{2\frac{m}{V}} V = \frac{\mathbf{p} \cdot \mathbf{p}}{2\rho} V \tag{2.30}$$

Let call K the kinetic energy per unity volume, so that its expression is:

$$K = \frac{\mathbf{p}\cdot\mathbf{p}}{2\rho} \quad \Rightarrow \quad E_{kin} = \int_{V_{cv}} k dV_{cv} = \int_V \phi k dV \tag{2.31}$$

In the last step of Eq. (2.31) the step function, defined in Sec. 2.1, to drop from the control volume to the universe volume in order to avoid the problem links to the boundaries movement. Using Eq. (2.8) the kinetic energy time derivative can be computed:

$$\begin{cases} F = E_{kin} \\ f = k \end{cases} \quad \Rightarrow \quad \begin{cases} \frac{\delta E_{kin}}{\delta k} = \phi \\ \frac{\delta E_{kin}}{\delta \phi} = k \end{cases}$$

$$\begin{aligned} \frac{dE_{kin}}{dt} &= \frac{d}{dt}\int_V \phi \frac{\mathbf{p}\cdot\mathbf{p}}{2\rho} dV = \int_V \frac{\partial}{\partial t}\left(\phi \frac{\mathbf{p}\cdot\mathbf{p}}{2\rho}\right) dV = \\ &= \int_V \frac{\mathbf{p}\cdot\mathbf{p}}{2\rho}\frac{\partial \phi}{\partial t} dV + \int_V \phi \frac{\partial}{\partial t}\left(\frac{\mathbf{p}\cdot\mathbf{p}}{2\rho}\right) dV = \\ &= -\int_V \frac{\mathbf{p}\cdot\mathbf{p}}{2\rho}\nabla\phi\cdot\mathbf{v_{cv}} dV + \int_V \phi \frac{\partial}{\partial t}\left(\frac{\mathbf{p}\cdot\mathbf{p}}{2\rho}\right) dV \\ \frac{dE_{kin}}{dt} &= \int_{V_{cv}} \nabla\cdot\left(\frac{\mathbf{p}\cdot\mathbf{p}}{2\rho}\mathbf{v_{cv}}\right) dV + \int_{V_{cv}} \frac{\partial}{\partial t}\left(\frac{\mathbf{p}\cdot\mathbf{p}}{2\rho}\right) dV \end{aligned} \tag{2.32}$$

Some mathematical steps have been skipped to derive Eq. (2.32) because the procedure is the same as used in the Sec. 2.1 and Sec. 2.2.

All the steps used for the kinetic energy are used also to compute the internal energy, the internal energy per volume unity e_{int} is introduced and with the Eq. (2.8) its time derivative is computed:

$$\begin{cases} F = E_{int} \\ f = e_{int} \end{cases} \quad \Rightarrow \quad \begin{cases} \frac{\delta E_{int}}{\delta e_{int}} = \phi \\ \frac{\delta E_{int}}{\delta \phi} = e_{int} \end{cases}$$

$$E_{int} = \int_{V_{cv}} \frac{E_{int}}{V} dV_{cv} = \int_V \phi e_{int} dV \tag{2.33}$$

The internal energy time derivative is:

$$\begin{aligned} \frac{dE_{int}}{dt} &= \frac{d}{dt}\int_V \phi e_{int} dV = \int_V \frac{\partial}{\partial t}(\phi e_{int}) dV = \\ &= \int_V \frac{\partial \phi}{\partial t} e_{int} dV + \int_V \phi \frac{\partial e_{int}}{\partial t} dV = \\ &= -\int_V \nabla\phi\cdot\mathbf{v_{cv}} e_{int} dV + \int_V \phi \frac{\partial e_{int}}{\partial t} dV = \\ &= \int_V \phi \nabla\cdot(\mathbf{v_{cv}} e_{int})\, dV + \int_V \phi \frac{\partial e_{int}}{\partial t} dV \\ \frac{dE_{int}}{dt} &= \int_{V_{cv}} \nabla\cdot(\mathbf{v_{cv}} e_{int})\, dV + \int_{V_{cv}} \frac{\partial e_{int}}{\partial t} dV \end{aligned} \tag{2.34}$$

Combining Eq. (2.32) and Eq. (2.34) the LHS of the first thermodynamic lw becomes:

$$\begin{aligned} \frac{dE}{dt} &= \int_{V_{cv}} \nabla\cdot(\mathbf{v_{cv}} e_{int})\, dV + \int_{V_{cv}} \frac{\partial e_{int}}{\partial t} dV + \\ &+ \int_{V_{cv}} \nabla\cdot\left(\frac{\mathbf{p}\cdot\mathbf{p}}{2\rho}\mathbf{v_{cv}}\right) dV + \int_{V_{cv}} \frac{\partial}{\partial t}\left(\frac{\mathbf{p}\cdot\mathbf{p}}{2\rho}\right) dV \end{aligned} \tag{2.35}$$

Now it's time to study the right-hand of the equation (2.28) starting from the work term

$\dot{W}$. This term is composed by two elements, one is the work done by the body forces and the another one is the work done by the stress acting on the control surface:

$$\begin{aligned}\dot{W} &= \int_{V_{cv}} \mathbf{f}\cdot\mathbf{u}dV - \int_{S_{cv}} (\underline{\underline{\sigma}}\cdot\mathbf{u})\cdot\mathbf{dA} = \\ &= \int_{V_{cv}} \mathbf{f}\cdot\mathbf{u}dV - \int_{V_{cv}} \nabla\cdot(\underline{\underline{\sigma}}\cdot\mathbf{u})dV = \\ &= \int_{V_{cv}} \mathbf{f}\cdot\mathbf{u}dV - \int_{V_{cv}} \nabla\cdot(p\mathbf{u})dV + \int_{V_{cv}} \nabla\cdot(\underline{\underline{\tau}}\cdot\mathbf{u})dV\end{aligned} \tag{2.36}$$

The energy flux $\dot{\Phi}$ is defined as:

$$\dot{\Phi} = -\int_{S_{cv}} \frac{E}{V}\mathbf{u}\cdot\mathbf{dA} - \int_{S_{cv}} \ddot{\mathbf{q}}_D\cdot\mathbf{dA} \tag{2.37}$$

where the first term is the advection term and the second in the diffusive term. The advection term can be split in two terms, internal energy and kinetic energy, therefore the final expression for energy flux is:

$$\dot{\Phi} = -\int_{S_{cv}} e_{int}\mathbf{u}\cdot\mathbf{dA} - \int_{S_{cv}} \frac{\mathbf{p}\cdot\mathbf{p}}{2\rho}\mathbf{u}\cdot\mathbf{dA} - \int_{S_{cv}} \ddot{\mathbf{q}}_D\cdot\mathbf{dA} \tag{2.38}$$

Thanks to the divergence theorem the surface integrals are transformed into volume integrals and then the final expression for the energy flux is:

$$\dot{\Phi} = -\int_{V_{cv}} \nabla\cdot(e_{int}\mathbf{u})\,dV - \int_{V_{cv}} \nabla\cdot\left(\frac{\mathbf{p}\cdot\mathbf{p}}{2\rho}\mathbf{u}\right)dV - \int_{V_{cv}} \nabla\cdot\ddot{\mathbf{q}}_D dV \tag{2.39}$$

Combining equations (2.35), (2.36) and (2.39) the integral form for the energy conservation law can be written:

$$\begin{aligned}&\int_{V_{cv}} \left[\nabla\cdot(\mathbf{v_{cv}}e_{int}) + \frac{\partial e_{int}}{\partial t} + \nabla\cdot\left(\frac{\mathbf{p}\cdot\mathbf{p}}{2\rho}\mathbf{v_{cv}}\right) + \frac{\partial}{\partial t}\left(\frac{\mathbf{p}\cdot\mathbf{p}}{2\rho}\right)\right]dV = \\ &= \int_{V_{cv}} \left[\mathbf{f}\cdot\mathbf{u} - \nabla\cdot(p\mathbf{u}) + \nabla\cdot(\underline{\underline{\tau}}\cdot\mathbf{u}) - \nabla\cdot(e_{int}\mathbf{u}) - \nabla\cdot\left(\frac{\mathbf{p}\cdot\mathbf{p}}{2\rho}\mathbf{u}\right) - \nabla\cdot\ddot{\mathbf{q}}_D\right]dV\end{aligned} \tag{2.40}$$

The equation (2.40) is the integral form of the energy conservation law, so the differential form is:

$$\begin{aligned}&\frac{\partial e_{int}}{\partial t} + \nabla\cdot(e_{int}\mathbf{u}) + \frac{\partial}{\partial t}\left(\frac{\mathbf{p}\cdot\mathbf{p}}{2\rho}\right) + \nabla\cdot(\frac{\mathbf{p}\cdot\mathbf{p}}{2\rho}\mathbf{u}) = \\ &-\nabla\cdot(\mathbf{v_{cv}}e_{int}) - \nabla\cdot\left(\frac{\mathbf{p}\cdot\mathbf{p}}{2\rho}\mathbf{v_{cv}}\right) - \nabla\cdot(p\mathbf{u}) + \nabla\cdot(\underline{\underline{\tau}}\cdot\mathbf{u}) - \nabla\cdot\ddot{\mathbf{q}}_D + \mathbf{f}\cdot\mathbf{u}\end{aligned} \tag{2.41}$$

The equation (2.41) is the energy conservation law expressed in the differential form. Once the total energy conservation law is derived it's possible to find a conservation expression for the *Internal energy* and for the *Kinetic Energy*. The idea is to write an equation for the kinetic energy and then computed the equation for the internal energy subtracting the kinetic energy to the total energy.

2.3.2 Kinetic energy equation

The kinetic energy definition suggests to apply the inner product between the quantity $\mathbf{p}/\rho$ and the momentum conservation law:

$$\underbrace{\frac{\partial\mathbf{p}}{\partial t}\cdot\frac{\mathbf{p}}{\rho}}_{=(*)} + \underbrace{[\nabla\cdot(\mathbf{up})]\cdot\frac{\mathbf{p}}{\rho}}_{=(**)} = -[\nabla\cdot(\mathbf{v_{cv}p})]\cdot\frac{\mathbf{p}}{\rho} - \nabla p\cdot\frac{\mathbf{p}}{\rho} + \left[\nabla\cdot\underline{\underline{\tau}}\right]\cdot\frac{\mathbf{p}}{\rho} + \mathbf{f}\cdot\frac{\mathbf{p}}{\rho} \tag{2.42}$$

$$(*) = \frac{\partial \mathbf{p}}{\partial t} \cdot \frac{\mathbf{p}}{\rho} = \frac{\partial}{\partial t}\left(\frac{\mathbf{p}\cdot\mathbf{p}}{2\rho}\right) + \frac{\mathbf{p}\cdot\mathbf{p}}{2\rho^2}\frac{\partial \rho}{\partial t}$$
$$(**) = [(\mathbf{u}\cdot\nabla)\mathbf{p} + (\nabla\cdot\mathbf{u})\mathbf{p}]\cdot\frac{\mathbf{p}}{\rho} = (\mathbf{u}\cdot\nabla)\mathbf{p}\cdot\frac{\mathbf{p}}{\rho} + (\nabla\cdot\mathbf{u})\mathbf{p}\cdot\frac{\mathbf{p}}{\rho} =$$
$$= (\mathbf{u}\cdot\nabla\mathbf{p})\cdot\frac{\mathbf{p}}{\rho} + (\nabla\cdot\mathbf{u})\frac{\mathbf{p}\cdot\mathbf{p}}{\rho} = (\nabla\cdot\mathbf{u})\frac{\mathbf{p}\cdot\mathbf{p}}{\rho} + \mathbf{u}\cdot\left[\nabla(\frac{\mathbf{p}\cdot\mathbf{p}}{2\rho}) + \frac{\mathbf{p}\cdot\mathbf{p}}{2\rho^2}\nabla\rho\right]$$

So the Eq. (2.42) LHS becomes:

$$(*) + (**) = \frac{\partial}{\partial t}\left(\frac{\mathbf{p}\cdot\mathbf{p}}{2\rho}\right) + \frac{\mathbf{p}\cdot\mathbf{p}}{2\rho^2}\frac{\partial\rho}{\partial t} + \underbrace{\frac{\mathbf{p}\cdot\mathbf{p}}{\rho}\nabla\cdot\mathbf{u}}_{=(***)} + \mathbf{u}\cdot\left[\nabla(\frac{\mathbf{p}\cdot\mathbf{p}}{2\rho} + \frac{\mathbf{p}\cdot\mathbf{p}}{2\rho^2}\nabla\rho\right] =$$

$$(***) = \frac{\mathbf{p}\cdot\mathbf{p}}{2\rho}\nabla\cdot\mathbf{u} + \frac{\mathbf{p}\cdot\mathbf{p}}{2\rho}\nabla\cdot\mathbf{u}$$

$$(*) + (**) = \frac{\partial}{\partial t}\left(\frac{\mathbf{p}\cdot\mathbf{p}}{2\rho}\right) + \frac{\mathbf{p}\cdot\mathbf{p}}{2\rho}\nabla\cdot\mathbf{u} + \mathbf{u}\cdot\nabla\left(\frac{\mathbf{p}\cdot\mathbf{p}}{2\rho}\right) + \frac{\mathbf{p}\cdot\mathbf{p}}{2\rho^2}\left[\frac{\partial\rho}{\partial t} + \rho\nabla\cdot\mathbf{u} + \mathbf{u}\cdot\nabla\rho\right] \tag{2.43}$$

The last therm of Eq. (2.43) right hand side of the last equation is the mass conservation, so combining the last equation with the Eq. (2.14) it's possible to rewrite the equation (2.42)

$$\begin{aligned}&\frac{\partial}{\partial t}\left(\frac{\mathbf{p}\cdot\mathbf{p}}{2\rho}\right) + \nabla\cdot\left(\frac{\mathbf{p}\cdot\mathbf{p}}{2\rho}\mathbf{u}\right) - \frac{\mathbf{p}\cdot\mathbf{p}}{2\rho^2}\nabla\cdot(\rho\mathbf{v_{cv}}) = \\ &= -\left[\nabla\cdot(\mathbf{v_{cv}}\mathbf{p})\right]\cdot\frac{\mathbf{p}}{\rho} - \nabla p\cdot\frac{\mathbf{p}}{\rho} + \left[\nabla\cdot\underline{\underline{\tau}}\right]\cdot\frac{\mathbf{p}}{\rho} + \mathbf{f}\cdot\frac{\mathbf{p}}{\rho}\end{aligned} \tag{2.44}$$

The last term in the Eq. (2.44) LHS and the first term in the Eq. (2.44) RHS can be expressed respectively as:

$$\frac{\mathbf{p}\cdot\mathbf{p}}{2\rho^2}\nabla\cdot(\rho\mathbf{v_{cv}}) = \frac{\mathbf{p}\cdot\mathbf{p}}{2\rho^2}\rho\nabla\cdot\mathbf{v_{cv}} + \frac{\mathbf{p}\cdot\mathbf{p}}{2\rho^2}\mathbf{v_{cv}}\cdot\nabla\rho \tag{2.45a}$$

$$\left[\nabla\cdot(\mathbf{v_{cv}}\mathbf{p})\right]\cdot\frac{\mathbf{p}}{\rho} = (\nabla\cdot\mathbf{v_{cv}})\frac{\mathbf{p}\cdot\mathbf{p}}{\rho} + \mathbf{v_{cv}}\cdot\left[\nabla\left(\frac{\mathbf{p}\cdot\mathbf{p}}{2\rho}\right) + \frac{\mathbf{p}\cdot\mathbf{p}}{2\rho^2}\nabla\rho\right] \tag{2.45b}$$

taking the difference term by term of equations (2.45a) and (2.45b) one gets:

$$\frac{\mathbf{p}\cdot\mathbf{p}}{2\rho^2}\nabla\cdot(\rho\mathbf{v_{cv}}) - \left[\nabla\cdot(\mathbf{v_{cv}}\mathbf{p})\right]\cdot\frac{\mathbf{p}}{\rho} = -\nabla\cdot\left(\frac{\mathbf{p}\cdot\mathbf{p}}{2\rho}\mathbf{v_{cv}}\right) \tag{2.46}$$

Finally Eq. (2.42) becomes:

$$\begin{aligned}&\frac{\partial}{\partial t}\left(\frac{\mathbf{p}\cdot\mathbf{p}}{2\rho}\right) + \nabla\cdot\left(\frac{\mathbf{p}\cdot\mathbf{p}}{2\rho}\mathbf{u}\right) = \\ &= -\nabla\cdot\left(\frac{\mathbf{p}\cdot\mathbf{p}}{2\rho}\mathbf{v_{cv}}\right) - \nabla p\cdot\frac{\mathbf{p}}{\rho} + \left[\nabla\cdot\underline{\underline{\tau}}\right]\cdot\frac{\mathbf{p}}{\rho} + \mathbf{f}\cdot\frac{\mathbf{p}}{\rho}\end{aligned} \tag{2.47}$$

So the final expression for the *Kinetic Energy Equation* is:

$$\frac{\partial K}{\partial t} + \nabla\cdot(K\mathbf{u}) = -\nabla\cdot(\mathbf{v_{cv}}K) - \nabla p\cdot\mathbf{u} + \left[\nabla\cdot\underline{\underline{\tau}}\right]\cdot\mathbf{u} + \mathbf{f}\cdot\mathbf{u} \tag{2.48}$$

2.3.3 Internal energy equation

After the kinetic energy equation the total energy conservation law can be written:

$$\begin{aligned}&\frac{\partial e_{int}}{\partial t} + \nabla\cdot[e_{int}\mathbf{u}] + \frac{\partial K}{\partial t} + \nabla\cdot(K\mathbf{u}) = \\ &-\nabla\cdot[e_{int}\mathbf{v_{cv}}] - \nabla\cdot(K\mathbf{v_{cv}}) - \mathbf{u}\cdot\nabla p - p\nabla\cdot\mathbf{u} + \\ &+\underline{\underline{\tau}}:\nabla\mathbf{u} + \mathbf{u}\cdot(\nabla\cdot\underline{\underline{\tau}}) - \nabla\cdot\ddot{\mathbf{q}}_D + \mathbf{f}\cdot\mathbf{u}\end{aligned} \tag{2.49}$$

To get the internal energy equation the kinetic energy equation (2.48) has to be subtracted from Eq. (2.49):

$$\frac{\partial e_{int}}{\partial t} + \nabla \cdot [e_{int}\mathbf{u}] = -\nabla \cdot [e_{int}\mathbf{v_{cv}}] - p\nabla \cdot \mathbf{u} + \underline{\underline{\tau}} : \nabla \mathbf{u} - \nabla \cdot \ddot{\mathbf{q}}_D \tag{2.50}$$

Equation (2.50) is the *Internal Energy Equation.*

2.3.4 Enthalpy equation

Once the conservation laws are derived as much as the kinetic energy equation and the internal energy equation an other useful equation can be derived, the *Enthalpy equation.* The enthalpy is defined as:

$$H = E_{int} + pV \tag{2.51}$$

or equally the enthalpy per volume unity:

$$h = e_{int} + p \tag{2.52}$$

Substituting Eq. (2.52) inside the internal energy equation (2.50) it gets:

$$\begin{aligned}
&\frac{\partial}{\partial t}(h-p) + \nabla \cdot [(h-p)\mathbf{u}] = -\nabla \cdot [(h-p)\mathbf{v_{cv}}] - p\nabla \cdot \mathbf{u} + \underline{\underline{\tau}} : \nabla \mathbf{u} - \nabla \cdot \ddot{\mathbf{q}}_D \\
&\frac{\partial h}{\partial t} + \nabla \cdot (h\mathbf{u}) = \\
&= -\nabla \cdot (h\mathbf{v_{cv}}) - \nabla \cdot (p\mathbf{v_{cv}}) + \frac{\partial p}{\partial t} + \nabla \cdot (p\mathbf{u}) - p\nabla \cdot \mathbf{u} + \underline{\underline{\tau}} : \nabla \mathbf{u} - \nabla \cdot \ddot{\mathbf{q}}_D = \\
&= -\nabla \cdot (h\mathbf{v_{cv}}) - \nabla \cdot (p\mathbf{v_{cv}}) + \frac{\partial p}{\partial t} + \mathbf{u} \cdot \nabla p + \underline{\underline{\tau}} : \nabla \mathbf{u} - \nabla \cdot \ddot{\mathbf{q}}_D
\end{aligned}$$

Rearranging the last equation it's possible to write the *Enthalpy Equation*:

$$\frac{\partial h}{\partial t} + \nabla \cdot (h\mathbf{u}) = -\nabla \cdot (h\mathbf{v_{cv}}) - \nabla \cdot (p\mathbf{v_{cv}}) + \frac{\partial p}{\partial t} + \mathbf{u} \cdot \nabla p + \underline{\underline{\tau}} : \nabla \mathbf{u} - \nabla \cdot \ddot{\mathbf{q}}_D \tag{2.53}$$

2.3.5 Temperature equation

Equation (2.53) is the starting point to derive an equation for the temperature. In generally way enthalpy is a function of several variable, *i.e.* temperature, concentration, pressure, phase field and go on:

$$H = H(T, p, c, \phi_i) \tag{2.54}$$

and its time derivative is defined as following:

$$\frac{\partial H}{\partial t} = \sum_i \left(\frac{\partial H}{\partial \lambda_i}\right) \frac{\partial \lambda_i}{\partial t} \tag{2.55}$$

making the assumption that all the derivative $\frac{\partial H}{\partial \lambda_i}$ are very small compared to $\frac{\partial H}{\partial T}$ it is possible to define the heat capacity at constant pressure:

$$\begin{aligned}
&H = H(T) \\
&\frac{\partial H}{\partial T}\Big|_p = c_p
\end{aligned} \tag{2.56}$$

or using the enthalpy per volume unity:

$$\begin{aligned}
&h = h(T) \\
&\frac{\partial h}{\partial T}\Big|_p = \rho c_p
\end{aligned} \tag{2.57}$$

The time and space derivatives of the enthalpy becomes:

$$\frac{\partial h}{\partial t} = \rho c_p \frac{\partial T}{\partial t} \tag{2.58a}$$

$$\nabla h = \rho c_p \nabla T \tag{2.58b}$$

Using the equations (2.58a) and (2.58b) in the enthalpy equation one obtains the successive equation:

$$\begin{aligned} \rho c_p \frac{\partial T}{\partial t} + \mathbf{u} \cdot \rho c_p \nabla T + h \nabla \cdot \mathbf{u} = -\mathbf{v_{cv}} \cdot \rho c_p \nabla T - h \nabla \cdot \mathbf{v_{cv}} - \\ - \nabla \cdot (p \mathbf{v_{cv}}) + \frac{\partial p}{\partial t} + \mathbf{u} \cdot \nabla p + \underline{\underline{\tau}} : \nabla \mathbf{u} - \nabla \cdot \ddot{\mathbf{q}}_D \end{aligned} \tag{2.59}$$

The equation (2.59) is the most general equation that describe the temperature evolution in space and in time.

Chapter 3

RANS equations

In the most of turbulent flows the Navier-Stokes equations are very hard to solve, this is due to the chaotic nature of the turbulence. By introducing a suitable average operation, it is possible to rewrite these equations in a simplified form.

In this section the *Reynolds Average Navier-Stokes equations*(*RANS*) are derived, these equations allow to evaluate the velocity field and the kinetic energy of the fluid. The derivation of RANSequation starts from the conservation laws derived in the Chapter2.The following derivation are based on some assumption, which will be used during all the derivation:

- Incompressible flow $\rightarrow \ \frac{\partial \rho}{\partial p} = 0$.
- Control volume fixed $\rightarrow \mathbf{v_{cv}} = 0$.

Although in the present work the density is considered constant, the fluctuating part is kept for completeness. With the assumptions introduced the conservations laws become:

$$\begin{cases} \nabla \cdot \mathbf{u} = 0 \\ \frac{\partial \mathbf{p}}{\partial t} + \nabla \cdot (\mathbf{up}) = -\nabla p + \nabla \cdot \underline{\underline{\tau}} + \mathbf{f} \\ \frac{\partial K}{\partial t} + \nabla \cdot (K\mathbf{u}) = -\nabla p \cdot \mathbf{u} + (\nabla \cdot \underline{\underline{\tau}}) \cdot \mathbf{u} + \mathbf{f} \cdot \mathbf{u} \end{cases} \tag{3.1}$$

3.1 Reynolds Decomposition

In a turbulent flows each quantity can be decomposed into two contributions: a mean value and a fluctuation, such as decomposition is called *Reynolds Decomposition*. The Reynolds can be applied to any variable concerning the turbulent flow:

$$\begin{cases} \mathbf{u} = \bar{\mathbf{u}} + \mathbf{u}' \\ p = \bar{p} + p' \\ \mathbf{f} = \bar{\mathbf{f}} + \mathbf{f}' \\ \rho = \bar{\rho} + \rho' \\ \mu = \bar{\mu} + \mu' \end{cases} \tag{3.2}$$

where the punctuation mark means the fluctuation while the bar over the variable means the mean value. The variables in a turbulent flows are statistically invariant, that is all the variable statistics under a shift of time, therefore a time average for a generic variable ϕ can be defined by:

$$\langle \phi \rangle = \lim_{\tau \to \infty} \frac{1}{\tau} \int_0^{\tau} \phi d\tau \tag{3.3}$$

Before to go ahead in the discussion let show some useful property of the average operation:

$$\langle \phi + \psi \rangle = \langle \phi \rangle + \langle \psi \rangle \tag{3.4a}$$

$$\langle \phi\psi \rangle = \bar{\phi}\bar{\psi} + \langle \phi'\psi' \rangle \tag{3.4b}$$

$$\langle \bar{\phi}\phi' \rangle = \bar{\phi}\langle \phi' \rangle = 0 \tag{3.4c}$$

$$\left\langle \frac{\partial \phi}{\partial t} \right\rangle = \frac{\partial}{\partial t}\langle \phi \rangle \tag{3.4d}$$

$$\langle \nabla\phi \rangle = \nabla\langle \phi \rangle \tag{3.4e}$$

$$\langle \int \phi d\mathbf{x} \rangle = \int \langle \phi \rangle d\mathbf{x} \tag{3.4f}$$

The time-average commutes with the summation, the differentiation and integration operations. Using the Eq. (3.3) is possible show that the time-average of the any fluctuation is equal to zero. Let be ϕ a variable that can be decomposed according to Reynolds decomposition and let apply the time-average to this variable:

$$\phi = \bar{\phi} + \phi' \overset{\langle\cdot\rangle}{\Rightarrow} \langle \phi \rangle = \langle \bar{\phi} \rangle + \langle \phi' \rangle \Rightarrow \bar{\phi} = \bar{\phi} + \langle \phi' \rangle$$

$$\Rightarrow \langle \phi' \rangle = 0 \tag{3.5}$$

Once all the tools necessary have been introduced they can be applied to Eq. (3.1) to obtain the RANS equation.

3.2 Continuity equation

The first equation in (3.1) is the mass conservation:

$$\begin{aligned}
\nabla \cdot \mathbf{u} = 0 \overset{\langle\cdot\rangle}{\Rightarrow} \langle \nabla \cdot \mathbf{u} \rangle &= 0 \\
\langle \nabla \cdot \mathbf{u} \rangle &= \langle \nabla \cdot (\bar{\mathbf{u}} + \mathbf{u}') \rangle = \\
&= \langle \nabla \cdot \bar{\mathbf{u}} + \nabla \cdot \mathbf{u}' \rangle = \\
&= \langle \nabla \cdot \bar{\mathbf{u}} \rangle + \langle \nabla \cdot \mathbf{u}' \rangle = \\
&= \nabla \cdot \bar{\mathbf{u}} + \nabla \cdot \langle \mathbf{u}' \rangle = \\
&= \nabla \cdot \bar{\mathbf{u}}
\end{aligned}$$

$$\nabla \cdot \bar{\mathbf{u}} = 0 \tag{3.6}$$

From equation (3.6) an equation for the fluctuation can be derived:

$$\nabla \cdot \mathbf{u}' = 0 \tag{3.7}$$

3.3 Momentum equation

Let consider the momentum conservation:

$$\frac{\partial(\rho\mathbf{u})}{\partial t} + \nabla \cdot (\rho\mathbf{u}\mathbf{u}) = -\nabla p + \nabla \cdot \underline{\underline{\tau}} + \mathbf{f} \tag{3.8}$$

where $\mathbf{p} = \rho\mathbf{u}$.
Using the Reynolds decomposition on the equation (3.8) one gets:

$$\frac{\partial}{\partial t}\left[(\bar{\rho} + \rho')(\bar{\mathbf{u}} + \mathbf{u}')\right] + \nabla \cdot \left[(\bar{\rho} + \rho')(\bar{\mathbf{u}} + \mathbf{u}')(\bar{\mathbf{u}} + \mathbf{u}')\right] = -\nabla(\bar{p} + p') + \nabla \cdot \underline{\underline{\tau}} + \left(\bar{\mathbf{f}} + \mathbf{f}'\right) \tag{3.9}$$

after the Eq. (3.9) is averaged. Firstly the attention is focused on the LHS of the equation (3.9), when the time average is applied the momentum time derivative becomes:

$$\begin{aligned}
\left\langle \frac{\partial}{\partial t}(\rho\mathbf{u}) \right\rangle &= \left\langle \rho\frac{\partial \mathbf{u}}{\partial t} \right\rangle + \left\langle \mathbf{u}\frac{\partial \rho}{\partial t} \right\rangle \\
\left\langle \rho\frac{\partial \mathbf{u}}{\partial t} \right\rangle &= \left\langle \bar{\rho}\frac{\partial \bar{\mathbf{u}}}{\partial t} \right\rangle + \left\langle \bar{\rho}\frac{\partial \mathbf{u}'}{\partial t} \right\rangle + \left\langle \rho'\frac{\partial \bar{\mathbf{u}}}{\partial t} \right\rangle + \left\langle \rho'\frac{\partial \mathbf{u}'}{\partial t} \right\rangle = \\
&= \bar{\rho}\left\langle \frac{\partial \bar{\mathbf{u}}}{\partial t} \right\rangle + \bar{\rho}\left\langle \frac{\partial \mathbf{u}'}{\partial t} \right\rangle + \langle \rho' \rangle \frac{\partial \bar{\mathbf{u}}}{\partial t} + \left\langle \rho'\frac{\partial \mathbf{u}'}{\partial t} \right\rangle = \\
&= \left\langle \rho'\frac{\partial \mathbf{u}'}{\partial t} \right\rangle \\
\left\langle \mathbf{u}\frac{\partial \rho}{\partial t} \right\rangle &= \left\langle \bar{\mathbf{u}}\frac{\partial \bar{\rho}}{\partial t} \right\rangle + \left\langle \bar{\mathbf{u}}\frac{\partial \rho'}{\partial t} \right\rangle + \left\langle \mathbf{u}'\frac{\partial \bar{\rho}}{\partial t} \right\rangle + \left\langle \mathbf{u}'\frac{\partial \rho'}{\partial t} \right\rangle = \\
&= \bar{\mathbf{u}}\left\langle \frac{\partial \bar{\rho}}{\partial t} \right\rangle + \bar{\mathbf{u}}\left\langle \frac{\partial \rho'}{\partial t} \right\rangle + \langle \mathbf{u}' \rangle \frac{\partial \bar{\rho}}{\partial t} + \left\langle \mathbf{u}'\frac{\partial \rho'}{\partial t} \right\rangle = \\
&= \left\langle \mathbf{u}'\frac{\partial \rho'}{\partial t} \right\rangle \\
\left\langle \frac{\partial}{\partial t}(\rho\mathbf{u}) \right\rangle &= \left\langle \mathbf{u}'\frac{\partial \rho'}{\partial t} \right\rangle + \left\langle \rho'\frac{\partial \mathbf{u}'}{\partial t} \right\rangle = \\
&= \left\langle \frac{\partial}{\partial t}(\rho'\mathbf{u}') \right\rangle = 0
\end{aligned}$$

Mean values are time independent therefore their time derivative is zero. The mathematical steps explained below are referred to the velocity fluctuation, but they can be applied at any fluctuation quantity.

$$\begin{aligned}
\left\langle \frac{\partial \mathbf{u}'}{\partial t} \right\rangle &= \lim_{\tau\to\infty} \frac{1}{\tau}\int_0^\tau \frac{\partial \mathbf{u}'}{\partial t} d\tau \\
&= \lim_{\tau\to\infty} \frac{1}{\tau}\int_{\mathbf{u}'(0)}^{\mathbf{u}'(\tau)} d\mathbf{u}' \\
&= \lim_{\tau\to\infty} \frac{\mathbf{u}'(\tau) - \mathbf{u}'(0)}{\tau} = 0
\end{aligned}$$

where the limit is equal to 0 because the fluctuation is a bounded function.
The divergence term inside the Eq. (3.9) LHS becomes:

$$\begin{aligned}
&\langle \nabla\cdot[(\bar{\rho}+\rho')(\bar{\mathbf{u}}+\mathbf{u}')(\bar{\mathbf{u}}+\mathbf{u}')]\rangle = \\
&= \langle \nabla\cdot(\bar{\rho}\bar{\mathbf{u}}\bar{\mathbf{u}}) + \nabla\cdot(\rho'\bar{\mathbf{u}}\bar{\mathbf{u}}) + \nabla\cdot(\bar{\rho}\bar{\mathbf{u}}\mathbf{u}') + \nabla\cdot(\rho'\bar{\mathbf{u}}\mathbf{u}') + \\
&+ \nabla\cdot(\bar{\rho}\mathbf{u}'\bar{\mathbf{u}}) + \nabla\cdot(\rho'\mathbf{u}'\bar{\mathbf{u}}) + \nabla\cdot(\bar{\rho}\mathbf{u}'\mathbf{u}') + \nabla\cdot(\rho'\mathbf{u}'\mathbf{u}')\rangle = \\
&= \langle \nabla\cdot(\bar{\rho}\bar{\mathbf{u}}\bar{\mathbf{u}})\rangle + \langle \nabla\cdot(\rho'\bar{\mathbf{u}}\bar{\mathbf{u}})\rangle + \langle \nabla\cdot(\bar{\rho}\bar{\mathbf{u}}\mathbf{u}')\rangle + \langle \nabla\cdot(\rho'\bar{\mathbf{u}}\mathbf{u}')\rangle + \\
&+ \langle \nabla\cdot(\bar{\rho}\mathbf{u}'\bar{\mathbf{u}})\rangle + \langle \nabla\cdot(\rho'\mathbf{u}'\bar{\mathbf{u}})\rangle + \langle \nabla\cdot(\bar{\rho}\mathbf{u}'\mathbf{u}')\rangle + \langle \nabla\cdot(\rho'\mathbf{u}'\mathbf{u}')\rangle
\end{aligned} \tag{3.10}$$

The equation (3.10) can be simplified using the fact that the average of a fluctuation is zero, the average of the average is the average itself and the time average commutes with the spatial derivative. Finally Eq. (3.10) becomes:

$$\langle \nabla\cdot[(\bar{\rho}+\rho')(\bar{\mathbf{u}}+\mathbf{u}')(\bar{\mathbf{u}}+\mathbf{u}')]\rangle = \nabla\cdot(\bar{\rho}\bar{\mathbf{u}}\bar{\mathbf{u}}) + \nabla\cdot\langle\rho'\left[(\bar{\mathbf{u}}\mathbf{u}') + (\bar{\mathbf{u}}\mathbf{u}')^T\right]\rangle + \nabla\cdot\langle\bar{\rho}\mathbf{u}'\mathbf{u}'\rangle + \nabla\cdot\langle\rho'\mathbf{u}'\mathbf{u}'\rangle$$

In the RHS of Eq. (3.9) the *stress tensor* the stress tensor can be expressed using the *Viscosity Newton's law*. The law is valid only for the Newtonian fluids, that is the fluids having the dynamic viscosity independent of the stress, and it states:

$$\underline{\underline{\tau}} = 2\mu\underline{\underline{\epsilon}} - \left(\frac{2}{3}\mu - \phi\right)\frac{1}{\rho}\frac{\partial\rho}{\partial p}\frac{Dp}{Dt}\,\underline{\underline{I}} \quad \text{with} \quad \underline{\underline{\epsilon}} = \frac{1}{2}\left(\nabla\mathbf{u} + \nabla\mathbf{u}^T\right) \tag{3.11}$$

where $\underline{\underline{\epsilon}}$ is the strain rate tensor, μ is the viscosity coefficient and the term with the pressure is the compressibility of the fluid. Using the assumption of incompressible flow, the compressible term vanish and the equation is rewritten as following:

$$\underline{\underline{\tau}} = 2\mu\underline{\underline{\epsilon}} \quad \text{with} \quad \underline{\underline{\epsilon}} = \frac{1}{2}\left(\nabla\mathbf{u} + \nabla\mathbf{u}^T\right) \tag{3.12}$$

Also for the strain rate tensor and viscosity coefficient, the Reynolds decomposition is applied:

$$\begin{cases} \mu = \bar{\mu} + \mu' \\ \underline{\underline{\epsilon}} = \underline{\underline{\bar{\epsilon}}} + \underline{\underline{\epsilon}}' \end{cases}$$

Now it is possible average the RHS of the equation (3.9):

$$\left\langle -\nabla p + \nabla \cdot \underline{\underline{\tau}} + \mathbf{f} \right\rangle = -\left\langle \nabla(\bar{p} + p') \right\rangle + \left\langle \nabla \cdot \left[2(\bar{\mu} + \mu')(\underline{\underline{\bar{\epsilon}}} + \underline{\underline{\epsilon}}') \right] \right\rangle + \left\langle \bar{\mathbf{f}} + \mathbf{f}' \right\rangle \tag{3.13}$$

Each term inside Eq. (3.13) is analyzed:

$$\begin{aligned} \langle \nabla p \rangle &= \langle \nabla(\bar{p} + p') \rangle = \\ &= \langle \nabla \bar{p} \rangle + \langle \nabla p' \rangle = \\ &= \nabla \langle \bar{p} \rangle + \nabla \langle p' \rangle = \\ &= \nabla \bar{p} \end{aligned}$$

$$\begin{aligned} \left\langle \nabla \cdot \left[2(\bar{\mu} + \mu')(\underline{\underline{\bar{\epsilon}}} + \underline{\underline{\epsilon}}') \right] \right\rangle &= 2\nabla \cdot \left\langle (\bar{\mu} + \mu')(\underline{\underline{\bar{\epsilon}}} + \underline{\underline{\epsilon}}') \right\rangle \\ \left\langle (\bar{\mu} + \mu')(\underline{\underline{\bar{\epsilon}}} + \underline{\underline{\epsilon}}') \right\rangle &= \left\langle \bar{\mu}\underline{\underline{\bar{\epsilon}}} + \mu'\underline{\underline{\bar{\epsilon}}} + \bar{\mu}\underline{\underline{\epsilon}}' + \mu'\underline{\underline{\epsilon}}' \right\rangle = \\ &= \left\langle \bar{\mu}\underline{\underline{\bar{\epsilon}}} \right\rangle + \left\langle \bar{\mu}\underline{\underline{\epsilon}}' \right\rangle + \left\langle \mu'\underline{\underline{\bar{\epsilon}}} \right\rangle + \left\langle \mu'\underline{\underline{\epsilon}}' \right\rangle = \\ &= \bar{\mu}\underline{\underline{\bar{\epsilon}}} + \left\langle \mu'\underline{\underline{\epsilon}}' \right\rangle \end{aligned}$$

$$\begin{aligned} \left\langle \nabla \cdot \left[2(\bar{\mu} + \mu')(\underline{\underline{\bar{\epsilon}}} + \underline{\underline{\epsilon}}') \right] \right\rangle &= \nabla \cdot (2\bar{\mu}\underline{\underline{\bar{\epsilon}}}) + \nabla \cdot \left\langle 2\mu'\underline{\underline{\epsilon}}' \right\rangle \\ \left\langle \bar{\mathbf{f}} + \mathbf{f}' \right\rangle &= \bar{\mathbf{f}} + \langle \mathbf{f}' \rangle = \\ &= \bar{\mathbf{f}} \end{aligned}$$

Equation (3.9) becomes:

$$\frac{\partial}{\partial t}(\bar{\rho}\bar{\mathbf{u}}) + \nabla \cdot (\bar{\rho}\bar{\mathbf{u}}\bar{\mathbf{u}}) + \nabla \cdot \left\langle \rho' \left[(\bar{\mathbf{u}}\mathbf{u}') + (\bar{\mathbf{u}}\mathbf{u}')^T \right] \right\rangle + \nabla \cdot \langle \bar{\rho}\mathbf{u}'\mathbf{u}' \rangle + \nabla \cdot \langle \rho'\mathbf{u}'\mathbf{u}' \rangle = -\nabla\bar{p} + \nabla \cdot (2\bar{\mu}\underline{\underline{\bar{\epsilon}}}) + \nabla \cdot \left\langle 2\mu'\underline{\underline{\epsilon}}' \right\rangle + \bar{\mathbf{f}} \tag{3.14}$$

The equation (3.14) is called *Momentum Reynolds Averaged Equation*. In the equation (3.14) a new tensor appears, it is the time average of the tensor product between the fluctuation vector and itself. These terms represent the turbulent transport and they are called *Reynolds stresses* and the tensor called *Reynolds stress tensor* is defined as following:

$$R = \bar{\rho}\mathbf{u}'\mathbf{u}' = \bar{\rho} \begin{bmatrix} u'^2 & u'v' & u'w' \\ v'u' & v'^2 & v'w' \\ w'u' & w'v' & w'^2 \end{bmatrix} \tag{3.15}$$

This tensor represents an unknown inside the mathematical model of the turbulence, which means the RANS equations are unclosed and need a closure model.

3.4 Turbulence Kinetic energy

As all the other quantity, the kinetic energy can be split into a mean value and a fluctuation through the Reynolds decomposition. Starting from the kinetic energy definition

it is possible to find an expression for the fluctuating term of the kinetic energy using the Reynolds decomposition and the average operation:

$$K = \frac{1}{2}\mathbf{u}\cdot\mathbf{u} = \frac{1}{2}(\bar{\mathbf{u}}+\mathbf{u}')\cdot(\bar{\mathbf{u}}+\mathbf{u}') = \frac{1}{2}\left[\bar{\mathbf{u}}\cdot\bar{\mathbf{u}} + \bar{\mathbf{u}}\cdot\mathbf{u}' + \mathbf{u}'\cdot\bar{\mathbf{u}} + \mathbf{u}'\cdot'\mathbf{u}'\right] \tag{3.16}$$

averaging equation (3.16) one gets:

$$\langle K\rangle = \frac{1}{2}(\bar{\mathbf{u}}\cdot\bar{\mathbf{u}}) + \frac{1}{2}\langle\mathbf{u}'\cdot\mathbf{u}'\rangle = \bar{K} + K' \tag{3.17}$$

The last term in the Eq. (3.17) is the fluctuation of the kinetic energy and it is called *Turbulence kinetic energy* k_T:

$$k_T = \frac{1}{2}\langle\mathbf{u}'\cdot\mathbf{u}'\rangle \tag{3.18}$$

The goal of this section is to find two different equations, one for the mean kinetic energy and the other one for the turbulence kinetic energy starting from the kinetic equation inside the system (3.1):

$$\frac{\partial K}{\partial t} + \nabla\cdot(\mathbf{u}K) = -\nabla p + (\nabla\cdot\underline{\underline{\tau}})\cdot\mathbf{u} + \mathbf{f}\cdot\mathbf{u} \tag{3.19}$$

As done in the previous section each sides of the equation is analyzed separately in order to simplify the derivation. The first term analyzed is the time derivative of the kinetic energy, introducing the density and energy Reynolds decomposition one gets:

$$\begin{aligned}\frac{\partial K}{\partial t} &= \frac{\partial}{\partial t}(\frac{1}{2}\rho\mathbf{u}\cdot\mathbf{u}) = \frac{\partial}{\partial t}\left[\frac{1}{2}(\bar{\rho}+\rho')(\bar{\mathbf{u}}+\mathbf{u}')\cdot(\bar{\mathbf{u}}+\mathbf{u}')\right] = \\ &= \frac{\partial}{\partial t}\left[\frac{1}{2}\bar{\rho}(\bar{\mathbf{u}}\cdot\bar{\mathbf{u}}+\bar{\mathbf{u}}\cdot\mathbf{u}'+\mathbf{u}'\cdot\bar{\mathbf{u}}+\mathbf{u}'\cdot\mathbf{u}') + \frac{1}{2}\rho'(\bar{\mathbf{u}}\cdot\bar{\mathbf{u}}+\bar{\mathbf{u}}\cdot\mathbf{u}'+\mathbf{u}'\cdot\bar{\mathbf{u}}+\mathbf{u}'\cdot\mathbf{u}')\right]\end{aligned}$$

$$\begin{aligned}&\left\langle\frac{\partial K}{\partial t}\right\rangle = \frac{\partial\langle K\rangle}{\partial t} = \\ &= \frac{\partial}{\partial t}\left\langle\left[\frac{1}{2}\bar{\rho}(\bar{\mathbf{u}}\cdot\bar{\mathbf{u}}+\bar{\mathbf{u}}\cdot\mathbf{u}'+\mathbf{u}'\cdot\bar{\mathbf{u}}+\mathbf{u}'\cdot\mathbf{u}') + \frac{1}{2}\rho'(\bar{\mathbf{u}}\cdot\bar{\mathbf{u}}+\bar{\mathbf{u}}\cdot\mathbf{u}'+\mathbf{u}'\cdot\bar{\mathbf{u}}+\mathbf{u}'\cdot\mathbf{u}')\right]\right\rangle \\ &= \frac{\partial}{\partial t}\left(\frac{1}{2}\bar{\rho}\bar{\mathbf{u}}\cdot\bar{\mathbf{u}}\right) + \frac{\partial}{\partial t}\left(\frac{1}{2}\bar{\rho}\langle\mathbf{u}'\cdot\mathbf{u}'\rangle\right) + \frac{\partial}{\partial t}\left(\frac{1}{2}\langle\rho'\bar{\mathbf{u}}\cdot\mathbf{u}'\rangle\right) + \frac{\partial}{\partial t}\left(\frac{1}{2}\langle\rho'\mathbf{u}'\cdot\bar{\mathbf{u}}\rangle\right) + \frac{\partial}{\partial t}\left(\frac{1}{2}\langle\rho'\mathbf{u}'\cdot\mathbf{u}'\rangle\right)\end{aligned}$$

$$\left\langle\frac{\partial K}{\partial t}\right\rangle = \frac{\partial\bar{K}}{\partial t} + \frac{\partial k_T}{\partial t} + \frac{\partial}{\partial t}\left(\frac{1}{2}\langle\rho'\bar{\mathbf{u}}\cdot\mathbf{u}'\rangle\right) + \frac{\partial}{\partial t}\left(\frac{1}{2}\langle\rho'\mathbf{u}'\cdot\bar{\mathbf{u}}\rangle\right) + \frac{\partial}{\partial t}\left(\frac{1}{2}\langle\rho'\mathbf{u}'\cdot\mathbf{u}'\rangle\right) \tag{3.20}$$

The second term analyzed is the transport term inside equation (3.19) LHS, the procedure is the same, the Reynolds decomposition is introduced and the average operation is applied:

$$\begin{aligned}&\nabla\cdot(\mathbf{u}K) = \nabla\cdot\left[(\bar{\mathbf{u}}+\mathbf{u}')\frac{1}{2}(\bar{\rho}+\rho')(\bar{\mathbf{u}}+\mathbf{u}')\cdot(\bar{\mathbf{u}}+\mathbf{u}')\right] \\ &(\bar{\mathbf{u}}+\mathbf{u}')\frac{1}{2}(\bar{\rho}+\rho')(\bar{\mathbf{u}}+\mathbf{u}')\cdot(\bar{\mathbf{u}}+\mathbf{u}') = \bar{\mathbf{u}}\frac{1}{2}\bar{\rho}(\bar{\mathbf{u}}\cdot\bar{\mathbf{u}}+\bar{\mathbf{u}}\cdot\mathbf{u}'+\mathbf{u}'\cdot\bar{\mathbf{u}}+\mathbf{u}'\cdot\mathbf{u}') \\ &+\bar{\mathbf{u}}\frac{1}{2}\rho'(\bar{\mathbf{u}}\cdot\bar{\mathbf{u}}+\bar{\mathbf{u}}\cdot\mathbf{u}'+\mathbf{u}'\cdot\bar{\mathbf{u}}+\mathbf{u}'\cdot\mathbf{u}') + \mathbf{u}'\frac{1}{2}\bar{\rho}(\bar{\mathbf{u}}\cdot\bar{\mathbf{u}}+\bar{\mathbf{u}}\cdot\mathbf{u}'+\mathbf{u}'\cdot\bar{\mathbf{u}}+\mathbf{u}'\cdot\mathbf{u}')+ \\ &+\mathbf{u}'\frac{1}{2}\rho'(\bar{\mathbf{u}}\cdot\bar{\mathbf{u}}+\bar{\mathbf{u}}\cdot\mathbf{u}'+\mathbf{u}'\cdot\bar{\mathbf{u}}+\mathbf{u}'\cdot\mathbf{u}')\end{aligned}$$

Once the Reynolds decomposition has been introduced the time average can be applied paying attention to the averages containing only a fluctuate term since they vanish:

$$\begin{aligned}
\langle \mathbf{u}K \rangle &= \bar{\mathbf{u}}\frac{1}{2}\bar{\rho}\bar{\mathbf{u}}\cdot\bar{\mathbf{u}} + \bar{\mathbf{u}}\frac{1}{2}\bar{\rho}\langle \mathbf{u}'\cdot\mathbf{u}'\rangle + \bar{\mathbf{u}}\frac{1}{2}\left[\langle\rho'\bar{\mathbf{u}}\cdot\mathbf{u}'\rangle + \langle\rho'\mathbf{u}'\cdot\bar{\mathbf{u}}\rangle + \langle\rho'\mathbf{u}'\cdot\mathbf{u}'\rangle\right] + \\
&+ \frac{1}{2}\bar{\rho}\left[\langle\mathbf{u}'\bar{\mathbf{u}}\cdot\mathbf{u}'\rangle + \langle\mathbf{u}'\mathbf{u}'\cdot\bar{\mathbf{u}}\rangle + \langle\mathbf{u}'\mathbf{u}'\cdot\mathbf{u}'\rangle\right] + \frac{1}{2}[\langle\rho'\mathbf{u}'\bar{\mathbf{u}}\cdot\bar{\mathbf{u}}\rangle + \langle\rho'\mathbf{u}'\bar{\mathbf{u}}\cdot\mathbf{u}'\rangle + \\
&+ \langle\rho'\mathbf{u}'\mathbf{u}'\cdot\bar{\mathbf{u}}\rangle + \langle\rho'\mathbf{u}'\mathbf{u}'\cdot\mathbf{u}'\rangle] = \\
&= \bar{K}\bar{\mathbf{u}} + k_T\bar{\mathbf{u}} + \langle\rho'\mathbf{u}'\rangle\bar{\mathbf{u}}\cdot\bar{\mathbf{u}} + \frac{1}{2}\langle\rho'\mathbf{u}'\bar{\mathbf{u}}\cdot\bar{\mathbf{u}}\rangle + \bar{\rho}\langle\mathbf{u}'\mathbf{u}'\rangle\cdot\bar{\mathbf{u}} + \frac{1}{2}\bar{\rho}\mathbf{u}'\mathbf{u}'\cdot\mathbf{u}'\rangle + \langle\rho'\mathbf{u}'\mathbf{u}'\rangle\cdot\bar{\mathbf{u}} \\
&+ \langle\rho'\mathbf{u}'\rangle\bar{\mathbf{u}}\cdot\bar{\mathbf{u}} + \frac{1}{2}\langle\rho'\mathbf{u}'\mathbf{u}'\cdot\mathbf{u}'\rangle
\end{aligned}$$

$$\begin{aligned}
\nabla\cdot\langle\mathbf{u}K\rangle = \nabla\cdot[&\bar{K}\bar{\mathbf{u}} + k_T\bar{\mathbf{u}} + \langle\rho'\mathbf{u}'\rangle\bar{\mathbf{u}}\cdot\bar{\mathbf{u}} + \frac{1}{2}\langle\rho'\mathbf{u}'\bar{\mathbf{u}}\cdot\bar{\mathbf{u}}\rangle + \bar{\rho}\langle\mathbf{u}'\mathbf{u}'\rangle\cdot\bar{\mathbf{u}} + \\
&+ \frac{1}{2}\bar{\rho}\langle\mathbf{u}'\mathbf{u}'\cdot\mathbf{u}'\rangle + \langle\rho'\mathbf{u}'\mathbf{u}'\rangle\cdot\bar{\mathbf{u}} + \langle\rho'\mathbf{u}'\rangle\bar{\mathbf{u}}\cdot\bar{\mathbf{u}} + \frac{1}{2}\langle\rho'\mathbf{u}'\mathbf{u}'\cdot\mathbf{u}'\rangle]
\end{aligned} \tag{3.21}$$

where the relations (A.4) and (A.5) have been employed.

The analysis now is focused on the LHS of the equation (3.19) which is analyzed term by terms. For the pressure term one gets:

$$\begin{aligned}
\nabla p\cdot\mathbf{u} &= \nabla(\bar{p}+p')\cdot(\bar{\mathbf{u}}+\mathbf{u}') = \nabla\bar{p}\cdot\bar{\mathbf{u}} + \nabla\bar{p}\cdot\mathbf{u}' + \nabla p'\cdot\bar{\mathbf{u}} + \nabla p'\cdot\mathbf{u}' \\
\langle\nabla p\cdot\mathbf{u}\rangle &= \nabla\bar{p}\cdot\bar{\mathbf{u}} + \nabla p'\cdot\mathbf{u}'
\end{aligned} \tag{3.22}$$

while for the force term is possible to write:

$$\begin{aligned}
\mathbf{f}\cdot\mathbf{u} &= (\bar{\mathbf{f}}+\mathbf{f}')\cdot(\bar{\mathbf{u}}+\mathbf{u}') = \bar{\mathbf{f}}\cdot\bar{\mathbf{u}} + \mathbf{f}'\cdot\bar{\mathbf{u}} + \bar{\mathbf{f}}\cdot\bar{\mathbf{u}} + \mathbf{f}'\cdot\mathbf{u}' \\
\langle\mathbf{f}\cdot\mathbf{u}\rangle &= \bar{\mathbf{f}}\cdot\bar{\mathbf{u}} + \langle\mathbf{f}'\cdot\mathbf{u}'\rangle
\end{aligned} \tag{3.23}$$

The viscous term requires more attention because it involves higher order correlation between the fluctuating terms. Applying the average operation to this term it can be written as following:

$$\begin{aligned}
\langle(\nabla\cdot\underline{\underline{\tau}})\cdot\mathbf{u}\rangle &= \langle\nabla\cdot(\underline{\underline{\tau}}\cdot\mathbf{u}) + \underline{\underline{\tau}} : \nabla\mathbf{u}\rangle \\
&= \langle\nabla\cdot(\underline{\underline{\tau}}\cdot\mathbf{u})\rangle + \langle\underline{\underline{\tau}} : \nabla\mathbf{u}\rangle \\
&= \nabla\cdot\langle\underline{\underline{\tau}}\cdot\mathbf{u}\rangle + \langle\underline{\underline{\tau}} : \nabla\mathbf{u}\rangle \\
\langle(\nabla\cdot\underline{\underline{\tau}})\cdot\mathbf{u}\rangle &= \nabla\cdot\langle\underline{\underline{\tau}}\cdot\mathbf{u}\rangle + \langle\underline{\underline{\tau}} : \nabla\mathbf{u}\rangle
\end{aligned} \tag{3.24}$$

The divergence term in the Eq. (3.24) RHS becomse:

$$\begin{aligned}
\underline{\underline{\tau}} \cdot \mathbf{u} &= (\bar{\underline{\underline{\tau}}} + \underline{\underline{\tau}}') \cdot (\bar{\mathbf{u}} + \mathbf{u}') = \bar{\underline{\underline{\tau}}} \cdot \bar{\mathbf{u}} + \bar{\underline{\underline{\tau}}} \cdot \mathbf{u}' + \underline{\underline{\tau}}' \cdot \bar{\mathbf{u}} + \underline{\underline{\tau}}' \cdot \mathbf{u}' \\
\langle \underline{\underline{\tau}} \cdot \mathbf{u} \rangle &= \bar{\underline{\underline{\tau}}} \cdot \bar{\mathbf{u}} + \langle \underline{\underline{\tau}}' \cdot \mathbf{u}' \rangle = \mu(\nabla \bar{\mathbf{u}} + \nabla \bar{\mathbf{u}}^T) \cdot \bar{\mathbf{u}} + \langle \mu(\nabla \mathbf{u}' + \nabla \mathbf{u}'^T) \cdot \mathbf{u}' \rangle = \\
&= \mu \nabla \bar{\mathbf{u}} \cdot \bar{\mathbf{u}} + \mu \nabla \bar{\mathbf{u}}^T \cdot \bar{\mathbf{u}} + \mu \langle \nabla \mathbf{u}' \cdot \mathbf{u}' + \nabla \mathbf{u}'^T \cdot \mathbf{u}' \rangle = \\
&= \mu \left[\nabla \left(\frac{1}{2} \bar{\mathbf{u}} \cdot \bar{\mathbf{u}} \right) + \nabla \bar{\mathbf{u}}^T \cdot \bar{\mathbf{u}} \right] + \mu \langle \nabla \left(\frac{1}{2} \mathbf{u}' \cdot \mathbf{u}' \right) + \nabla \mathbf{u}'^T \cdot \mathbf{u}' \rangle
\end{aligned}$$

Let us analyze the RHS of the last equation term by term:

$$\begin{aligned}
\nabla \left(\frac{1}{2} \bar{\mathbf{u}} \cdot \bar{\mathbf{u}} \right) &= \nabla \left(\frac{1}{2} \bar{\rho} \bar{\mathbf{u}} \cdot \bar{\mathbf{u}} \right) - \frac{1}{2} \bar{\mathbf{u}} \cdot \bar{\mathbf{u}} \nabla \bar{\rho} = \nabla \bar{K} - \frac{\bar{K}}{\bar{\rho}} \nabla \bar{\rho} \\
\langle \nabla \left(\frac{1}{2} \mathbf{u}' \cdot \mathbf{u}' \right) \rangle &= \nabla \left(\frac{1}{2} \bar{\rho} \langle \mathbf{u}' \cdot \mathbf{u}' \rangle \right) - \frac{1}{2} \langle \mathbf{u}' \cdot \mathbf{u}' \rangle \nabla \bar{\rho} = \nabla k_T - \frac{k_T}{\bar{\rho}} \nabla \bar{\rho}
\end{aligned}$$

finally the average of the inner product between the stress tensor and the velocity becomes:

$$\langle \underline{\underline{\tau}} \cdot \mathbf{u} \rangle = \mu \left[\nabla \bar{K} + \nabla k_T \right] - \mu \left[\frac{\bar{K}}{\bar{\rho}} + \frac{k_T}{\bar{\rho}} \right] \nabla \bar{\rho} + \mu \left[\nabla \bar{\mathbf{u}}^T \cdot \bar{\mathbf{u}} + \nabla \mathbf{u}'^T \cdot \mathbf{u}' \right]$$

Using the vector identity (A.6) the divergence term inside the equation (3.24) is rewritten in the following manner:

$$\begin{aligned}
\nabla \cdot \langle \underline{\underline{\tau}} \cdot \mathbf{u} \rangle = \mu \left[\nabla^2 \bar{K} + \nabla^2 k_T \right] - \mu \left[\frac{\bar{K}}{\bar{\rho}} + \frac{k_T}{\bar{\rho}} \right] \nabla^2 \bar{\rho} - \mu \left[\nabla \frac{\bar{K}}{\bar{\rho}} + \nabla \frac{k_T}{\bar{\rho}} \right] \cdot \nabla \bar{\rho} + \\
+ \mu \left[\nabla (\nabla \cdot \bar{\mathbf{u}}) \cdot \bar{\mathbf{u}} + \nabla \bar{\mathbf{u}} : \nabla \bar{\mathbf{u}}^T \right] + \mu \langle \nabla (\nabla \cdot \mathbf{u}') \cdot \mathbf{u}' + \nabla \mathbf{u}' : \nabla \mathbf{u}'^T \rangle
\end{aligned} \tag{3.25}$$

The inner product between the two tensors in Eq. (3.24) is:

$$\underline{\underline{\tau}} : \nabla \mathbf{u} = (\bar{\underline{\underline{\tau}}} + \underline{\underline{\tau}}') : (\nabla \bar{\mathbf{u}} + \nabla \mathbf{u}') = \bar{\underline{\underline{\tau}}} : \nabla \bar{\mathbf{u}} + \bar{\underline{\underline{\tau}}} : \nabla \mathbf{u}' + \underline{\underline{\tau}}' : \nabla \bar{\mathbf{u}} + \underline{\underline{\tau}}' : \nabla \mathbf{u}'$$

applying the average one obtains:

$$\begin{aligned}
\langle \underline{\underline{\tau}} : \nabla \mathbf{u} \rangle &= \bar{\underline{\underline{\tau}}} : \nabla \bar{\mathbf{u}} + \langle \underline{\underline{\tau}}' : \nabla \mathbf{u}' \rangle = \\
&= \mu \left[\nabla \bar{\mathbf{u}} : \nabla \bar{\mathbf{u}} + \nabla \bar{\mathbf{u}}^T : \nabla \bar{\mathbf{u}} \right] + \mu \langle \nabla \mathbf{u}' : \nabla \mathbf{u}' + \nabla \mathbf{u}'^T : \nabla \mathbf{u}' \rangle
\end{aligned} \tag{3.26}$$

Substituting equations (3.25) and (3.26) inside Eq. (3.24) the final expression for the viscous terms is:

$$\begin{aligned}
\langle (\nabla \cdot \underline{\underline{\tau}}) \cdot \mathbf{u} \rangle &= \nabla \cdot \langle \underline{\underline{\tau}} \cdot \mathbf{u} \rangle + \langle \underline{\underline{\tau}} : \nabla \mathbf{u} \rangle = \\
&= \mu \left[\nabla^2 \bar{K} + \nabla^2 k_T \right] - \mu \left[\frac{\bar{K}}{\bar{\rho}} + \frac{k_T}{\bar{\rho}} \right] \nabla^2 \bar{\rho} - \mu \left[\nabla \frac{\bar{K}}{\bar{\rho}} + \nabla \frac{k_T}{\bar{\rho}} \right] \cdot \nabla \bar{\rho} + \\
&+ \mu \left[\nabla (\nabla \cdot \bar{\mathbf{u}}) \cdot \bar{\mathbf{u}} - \nabla \bar{\mathbf{u}} : \nabla \bar{\mathbf{u}} \right] + \mu \left[\langle \nabla (\nabla \cdot \mathbf{u}') \cdot \mathbf{u}' \rangle - \langle \nabla \mathbf{u}' : \nabla \mathbf{u}' \rangle \right]
\end{aligned} \tag{3.27}$$

Combining equations (3.20),(3.21),(3.22),(3.23) and (3.27) the averaged equation for the total kinetic energy can be derived:

$$\begin{aligned}
&\frac{\partial \bar{K}}{\partial t} + \frac{\partial k_T}{\partial t} + \frac{\partial}{\partial t}\left(\frac{1}{2}\langle\rho'\bar{\mathbf{u}}\cdot\mathbf{u}'\rangle\right) + \frac{\partial}{\partial t}\left(\frac{1}{2}\langle\rho'\mathbf{u}'\cdot\bar{\mathbf{u}}\rangle\right) + \frac{\partial}{\partial t}\left(\frac{1}{2}\langle\rho'\mathbf{u}'\cdot\mathbf{u}'\rangle\right) + \\
&+ \nabla\cdot\left[\bar{K}\bar{\mathbf{u}} + k_T\bar{\mathbf{u}} + \langle\rho'\mathbf{u}'\rangle\bar{\mathbf{u}}\cdot\bar{\mathbf{u}} + \frac{1}{2}\langle\rho'\mathbf{u}'\bar{\mathbf{u}}\cdot\bar{\mathbf{u}}\rangle + \bar{\rho}\langle\mathbf{u}'\mathbf{u}'\rangle\cdot\bar{\mathbf{u}} + \frac{1}{2}\bar{\rho}\langle\mathbf{u}'\mathbf{u}'\cdot\mathbf{u}'\rangle + \right. \\
&\left. + \langle\rho'\mathbf{u}'\mathbf{u}'\rangle\cdot\bar{\mathbf{u}} + \langle\rho'\mathbf{u}'\rangle\bar{\mathbf{u}}\cdot\bar{\mathbf{u}} + \frac{1}{2}\langle\rho'\mathbf{u}'\mathbf{u}'\cdot\mathbf{u}'\rangle\right] = -\nabla\bar{p}\cdot\bar{\mathbf{u}} - \nabla p'\cdot\mathbf{u}' + \mu\left[\nabla^2\bar{K} + \nabla^2 k_T\right] - \\
&- \mu\left[\frac{\bar{K}}{\bar{\rho}} + \frac{k_T}{\bar{\rho}}\right]\nabla^2\bar{\rho} - \mu\left[\nabla\frac{\bar{K}}{\bar{\rho}} + \nabla\frac{k_T}{\bar{\rho}}\right]\cdot\nabla\bar{\rho} + \mu\left[\nabla(\nabla\cdot\bar{\mathbf{u}})\cdot\bar{\mathbf{u}} - \nabla\bar{\mathbf{u}} : \nabla\bar{\mathbf{u}}\right] + \\
&+ \mu\left[\langle\nabla(\nabla\cdot\mathbf{u}')\cdot\mathbf{u}'\rangle - \langle\nabla\mathbf{u}' : \nabla\mathbf{u}'\rangle\right] + \bar{\mathbf{f}}\cdot\bar{\mathbf{u}} + \langle\mathbf{f}'\cdot\mathbf{u}'\rangle
\end{aligned} \tag{3.28}$$

Equation (3.28) can be split into two equations, one for the mean kinetic energy and the other one for the turbulence kinetic energy. The mean kinetic energy equation states:

$$\frac{\partial\bar{K}}{\partial t} + \nabla\cdot(\bar{K}\bar{\mathbf{u}}) = -\nabla\bar{p}\cdot\bar{\mathbf{u}} + \mu\nabla^2\bar{K} - \mu\frac{\bar{K}}{\bar{\rho}}\nabla^2\bar{\rho} - \mu\nabla\frac{\bar{K}}{\bar{\rho}}\cdot\nabla\bar{\rho} + \mu\left[\nabla(\nabla\cdot\bar{\mathbf{u}})\cdot\bar{\mathbf{u}} - \nabla\bar{\mathbf{u}} : \nabla\bar{\mathbf{u}}\right] + \bar{\mathbf{f}}\cdot\bar{\mathbf{u}} \tag{3.29}$$

The turbulence kinetic energy is composed by all the fluctuating terms:

$$\begin{aligned}
&\frac{\partial k_T}{\partial t} + \nabla\cdot(k_T\bar{\mathbf{u}}) + \frac{\partial}{\partial t}\left(\frac{1}{2}\langle\rho'\bar{\mathbf{u}}\cdot\mathbf{u}'\rangle\right) + \frac{\partial}{\partial t}\left(\frac{1}{2}\langle\rho'\mathbf{u}'\cdot\bar{\mathbf{u}}\rangle\right) + \frac{\partial}{\partial t}\left(\frac{1}{2}\langle\rho'\mathbf{u}'\cdot\mathbf{u}'\rangle\right) = \\
&= -\nabla\cdot\left[\langle\rho'\mathbf{u}'\rangle\bar{\mathbf{u}}\cdot\bar{\mathbf{u}} + \frac{1}{2}\langle\rho'\mathbf{u}'\bar{\mathbf{u}}\cdot\bar{\mathbf{u}}\rangle + \bar{\rho}\langle\mathbf{u}'\mathbf{u}'\rangle\cdot\bar{\mathbf{u}} + \frac{1}{2}\bar{\rho}\langle\mathbf{u}'\mathbf{u}'\cdot\mathbf{u}'\rangle + \right. \\
&\left. + \langle\rho'\mathbf{u}'\mathbf{u}'\rangle\cdot\bar{\mathbf{u}} + \langle\rho'\mathbf{u}'\rangle\bar{\mathbf{u}}\cdot\bar{\mathbf{u}} + \frac{1}{2}\langle\rho'\mathbf{u}'\mathbf{u}'\cdot\mathbf{u}'\rangle\right] - \nabla p'\cdot\mathbf{u}' + \mu\nabla^2 k_T - \\
&- \mu\frac{k_T}{\bar{\rho}}\nabla^2\bar{\rho} - \mu\nabla\frac{k_T}{\bar{\rho}}\cdot\nabla\bar{\rho} + \mu\left[\langle\nabla(\nabla\cdot\mathbf{u}')\cdot\mathbf{u}'\rangle - \langle\nabla\mathbf{u}' : \nabla\mathbf{u}'\rangle\right] + \langle\mathbf{f}'\cdot\mathbf{u}'\rangle
\end{aligned} \tag{3.30}$$

The equation (3.30) describes the evolution of the turbulence kinetic energy and in the RHS an important term appear, the *Turbulence kinetic energy dissipation* term. It is defined as

$$\mu\nabla\mathbf{u}' : \nabla\mathbf{u}' \tag{3.31}$$

the dissipation is essentially the mean rate at which work is done by the fluctuating strain rate against fluctuating viscous stresses, the result is the conversion of turbulence kinetic energy into internal energy. This term is non-negative hence it always acts as sink term for the turbulence kinetic energy.

The dissipation terms is a fundamental variable and an equation describing it will derive in the next section.

3.5 Turbulence kinetic energy dissipation equation

The starting point to derive the dissipation equation is the momentum equation (3.9):

$$\frac{\partial\mathbf{p}}{\partial t} + \nabla\cdot(\mathbf{up}) = -\nabla p + \nabla\cdot\underline{\underline{\tau}} + \mathbf{f} \tag{3.32}$$

We develop the LHS of equation (3.32):

$$\begin{aligned}
\rho\frac{\partial\mathbf{u}}{\partial t} + \mathbf{u}\frac{\partial\rho}{\partial t} + \nabla\cdot(\rho\mathbf{uu}) &= \rho\frac{\partial\mathbf{u}}{\partial t} + \mathbf{u}\frac{\partial\rho}{\partial t} + \mathbf{uu}\cdot\nabla\rho + \rho\nabla\cdot(\mathbf{uu}) = \\
&= \rho\frac{\partial\mathbf{u}}{\partial t} + \mathbf{u}\frac{\partial\rho}{\partial t} + \mathbf{uu}\nabla\rho + \rho(\nabla\cdot\mathbf{u})\mathbf{u} + \rho\mathbf{u}\cdot\nabla\mathbf{u} = \\
&= \rho\left[\frac{\partial\mathbf{u}}{\partial t} + (\mathbf{u}\cdot\nabla)\mathbf{u}\right] + \mathbf{u}\left[\frac{\partial\rho}{\partial t} + \mathbf{u}\cdot\nabla\rho + \rho\nabla\cdot\mathbf{u}\right]
\end{aligned} \tag{3.33}$$

Using the continuity equation

$$\frac{\partial \rho}{\partial t} + \mathbf{u} \cdot \nabla \rho = -\rho \nabla \cdot \mathbf{u} \tag{3.34}$$

the equation (3.32) LHS becomes:

$$\frac{\partial \mathbf{p}}{\partial t} + \nabla \cdot (\mathbf{up}) = \rho \left[\frac{\partial \mathbf{u}}{\partial t} + (\mathbf{u} \cdot \nabla)\mathbf{u} \right] \tag{3.35}$$

Equation (3.32) is rewritten as:

$$\rho \left[\frac{\partial \mathbf{u}}{\partial t} + (\mathbf{u} \cdot \nabla)\mathbf{u} \right] = -\nabla p + \nabla \cdot \underline{\underline{\tau}} + \mathbf{f} \tag{3.36}$$

Let us introduce the Reynolds decomposition into Eq. (3.36), therefore one gets:

$$(\bar{\rho} + \rho') \left[\frac{\partial \bar{\mathbf{u}}}{\partial t} + \frac{\partial \mathbf{u}'}{\partial t} + (\bar{\mathbf{u}} + \mathbf{u}') \cdot \nabla(\bar{\mathbf{u}} + \mathbf{u}') \right] = -\nabla(\bar{p} + p') + \nabla \cdot (\underline{\underline{\bar{\tau}}} + \underline{\underline{\tau}}') + \bar{\mathbf{f}} + \mathbf{f}' \tag{3.37}$$

averaging equation (3.37), an averaged equation for the momentum is obtained:

$$\begin{aligned} &\bar{\rho} \left[\frac{\partial \bar{\mathbf{u}}}{\partial t} + \bar{\mathbf{u}} \cdot \nabla \bar{\mathbf{u}} + \langle \mathbf{u}' \cdot \nabla \mathbf{u}' \rangle \right] + \langle \rho' \frac{\partial \mathbf{u}'}{\partial t} \rangle + \langle \rho' \bar{\mathbf{u}} \cdot \nabla \mathbf{u}' \rangle + \langle \rho' \mathbf{u}' \cdot \nabla \bar{\mathbf{u}} \rangle + \langle \rho' \mathbf{u}' \cdot \nabla \mathbf{u}' \rangle = \\ &= -\nabla \bar{p} + \nabla \cdot \underline{\underline{\bar{\tau}}} + \bar{\mathbf{f}} \end{aligned} \tag{3.38}$$

The scope of the derivation is to find an equation for the dissipation, quantity links to the velocity fluctuations. A way to obtain such an equation the idea is to subtract Eq. (3.38) from Eq. (3.37) to an equation for the fluctuate terms. The resultant equation is:

$$\begin{aligned} &\bar{\rho} \left[\frac{\partial \mathbf{u}'}{\partial t} + \bar{\mathbf{u}} \cdot \nabla \mathbf{u}' + \mathbf{u}' \cdot \nabla \bar{\mathbf{u}} + \mathbf{u}' \cdot \nabla \mathbf{u}' - \langle \mathbf{u}' \cdot \nabla \mathbf{u}' \rangle \right] + \rho' \left[\frac{\partial \bar{\mathbf{u}}}{\partial t} + \frac{\partial \mathbf{u}'}{\partial t} + (\bar{\mathbf{u}} + \mathbf{u}') \cdot \nabla(\bar{\mathbf{u}} + \mathbf{u}') \right] - \\ &- \langle \rho' \frac{\partial \mathbf{u}'}{\partial t} \rangle - \langle \rho' \bar{\mathbf{u}} \cdot \nabla \mathbf{u}' \rangle + \langle \rho' \mathbf{u}' \cdot \nabla \bar{\mathbf{u}} \rangle - \langle \rho' \mathbf{u}' \cdot \nabla \mathbf{u}' \rangle = -\nabla p' + \nabla \cdot \underline{\underline{\tau}}' + \mathbf{f}' \end{aligned} \tag{3.39}$$

Equation (3.39) is an averaged equation for the fluctuate velocity, therefore, reminding the definition of ε in (3.31), the gradient for (3.39) is taken. At the resultant equation the inner product with the tensor $\nabla \mathbf{u}'$ defined in (A.8)[5] is applied. Finally the average is taken.
Let analyze term by term of Eq. (3.39). The time derivative becomes:

$$\bar{\rho} \frac{\partial \mathbf{u}'}{\partial t} \quad \Rightarrow \quad \langle \nabla \mathbf{u}' : \nabla \left(\bar{\rho} \frac{\partial \mathbf{u}'}{\partial t} \right) \rangle$$

$$\nabla \left(\bar{\rho} \frac{\partial \mathbf{u}'}{\partial t} \right) = \nabla \left[\frac{\partial (\bar{\rho} \mathbf{u}')}{\partial t} - \mathbf{u}' \frac{\partial \bar{\rho}}{\partial t} \right] = \nabla \left(\frac{\partial (\bar{\rho} \mathbf{u}')}{\partial t} \right) = \frac{\partial}{\partial t} \nabla (\bar{\rho} \mathbf{u}') = \frac{\partial}{\partial t} \left(\bar{\rho} \nabla \mathbf{u}' + \mathbf{u}' \nabla \bar{\rho} \right)$$

in the last equation the time derivative of the density mean value vanishes and the time and space derivative commute.

$$\nabla \mathbf{u}' : \frac{\partial}{\partial t} \left(\bar{\rho} \nabla \mathbf{u}' + \mathbf{u}' \nabla \bar{\rho} \right) = \bar{\rho} \left(\frac{\partial}{\partial t} \nabla \mathbf{u}' \right) : \nabla \mathbf{u}' + \nabla \mathbf{u}' : \frac{\partial}{\partial t} \left(\mathbf{u}' \nabla \bar{\rho} \right) = \bar{\rho} \frac{\partial}{\partial t} \left(\frac{1}{2} \nabla \mathbf{u}' : \nabla \mathbf{u}' \right) + \nabla \mathbf{u}' : \frac{\partial}{\partial t} \left(\mathbf{u}' \nabla \bar{\rho} \right)$$

$$\langle \nabla \mathbf{u}' : \nabla \left(\bar{\rho} \frac{\partial \mathbf{u}'}{\partial t} \right) \rangle = \bar{\rho} \frac{\partial}{\partial t} \left(\frac{1}{2} \langle \nabla \mathbf{u}' : \nabla \mathbf{u}' \rangle \right) + \langle \nabla \mathbf{u}' : \frac{\partial}{\partial t} \left(\mathbf{u}' \nabla \bar{\rho} \right) \rangle = \bar{\rho} \frac{\partial}{\partial t} \left(\frac{1}{2} \langle \nabla \mathbf{u}' : \nabla \mathbf{u}' \rangle \right) + \langle \nabla \mathbf{u}' : \nabla \bar{\rho} \frac{\partial \mathbf{u}'}{\partial t} \rangle$$

$$\bar{\rho}\bar{\mathbf{u}}\cdot\nabla\mathbf{u}' \quad \Rightarrow \quad \langle\nabla\mathbf{u}' : \nabla(\bar{\rho}\bar{\mathbf{u}}\cdot\nabla\mathbf{u}')\rangle$$
$$\nabla(\bar{\rho}\bar{\mathbf{u}}\cdot\nabla\mathbf{u}') = \nabla(\bar{\rho}\bar{\mathbf{u}})\odot\nabla\mathbf{u}' + (\bar{\rho}\bar{\mathbf{u}}\cdot\nabla)\nabla\mathbf{u}'$$

In the last equation the relation (A.7) has been introduced, where $\odot$ states the matrix product.

$$\nabla\mathbf{u}' : [\nabla(\bar{\rho}\bar{\mathbf{u}})\odot\nabla\mathbf{u}' + (\bar{\rho}\bar{\mathbf{u}}\cdot\nabla)\nabla\mathbf{u}'] = \nabla\mathbf{u}' : \nabla(\bar{\rho}\bar{\mathbf{u}})\odot\nabla\mathbf{u}' + \bar{\rho}\bar{\mathbf{u}}\cdot\nabla\left[\frac{1}{2}(\nabla\mathbf{u}' : \nabla\mathbf{u}')\right]$$
$$\langle\nabla\mathbf{u}' : [\nabla\left(\bar{\rho}\bar{\mathbf{u}}\cdot\nabla\mathbf{u}'\right)]\rangle = \langle\nabla\mathbf{u}' : [\nabla(\bar{\rho}\bar{\mathbf{u}})\odot\nabla\mathbf{u}']\rangle + \langle\bar{\rho}\bar{\mathbf{u}}\cdot\nabla\left[\frac{1}{2}(\nabla\mathbf{u}' : \nabla\mathbf{u}')\right]\rangle$$

The mathematical steps for the third and fourth term in Eq. (3.39) are the same therefore the mathematical steps are skipped and only the final expression is provided.

$$\bar{\rho}\mathbf{u}'\cdot\nabla\bar{\mathbf{u}} \quad \Rightarrow \quad \langle\nabla\mathbf{u}' : [\nabla\left(\bar{\rho}\mathbf{u}'\right)\odot\nabla\bar{\mathbf{u}}]\rangle + \langle\nabla\mathbf{u}' : [(\bar{\rho}\mathbf{u}'\cdot\nabla)\nabla\bar{\mathbf{u}}]\rangle$$
$$\bar{\rho}\mathbf{u}'\cdot\nabla\mathbf{u}' \quad \Rightarrow \quad \langle\nabla\mathbf{u}' : [\nabla\left(\bar{\rho}\mathbf{u}'\right)\odot\nabla\mathbf{u}']\rangle + \langle\bar{\rho}\mathbf{u}'\cdot\nabla\left[\frac{1}{2}\left(\nabla\mathbf{u}' : \nabla\mathbf{u}'\right)\right]\rangle$$

The last term of the constant density part is:

$$\bar{\rho}\langle\mathbf{u}'\cdot\nabla\mathbf{u}'\rangle \quad \Rightarrow \quad \langle\nabla\mathbf{u}' : \nabla\left[\bar{\rho}\langle\mathbf{u}'\cdot\nabla\mathbf{u}'\rangle\right]\rangle$$
$$\nabla(\bar{\rho}\langle\mathbf{u}'\cdot\nabla\mathbf{u}'\rangle) = \nabla\bar{\rho}\langle\mathbf{u}'\cdot\nabla\mathbf{u}'\rangle + \nabla\langle\mathbf{u}'\cdot\nabla\mathbf{u}'\rangle\bar{\rho}$$
$$\langle\nabla\mathbf{u}' : \nabla\left[\bar{\rho}\langle\mathbf{u}'\cdot\nabla\mathbf{u}'\rangle\right]\rangle = \langle\nabla\mathbf{u}' : \nabla\bar{\rho}\langle\mathbf{u}'\cdot\nabla\mathbf{u}'\rangle\rangle + \langle\nabla\mathbf{u}' : \left(\nabla\langle\mathbf{u}'\cdot\nabla\mathbf{u}'\rangle\right)\bar{\rho}\rangle =$$

the term $\langle\mathbf{u}'\cdot\nabla\mathbf{u}'\rangle$ is an averaged quantity, therefore it can be extracted out from the average operation as well as $\nabla\bar{\rho}$. The same observation is made for $\nabla\langle\mathbf{u}'\cdot\nabla\mathbf{u}'\rangle$.

$$\begin{aligned}
&= \langle\nabla\mathbf{u}'\rangle : \nabla\bar{\rho}\langle\mathbf{u}'\cdot\nabla\mathbf{u}'\rangle + \langle\nabla\mathbf{u}'\rangle : \nabla\langle\mathbf{u}'\cdot\nabla\mathbf{u}'\rangle\bar{\rho} = \\
&= \nabla\langle\mathbf{u}'\rangle : \nabla\bar{\rho}\langle\mathbf{u}'\cdot\nabla\mathbf{u}'\rangle + \nabla\langle\mathbf{u}'\rangle : \nabla\langle\mathbf{u}'\cdot\nabla\mathbf{u}'\rangle\bar{\rho} = \\
&= 0
\end{aligned}$$

Let study the terms containing the density fluctuations.

$$\rho'\frac{\partial\mathbf{u}'}{\partial t} \quad \rightarrow \quad \langle\nabla\mathbf{u}' : \nabla\left(\rho'\frac{\partial\mathbf{u}'}{\partial t}\right)\rangle$$
$$\nabla\left(\rho'\frac{\partial\mathbf{u}'}{\partial t}\right) = \nabla\rho'\frac{\partial\mathbf{u}'}{\partial t} + \rho'\nabla\frac{\partial\mathbf{u}'}{\partial t} = \nabla\rho'\frac{\partial\mathbf{u}'}{\partial t} + \rho'\frac{\partial}{\partial t}\nabla\mathbf{u}'$$
$$\nabla\mathbf{u}' : \nabla\left(\rho'\frac{\partial\mathbf{u}'}{\partial t}\right) = \nabla\mathbf{u}' : \left(\nabla\rho'\frac{\partial\mathbf{u}'}{\partial t}\right) + \nabla\mathbf{u}' : \rho'\frac{\partial}{\partial t}\left(\nabla\mathbf{u}'\right)$$
$$= \nabla\mathbf{u}' : \left(\nabla\rho'\frac{\partial\mathbf{u}'}{\partial t}\right) + \rho'\frac{\partial}{\partial t}\left(\frac{1}{2}\nabla\mathbf{u}' : \nabla\mathbf{u}'\right)$$
$$\langle\nabla\mathbf{u}' : \nabla\left(\rho'\frac{\partial\mathbf{u}'}{\partial t}\right)\rangle = \langle\nabla\mathbf{u}' : \left(\nabla\rho'\frac{\partial\mathbf{u}'}{\partial t}\right)\rangle + \langle\rho'\frac{\partial}{\partial t}\nabla\left(\frac{1}{2}\nabla\mathbf{u}' : \nabla\mathbf{u}'\right)\rangle$$

The term $\rho'(\bar{\mathbf{u}}+\mathbf{u}')\cdot\nabla(\bar{\mathbf{u}}+\mathbf{u}')$ is similar to those analyzed before, moreover the same mathematical steps:

$$\rho'(\bar{\mathbf{u}}+\mathbf{u}')\cdot\nabla(\bar{\mathbf{u}}+\mathbf{u}') \quad \Rightarrow \quad \langle\nabla\mathbf{u}' : \nabla\left[\rho'(\bar{\mathbf{u}}+\mathbf{u}')\cdot\nabla(\bar{\mathbf{u}}+\mathbf{u}')\right]\rangle$$
$$\rho'\bar{\mathbf{u}}\cdot\nabla\bar{\mathbf{u}} \quad \Rightarrow \quad \langle\nabla\mathbf{u}' : [\nabla(\rho'\bar{\mathbf{u}})\odot\nabla\bar{\mathbf{u}}]\rangle + \langle\nabla\mathbf{u}' : (\rho'\bar{\mathbf{u}}\cdot\nabla)\nabla\bar{\mathbf{u}}\rangle$$
$$\rho'\bar{\mathbf{u}}\cdot\nabla\mathbf{u}' \quad \Rightarrow \quad \langle\nabla\mathbf{u}' : [\nabla(\rho'\bar{\mathbf{u}})\odot\nabla\mathbf{u}']\rangle + \langle\rho'\bar{\mathbf{u}}\cdot\nabla\left[\bar{\mathbf{u}}(\nabla\mathbf{u}' : \nabla\mathbf{u}')\right]\rangle$$
$$\rho'\mathbf{u}'\cdot\nabla\bar{\mathbf{u}} \quad \Rightarrow \quad \langle\nabla\mathbf{u}' : [\nabla(\rho'\mathbf{u}')\odot\nabla\bar{\mathbf{u}}]\rangle + \langle\nabla\mathbf{u}' : [(\rho'\mathbf{u}'\cdot\nabla)\nabla\bar{\mathbf{u}}]\rangle$$
$$\rho'\mathbf{u}'\cdot\nabla\mathbf{u}' \quad \Rightarrow \quad \langle\nabla\mathbf{u}' : [\nabla(\rho'\mathbf{u}')\odot\nabla\mathbf{u}']\rangle + \langle\rho'\mathbf{u}'\cdot\nabla\left[\frac{1}{2}(\nabla\mathbf{u}' : \nabla\mathbf{u}')\right]\rangle$$

In Eq. (3.39) LHS there are some averaged terms, those are manipulated in the same way done before. The results is the average of a tensor product between a fluctuate term and an average term. This expression is equal to zero.

Below only one term is shown, but for the others the mathematical steps are exactly the same.

$$\begin{aligned}
\langle \rho' \frac{\partial \mathbf{u}'}{\partial t} \rangle \quad &\Rightarrow \quad \langle \nabla \mathbf{u}' : \nabla \langle \rho' \frac{\partial \mathbf{u}'}{\partial t} \rangle \rangle \\
\nabla \langle \rho' \frac{\partial \mathbf{u}'}{\partial t} \rangle &= \left\langle \nabla \left(\rho' \frac{\partial \mathbf{u}'}{\partial t} \right) \right\rangle \\
\left\langle \nabla \mathbf{u}' : \langle \nabla \left(\rho' \frac{\partial \mathbf{u}'}{\partial t} \right) \rangle \right\rangle &= \langle \nabla \mathbf{u}' \rangle : \langle \nabla \left(\rho' \frac{\partial \mathbf{u}'}{\partial t} \right) \rangle = \\
&= \nabla \langle \mathbf{u}' \rangle : \langle \nabla \left(\rho' \frac{\partial \mathbf{u}'}{\partial t} \right) \rangle = \\
&= 0
\end{aligned}$$

For the RHS of the equation (3.39), as before we study each term alone.

$$\begin{aligned}
\nabla p' \quad &\rightarrow \quad \langle \nabla \mathbf{u}' : \nabla (\nabla p') \rangle \\
\mathbf{f}' \quad &\rightarrow \quad \langle \nabla \mathbf{u}' : \nabla \mathbf{f}' \rangle \\
\nabla \cdot \underline{\underline{\tau}}' \quad &\rightarrow \quad \langle \nabla \mathbf{u}' : \nabla (\nabla \cdot \underline{\underline{\tau}}') \rangle \\
\nabla (\nabla \cdot \underline{\underline{\tau}}') &= \nabla (\mu \nabla^2 \mathbf{u}' + \mu \nabla \cdot \nabla \mathbf{u}'^T) = \mu \nabla \nabla^2 \mathbf{u}' + \mu \nabla (\nabla \cdot \nabla \mathbf{u}'^T)
\end{aligned}$$

Collecting all the terms analyzed an equation for the dissipation can be written.

$$\begin{aligned}
&\frac{1}{2}\bar{\rho}\frac{\partial}{\partial t}\left(\langle \nabla \mathbf{u}' : \nabla \mathbf{u}' \rangle\right) + \langle \nabla \mathbf{u}' : \nabla \bar{\rho} \frac{\partial \mathbf{u}'}{\partial t} \rangle + \langle \nabla \mathbf{u}' : [\nabla (\bar{\rho}\bar{\mathbf{u}}) \odot \nabla \mathbf{u}'] \rangle + \frac{1}{2}\bar{\rho}\bar{\mathbf{u}} \cdot \nabla \langle \nabla \mathbf{u}' : \nabla \mathbf{u}' \rangle + \\
&+ \langle \nabla \mathbf{u}' : [\nabla (\bar{\rho}\mathbf{u}') \odot \nabla \bar{\mathbf{u}}] \rangle + \langle \nabla \mathbf{u}' : [(\bar{\rho}\mathbf{u}' \cdot \nabla) \nabla \bar{\mathbf{u}}] \rangle + \langle \nabla \mathbf{u}' : [\nabla (\bar{\rho}\mathbf{u}') \odot \nabla \mathbf{u}'] \rangle + \\
&+ \frac{1}{2}\bar{\rho} \langle \mathbf{u}' \cdot \nabla \left[(\nabla \mathbf{u}' : \nabla \mathbf{u}') \right] \rangle + \langle \nabla \mathbf{u}' : \left(\nabla \rho' \frac{\partial \mathbf{u}'}{\partial t} \right) \rangle + \frac{1}{2} \langle \rho' \frac{\partial}{\partial t} \nabla (\nabla \mathbf{u}' : \nabla \mathbf{u}') \rangle \\
&+ \langle \nabla \mathbf{u}' : [\nabla (\rho' \bar{\mathbf{u}}) \odot \nabla \bar{\mathbf{u}}] \rangle + \langle \nabla \mathbf{u}' : (\rho' \bar{\mathbf{u}} \cdot \nabla) \nabla \bar{\mathbf{u}} \rangle + \langle \nabla \mathbf{u}' : [\nabla (\rho' \bar{\mathbf{u}}) \odot \nabla \mathbf{u}'] \rangle + \\
&+ \langle \rho' \bar{\mathbf{u}} \cdot \nabla \left[\bar{\mathbf{u}} (\nabla \mathbf{u}' : \nabla \mathbf{u}') \right] \rangle + \langle \nabla \mathbf{u}' : [\nabla (\rho' \mathbf{u}') \odot \nabla \bar{\mathbf{u}}] \rangle + \\
&+ \langle \nabla \mathbf{u}' : [(\rho' \mathbf{u}' \cdot \nabla) \nabla \bar{\mathbf{u}}] \rangle + \langle \nabla \mathbf{u}' : [\nabla (\rho' \mathbf{u}') \odot \nabla \mathbf{u}'] \rangle + \frac{1}{2} \langle \rho' \mathbf{u}' \cdot \nabla \left(\nabla \mathbf{u}' : \nabla \mathbf{u}' \right) \rangle = \\
&= -\langle \nabla \mathbf{u}' : \nabla (\nabla p') \rangle + \langle \nabla \mathbf{u}' : \mu \nabla \nabla^2 \mathbf{u}' \rangle + \langle \nabla \mathbf{u}' : \mu \nabla (\nabla \cdot \nabla \mathbf{u}'^T) \rangle + \langle \nabla \mathbf{u}' : \nabla \mathbf{f}' \rangle
\end{aligned} \tag{3.40}$$

Equation (3.40) represents the dissipation expression that allows to close the model and to solve the kinetic energy equation. Further assumptions can be introduced:

- Constant density $\rho' = 0 \rightarrow \rho = \bar{\rho}$.
- Constant density means that $\frac{D\rho}{Dt} = 0 \rightarrow \nabla \cdot \mathbf{u} = 0$.
- Velocity divergence equal to zero means that $\nabla \cdot \mathbf{u}' = 0 \rightarrow \nabla \cdot \underline{\underline{\tau}}' = \mu \nabla^2 \mathbf{u}'$.

With these assumption equation (3.40) can be modified as following:

$$\begin{aligned}
&\frac{1}{2}\bar{\rho}\frac{\partial}{\partial t}(\langle \nabla \mathbf{u}' : \nabla \mathbf{u}' \rangle) + \bar{\rho} \langle \nabla \mathbf{u}' : [\nabla (\bar{\mathbf{u}}) \odot \nabla \mathbf{u}'] \rangle + \frac{1}{2}\bar{\rho}\bar{\mathbf{u}} \cdot \nabla \langle \nabla \mathbf{u}' : \nabla \mathbf{u}' \rangle + \\
&+ \bar{\rho} \langle \nabla \mathbf{u}' : [\nabla (\mathbf{u}') \odot \nabla \bar{\mathbf{u}}] \rangle + \bar{\rho} \langle \nabla \mathbf{u}' : [(\mathbf{u}' \cdot \nabla) \nabla \bar{\mathbf{u}}] \rangle + \bar{\rho} \langle \nabla \mathbf{u}' : [\nabla (\mathbf{u}') \odot \nabla \mathbf{u}'] \rangle + \\
&+ \frac{1}{2}\bar{\rho} \langle \mathbf{u}' \cdot \nabla \left[(\nabla \mathbf{u}' : \nabla \mathbf{u}') \right] \rangle = -\langle \nabla \mathbf{u}' : \nabla (\nabla p') \rangle + \langle \nabla \mathbf{u}' : \mu \nabla \nabla^2 \mathbf{u}' \rangle + \langle \nabla \mathbf{u}' : \nabla \mathbf{f}' \rangle
\end{aligned} \tag{3.41}$$

Defining the dissipation as: $\varepsilon = \nu\langle\nabla\mathbf{u}' : \nabla\mathbf{u}'\rangle$, where $\nu = \mu/\rho$, Eq. (3.41) is divided by ρ and multiplied for $2\nu\rho$. One gets:

$$\begin{aligned}
&\bar{\rho}\frac{\partial\varepsilon}{\partial t} + 2\mu\langle\nabla\mathbf{u}' : [\nabla(\bar{\mathbf{u}}) \odot \nabla\mathbf{u}']\rangle + \bar{\rho}\bar{\mathbf{u}}\cdot\nabla\varepsilon + 2\mu\langle\nabla\mathbf{u}' : [\nabla(\mathbf{u}') \odot \nabla\bar{\mathbf{u}}]\rangle + \\
&+ 2\mu\langle\nabla\mathbf{u}' : [(\mathbf{u}'\cdot\nabla)\nabla\bar{\mathbf{u}}]\rangle + 2\mu\langle\nabla\mathbf{u}' : [\nabla(\mathbf{u}') \odot \nabla\mathbf{u}']\rangle + 2\mu\langle\mathbf{u}'\cdot\nabla\left[(\nabla\mathbf{u}' : \nabla\mathbf{u}')\right]\rangle = \\
&= -2\nu\langle\nabla\mathbf{u}' : \nabla(\nabla p')\rangle + 2\nu\mu\langle\nabla\mathbf{u}' : \nabla\nabla^2\mathbf{u}'\rangle + 2\nu\langle\nabla\mathbf{u}' : \nabla\mathbf{f}'\rangle
\end{aligned} \tag{3.42}$$

Rearranging all the term, equation 3.42 becomes:

$$\begin{aligned}
\bar{\rho}\frac{\partial\varepsilon}{\partial t} + \bar{\rho}\bar{\mathbf{u}}\cdot\nabla\varepsilon = & \\
&= -2\mu\langle\nabla\mathbf{u}' : [\nabla(\bar{\mathbf{u}}) \odot \nabla\mathbf{u}']\rangle - 2\mu\langle\nabla\mathbf{u}' : [\nabla(\mathbf{u}') \odot \nabla\bar{\mathbf{u}}]\rangle - \\
&- 2\mu\langle\nabla\mathbf{u}' : [(\mathbf{u}'\cdot\nabla)\nabla\bar{\mathbf{u}}]\rangle - 2\mu\langle\nabla\mathbf{u}' : [\nabla(\mathbf{u}') \odot \nabla\mathbf{u}']\rangle \\
&- 2\mu\langle\mathbf{u}'\cdot\nabla\left[(\nabla\mathbf{u}' : \nabla\mathbf{u}')\right]\rangle - 2\nu\langle\nabla\mathbf{u}' : \nabla(\nabla p')\rangle + \\
&+ 2\nu\mu\langle\nabla\mathbf{u}' : \nabla\nabla^2\mathbf{u}'\rangle + 2\nu\langle\nabla\mathbf{u}' : \nabla\mathbf{f}'\rangle
\end{aligned} \tag{3.43}$$

Using equation (A.9) some simplifications can be made:

$$\begin{aligned}
\nabla\mathbf{u}' : \nabla\nabla^2\mathbf{u}' = \nabla\mathbf{u}' : \nabla^2\nabla\mathbf{u}' = \nabla\left(\nabla\mathbf{u}' : \nabla\nabla\mathbf{u}'\right) - \nabla\nabla\mathbf{u}' : \nabla\nabla\mathbf{u}' = & \\
= \nabla\left[\nabla(\frac{1}{2}\nabla\mathbf{u}' : \nabla\mathbf{u}')\right] - \nabla\nabla\mathbf{u}' : \nabla\nabla\mathbf{u}' & \\
2\nu\mu\langle\nabla\mathbf{u}' : \nabla\nabla^2\mathbf{u}\rangle = 2\nu\mu\frac{1}{2}\nabla\left[\nabla\langle\nabla\mathbf{u}' : \nabla\mathbf{u}'\rangle\right] - 2\nu\mu\langle\nabla\nabla\mathbf{u}' : \nabla\nabla\mathbf{u}'\rangle = & \\
= \mu\nabla(\nabla\varepsilon) - 2\nu\mu\langle\nabla\nabla\mathbf{u}' : \nabla\nabla\mathbf{u}'\rangle &
\end{aligned}$$

The final form for the dissipation equation is:

$$\begin{aligned}
\bar{\rho}\frac{\partial\varepsilon}{\partial t} + \bar{\rho}\bar{\mathbf{u}}\cdot\nabla\varepsilon = & \\
&= -2\mu\langle\nabla\mathbf{u}' : [\nabla\bar{\mathbf{u}} \odot \nabla\mathbf{u}']\rangle - 2\mu\langle\nabla\mathbf{u}' : [\nabla\mathbf{u}' \odot \nabla\bar{\mathbf{u}}]\rangle - \\
&- 2\mu\langle\nabla\mathbf{u}' : [(\mathbf{u}'\cdot\nabla)\nabla\bar{\mathbf{u}}]\rangle - 2\mu\langle\nabla\mathbf{u}' : [\nabla\mathbf{u}' \odot \nabla\mathbf{u}']\rangle - \\
&- 2\mu\langle\mathbf{u}'\cdot\nabla\left[(\nabla\mathbf{u}' : \nabla\mathbf{u}')\right]\rangle - 2\nu\langle\nabla\mathbf{u}' : \nabla(\nabla p')\rangle + \\
&+ \mu\nabla(\nabla\varepsilon) - 2\nu\mu\langle\nabla\nabla\mathbf{u}' : \nabla\nabla\mathbf{u}'\rangle + 2\nu\langle\nabla\mathbf{u}' : \nabla\mathbf{f}'\rangle
\end{aligned} \tag{3.44}$$

Chapter 4

Turbulence Model

This chapter is dedicated to the turbulence phenomenon and its modelling. In the first part the mechanisms referred to the turbulence are briefly outlined in order to understand which assumptions are used to model the phenomenon. In the second section the $k-\varepsilon$ turbulence model is presented.

4.1 The nature of Turbulence

There are many situations where a turbulent flow is observed in the everyday surroundings, water in a river or in a waterfall, the plume formed by a rocket engine or also the smoke from a cigarette, these are only a few examples but the list can be very long. In engineering turbulent flows are prevalent, one can think about the flows around the vehicles,*e.g.*airplanes cars, or about the flows inside vessels or heat exchanger. This large diffusion of the turbulent flows is due to its ability to transport and mix fluid much more effectively than comparable laminar flows.

The main characteristic is a chaotic and random flow where eddies of different sizes realize the exchange of mass, momentum and energy inside the flow. In this chaotic flow the velocity keep changing in space and time, therefore it is decomposed into a mean value and a fluctuation. The fundamental parameter characterizing the turbulent flow is the *Reynolds Number*, a dimensionless number that evaluates the ratio between the inertial forces and the viscous forces:

$$Re_D = \frac{vD}{\nu} \tag{4.1}$$

where ν is the fluid viscosty, v and D are respectively a characteristic velocity and a characteristic length scale of the flow. Depending on the value of the Reynolds number it's possible to discern who prevails between the inertial and viscous effects. Turbulence regime is triggered at high Re numbers, when the non linear term within the Navier-Stoke equations is much bigger than the linear term.

Before to go ahead in the description of the mechanisms that characterizes the turbulence, it's important to introduce some statistical definitions. First of all the use of probability density functions to describe the random variables allow to generalized the discussion to any turbulent flows. A random field is statistically stationary if all statistics are invariant under a shift in time and it is called statistically homogenous if all the statistics are invariant under any translation. If a field is statistically homogenous it follows that the mean field is uniform and, with an appropriate choice of frame, can be taken equal to zero. If the statistics of the field is also invariant under rotations and reflections of the coordinate systems then it's statistically isotropic.

In homogenous turbulence the fluctuating velocity field is statistically homogenous.

It should be underlined that even if a flow is statistically homogenous, nevertheless all the components of any field can vary inside the coordinate system and in time, it's

only the statistics that are independent of some coordinate directions.

Turbulence is an eddying motion which has a wide spectrum of eddy sizes and a corresponding spectrum of fluctuation frequencies. Its motion is always rotational and can be thought of as a tangle of vortex elements whose vorticity can be aligned in all directions and are highly unsteady. The largest eddies are determined by the boundary conditions of the flow and their size is of the same order of magnitude as the main flow. The smallest eddies are determined by the viscous forces.

The eddies can be considered as vortex element which stretch each other through a process called *vortex stretching*. Due to this process the energy is passed from the larger eddies to the smaller and smaller eddies until the viscous forces became active and dissipate the energy. The energy flow, from the larger eddies to the smaller eddies, is called *Energy Cascade*.

4.1.1 The energy cascade

As explained before turbulent flows are characterized by eddies with a wide range of length scales. An eddy can be though as a turbulent motion localized within a region of size l. The larger eddies are characterized by a lengthscale l_0 that is comparable to the scale of the main flow as well as the velocity u_0 is in the same order of the main velocity, therefore the Re number of the larger eddies is high and the direct effects of the viscosity on the larger eddies are negligible. Afterward Richardson's turbulence formulation[24] the larger eddies are unstable and breaks up transferring their energy to the smaller eddies, which undergo a similar break-up process and transfer their energy to smaller eddies. This mechanism is called *energy cascade*. The large eddies interact with the mean flow, thereby extracting kinetic energy from the mean motion and feeding it into the larger scale turbulent motion. Through the stretching vortex the energy passes to the smaller scales and finally be dissipated. Therefore the rate of energy dissipated is also determined by the large scale motion although the dissipation is a viscous process and takes place at the smallest eddies. The viscosity determines the amount of dissipated energy and the scale at which dissipation takes place. Moreover at high Reynolds number the viscosity effects are small as well as the dissipative eddies.

Kolmogorov[15], through a theory stated in the form of three hypotheses, tried to quantify the Richardson's description and to understand which are the time and length scales characterizing the energy cascade.

4.1.2 Kolmogorov hypotheses

The first hypothesis proposed by Kolmogorov concerns the isotropy of the small eddies at high Re number. Kolmogorov argued that all the information about the geometry of the large eddies is lost during the cascade and hence the small scale motions are *locally isotropic*. Locally isotropic means that the isotropy is respected in a small domain compared to the main flow domain and far from the boundary of the flow or other singularities. Therefore the smaller eddies have similar statistics in every high Reynolds number turbulent flow.

It is useful introduce a lengthscale, $l_{EI} \approx \frac{1}{6} l_0$[22], as the demarcation between the anisotropic large eddies and the isotropic small eddies,$l \leq l_{EI}$. In the small eddies range, during the energy cascade, the dominant parameters are the energy rate at which the small scales receive energy and viscous dissipation. The dissipation rate ε is determined by the energy transfer rate, therefore it has assumed that the energy rate and the dissipation are equals.

Therefore the first consequence of the locally isotropy is represented by the *Kolmogorov's first similarity hypothesis*. For high Re number in a turbulent flows the characteristics of the small scale motions have an universal form and are determined by $\nu \left[m^2/s\right]$ and $\varepsilon \left[m^2/s^3\right]$.

With this two parameters, through dimensional analysis, it's possible to define an unique length, velocity and time scale for the small eddies range:

$$\eta \equiv \left(\frac{\nu^3}{\varepsilon}\right)^{1/4} \tag{4.2a}$$

$$u_\eta \equiv (\varepsilon\nu)^{1/4} \tag{4.2b}$$

$$\tau_\eta \equiv \left(\frac{\nu}{\varepsilon}\right)^{1/2} \tag{4.2c}$$

Using equations (4.2) the Re number, related to the small eddies, can be evaluated:

$$Re = \frac{u_\eta \eta}{\nu} = \frac{(\varepsilon\nu)^{1/4}(\nu^3/\varepsilon)^{1/4}}{\nu} = \frac{\varepsilon^{1/4}\nu}{\nu\varepsilon^{1/4}} = 1 \tag{4.3}$$

and also the dissipation rate can be derived:

$$\varepsilon = \nu\left(\frac{u_\eta}{\eta}\right)^2 = \frac{\nu}{\tau_\eta^2} \tag{4.4}$$

Equation (4.3) is consistent with the notion that the cascade proceeds to smaller and smaller scales until the Reynolds number is small enough for dissipation to be effective.

The ratios of the smallest to largest scales are determined from the equation set (4.2) and from the scaling $\varepsilon \sim u_0/l_0$:

$$\eta/l_0 \sim Re^{\,-3/4} \tag{4.5a}$$

$$u_\eta/u_0 \sim Re^{\,-1/4} \tag{4.5b}$$

$$\tau_\eta/\tau_0 \sim Re^{\,-1/2} \tag{4.5c}$$

As at high Re number all the small eddies scales are smaller compared to the largest eddies, there is a range of scales l that are very small compared with the largest ones l_0 and yet very large compared to η,*i.e.*$\eta \ll l \ll l_0$. Since eddies in this range are much bigger than the dissipative eddies, it may be supposed that their Re number is large and consequently they are little affected by viscosity. Following that idea Kolmogorov formulated his *second similarity hypothesis*. At high Re number in a turbulent flow the statistics of the motions of scale l in the range $\eta \ll l \ll l_0$ have an universal form that is determined by ε independent by ν.

As done before it's convenient to introduce a lengthscale $l_{DI} \approx 60\eta$ in order to split the range of the small eddies in two parts. The first range, $l_{DI} \leq l \leq l_{EI}$, is called *inertial subrange*. In this range the motions are determined by the inertial effects and viscous effects being negligible. The second is called *dissipation subrange* and it is the range where the viscous effects are dominant and are responsible for the dissipation process.

Using the dimensional analysis it is possible to derive characteristic scales for length, velocity and time. Since the viscous effect are negligible inside the inertial zone the it's meaningless to use the cinematic viscosity coupled with the dissipation rate to form the fundamental scales, furthermore it is impossible to generate the scales using only the dissipation rate. Therefore for a given eddy size l characteristic velocity and time are formed from ε and l:

$$u(l) = (\varepsilon l)^{1/3} \tag{4.6a}$$

$$\tau\,(l) = \left(\frac{l^2}{\varepsilon}\right)^{1/3} \tag{4.6b}$$

The rate at which energy is transferred from eddies larger than l to those smaller than l is denoted $T(l)$ and using the equations (4.6) is possible to find a relation for T:

$$T \sim \frac{u^2(l)}{\tau(l)} \quad \text{but} \quad \varepsilon = \frac{u^2(l)}{\tau(l)} \quad \Rightarrow \quad T \sim \varepsilon \tag{4.7}$$

Last equation shows that, inside the inertial range, the energy transferred rate is independent from the eddy size. Therefore the energy transferred from the large scales to small scales, which determines the constant rate of energy in the inertial range, defines the dissipation rate ε. In Fig. 4.1 the energy cascade is sketched with the different ranges.

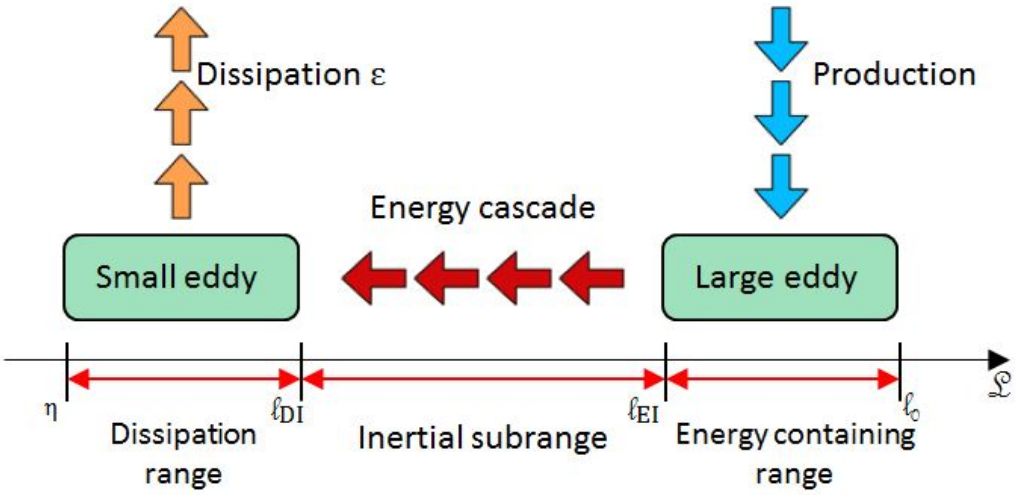

Fig. 4.1: Schematic diagram of the energy cascade at very high Reynolds number.

4.1.3 The energy spectrum

The previous section has shown how the turbulent kinetic energy is transferred between the different eddies, it remains to see how the turbulent kinetic energy is distributed among the various eddies.

All the fluctuating properties of a turbulent flow contain energy across a wide range of frequencies or wavenumbers, $\kappa = 2\pi/l$ where l is the length scale, thus the energy contains in a wavenumber range $[\kappa_a, \kappa_b]$ is equal to:

$$k_T = \int_{\kappa_a}^{\kappa_b} E(\kappa) d\kappa \tag{4.8}$$

Yet it is possible to write an equation for the dissipation inside the same wavenumber range:

$$\varepsilon = \int_{\kappa_a}^{\kappa_b} 2\nu\kappa^2 E(\kappa) d\kappa \tag{4.9}$$

Applying the Kolmogorov's hypotheses, an expression for the turbulent kinetic within the inertial range can be written. It follows from the first similarity hypothesis that for $l < l_{EI} \rightarrow \kappa > \kappa_{EI} \equiv 2\pi/l_{EI}$ the energy spectrum is an universal function of ε and ν. Through the second similarity hypothesis it follows that for a lengthscales $l_{DI} < l < l_{EI}$ the energy spectrum depends only by the turbulent dissipation. In the inertial range $(\kappa_{EI}; \kappa_{DI})$ the energy spectrum is[22]:

$$E(\kappa) = C\varepsilon^{2/3}\kappa^{-5/3} \tag{4.10}$$

Equation (4.10) is called *Kolmogorov's* 5/3 law and, although it applies only in the inertial range, it consistent with the idea that the bulk of the energy is in the large scales, small wavenumbers, and that the bulk of the dissipation is in the small scales, big wavenumbers. In Fig. 4.2 the spectral energy $E(\kappa)$ is shown as a function of the wavenumber $k = 2\pi/l$. The spectral energy is defined as kinetic energy per unit of mass and per unit wavenumber. The plot displays that the large eddies are the most energetic and $E(\kappa)$ rapidly decreases as the the wavenumber increases, therefore the smallest eddies have the lowest energy contents.

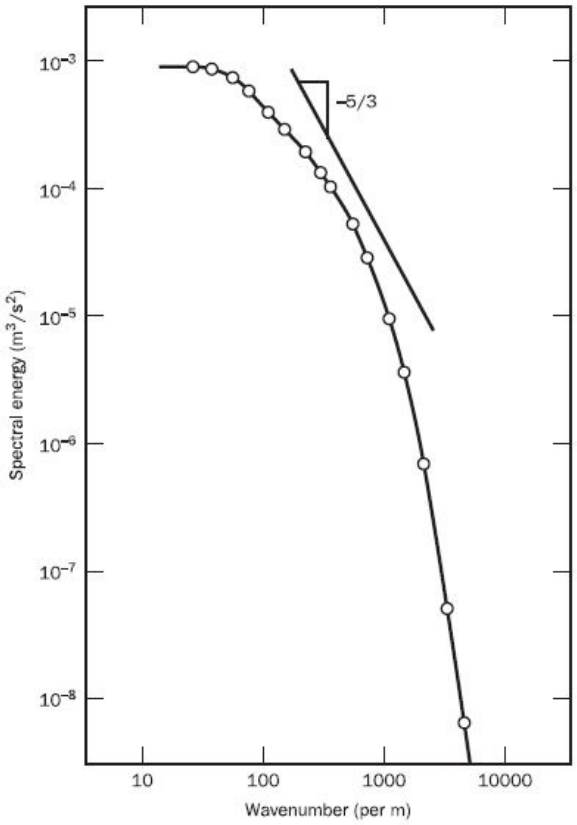

Fig. 4.2: Energy spectrum in function of the wavenumber[29].

4.2 k-ε model

In the present work a turbulence model for the Reynolds average Navier Stokes equations is applied: the $k-\varepsilon$ model[18]. This model belongs to the class of *two-equations models*, in which model transport equations are solved for two turbulence quantities, in the $k-\varepsilon$ model these quantities are the turbulence kinetic energy k_T and the dissipation of turbulence kinetic energy ε. The model is based on the Kolmogorov's hypothesis.

The model is the most widely used to model the turbulence, it is incorporated in most commercial CFD codes and it is acceptably accurate for simple flows.

The model is based on k-equation (3.30) and ε-equation (3.44). The equations have to be modeled, finding the physical mean of each term and trying to write them in order to evaluate the dissipation.

The equations modeling is achieved by two steps, first one models every term of each equation introducing some coefficients and then one closes the system finding the values for the coefficients introduced. The problem of closure arises because of the presence of fluctuations, indeed close the system means find a way to write and evaluate these fluctuating terms. Our closure model is based on some assumptions that introduce some approximations in the model with the risk to not get an exact solution.

Introducing the assumptions used to derive the ε-equation , equation (3.30) becomes:

$$\frac{\partial k_T}{\partial t}+\bar{\mathbf{u}}\cdot\nabla k_T = -\nabla\cdot(\bar{\rho}\langle\mathbf{u}'\mathbf{u}'\rangle\cdot\bar{\mathbf{u}})-\rho\varepsilon+\nabla\cdot\left[\mu\nabla k_T - p'\mathbf{u}' - \frac{1}{2}\rho\langle\mathbf{u}'\mathbf{u}'\cdot\mathbf{u}'\rangle\right]+\langle\mathbf{f}'\cdot\mathbf{u}'\rangle \quad (4.11)$$

The different terms in the equation (4.11) describe the transport processes for the turbulence kinetic energy.

The LHS gives the rate of change of k following a fluid particle while the RHS is a bit more complicated. The first term of the RHS is the production term and represents the rate at which kinetic energy is transferred from the main flow to the turbulence and it represents the production term. The second term, $\rho\varepsilon$, is the dissipation term and represents the loss of turbulence kinetic energy that is the rate at which the turbulence kinetic energy is converted into internal energy. The pressure term is the pressure diffusion contributing to the turbulent transport, called *pressure diffusion* resulting from the correlation between the pressure and velocity fluctuations. The laplacian term is called *molecular diffusion* and represents the diffusion of turbulence energy caused by the molecular transport process and, finally, the triple velocity correlation is the *turbulent transport*[34]. This last term is the rate at which the turbulence energy is transported through the fluid by the turbulent fluctuations.

Assuming a gradient-diffusion transport mechanism, as the Fick's law, the pressure term and the turbulent transport can be assumed proportional to the gradient of turbulence kinetic energy:

$$\begin{aligned} p'\mathbf{u}' + \frac{1}{2}\rho\langle\mathbf{u}'\mathbf{u}'\cdot\mathbf{u}'\rangle &\propto \nabla k_T \\ p'\mathbf{u}' + \frac{1}{2}\rho\langle\mathbf{u}'\mathbf{u}'\cdot\mathbf{u}'\rangle &= \frac{\mu_T}{\sigma_k}\nabla k_T \end{aligned} \tag{4.12}$$

where μ_T is the the eddy viscosity while σ_k is a closure coefficient known as the turbulent Prandtl number. The turbulent Prandtl number can be used to related the eddy viscosity to the eddy diffusivity coefficient, defined as $\Gamma_T = \mu_T/\sigma_k$. The equation (4.11) becomes:

$$\frac{\partial k_T}{\partial t} + \bar{\mathbf{u}}\cdot\nabla k_T = -\nabla\cdot(\rho\langle\mathbf{u}'\mathbf{u}'\rangle\cdot\bar{\mathbf{u}}) - \rho\varepsilon + \nabla\cdot\left[\left(\mu + \frac{\mu_t}{\sigma_k}\right)\nabla k_T\right] + \langle\mathbf{f}'\cdot\mathbf{u}\rangle \tag{4.13}$$

Defined an equation for the turbulence kinetic energy, the dissipation equation has to be analyzed in order to describe each term within it. As it has been done for the kinetic energy every term is analyzed and using dimensional analysis and physical sense the equation is rewritten introducing closure coefficients. The ε-equation is:

$$\begin{aligned} \bar{\rho}\frac{\partial\varepsilon}{\partial t} + \bar{\rho}\bar{\mathbf{u}}\cdot\nabla\varepsilon = & \\ &= -2\mu\langle\nabla\mathbf{u}' : [\nabla\bar{\mathbf{u}}\odot\nabla\mathbf{u}']\rangle - 2\mu\langle\nabla\mathbf{u}' : [\nabla\mathbf{u}'\odot\nabla\bar{\mathbf{u}}]\rangle - \\ &- 2\mu\langle\nabla\mathbf{u}' : [(\mathbf{u}'\cdot\nabla)\nabla\bar{\mathbf{u}}]\rangle - 2\mu\langle\nabla\mathbf{u}' : [\nabla\mathbf{u}'\odot\nabla\mathbf{u}']\rangle - \\ &- 2\mu\langle\mathbf{u}'\cdot\nabla\left[(\nabla\mathbf{u}' : \nabla\mathbf{u}')\right]\rangle - 2\nu\langle\nabla\mathbf{u}' : \nabla(\nabla p')\rangle + \\ &+ \mu\nabla(\nabla\varepsilon) - 2\nu\mu\langle\nabla\nabla\mathbf{u}' : \nabla\nabla\mathbf{u}'\rangle + 2\nu\langle\nabla\mathbf{u}' : \nabla\mathbf{f}'\rangle \end{aligned} \tag{4.14}$$

The first terms analyzed are those containing the derivative of the mean velocity, they represent the production of dissipation due to interactions between the mean flow and the products of the turbulent fluctuations. This interpretation follows from the presumption that the product of the turbulent fluctuations have negative correlations in regions with positive velocity gradients[6].

$$P_\varepsilon = -2\mu\langle\nabla\mathbf{u}' : [\nabla\bar{\mathbf{u}}\odot\nabla\mathbf{u}']\rangle - 2\mu\langle\nabla\mathbf{u}' : [\nabla\mathbf{u}'\odot\nabla\bar{\mathbf{u}}]\rangle - 2\mu\langle\nabla\mathbf{u}' : [(\mathbf{u}'\cdot\nabla)\nabla\bar{\mathbf{u}}]\rangle \tag{4.15}$$

To model this term the assumption of the local equilibrium is made, it means that the production of turbulence kinetic energy and its dissipation are almost equal locally. With this assumption one can say that the turbulent and mean flow quantities are locally proportional at any point in the flow, therefore the ratio of turbulent and mean quantities is constant. The local equilibrium states:

$$\begin{aligned} \nabla\cdot(\rho\langle\mathbf{u}'\mathbf{u}'\rangle : \nabla\bar{\mathbf{u}}) &\approx \varepsilon \\ P_k = \nabla\cdot(\rho\langle\mathbf{u}'\mathbf{u}'\rangle : \nabla\bar{\mathbf{u}}) &\approx \varepsilon \end{aligned} \tag{4.16}$$

Through a dimensional analysis it is possible to write:

$$P_\varepsilon \propto \frac{P_k}{t_{ch}} = \mu \left(\langle \mathbf{u}'\mathbf{u}' \rangle : \nabla \bar{\mathbf{u}} \right) t_{ch}^{-1} \tag{4.17}$$

where t_{ch} is the characteristic time scale for the production of ε.

As the local equilibrium has been assumed the production rate of the turbulence kinetic energy is the same as the one of the dissipation, therefore one can imagine that a proportional relation exists between these two quantities:

$$k_T \propto \varepsilon$$

a time scale can be derived using the dimensional analysis. The ratio between k_T and ε is equal to the time scale for the turbulent dissipation.

$$t_{ch} = \frac{k_T}{\varepsilon} \tag{4.18}$$

which gives:

$$\begin{aligned} P_\varepsilon &\propto \frac{\varepsilon}{k_T} \langle \mathbf{u}'\mathbf{u}' \rangle : \nabla \bar{\mathbf{u}} \\ P_\varepsilon &= C_{\varepsilon 1} \frac{\varepsilon}{k_T} \langle \mathbf{u}'\mathbf{u}' \rangle : \nabla \bar{\mathbf{u}} \end{aligned} \tag{4.19}$$

where $C_{\varepsilon 1}$ is a constant value.

The velocity fluctuations represent the time rate at which the dissipation is destroyed or dissipated.

$$D_\varepsilon = -2\mu \langle \nabla \mathbf{u}' : [\nabla \mathbf{u}' \odot \nabla \mathbf{u}'] \rangle - 2\mu\nu \langle \nabla\nabla \mathbf{u}' : \nabla\nabla \mathbf{u}' \rangle \tag{4.20}$$

Using a dimensional analysis one can write:

$$\begin{aligned} D_\varepsilon &\approx \frac{\varepsilon}{t_{ch}} \\ D_\varepsilon &= C_{\varepsilon 2} \frac{\varepsilon^2}{k_T} \end{aligned} \tag{4.21}$$

where $C_{\varepsilon 2}$ is a constant value.

The remaining terms to analyze are:

$$\mu \nabla(\nabla \varepsilon) - 2\nu \langle \nabla \mathbf{u}' : \nabla(\nabla p') \rangle - 2\mu \langle \mathbf{u}' \cdot \nabla \left[\nabla \mathbf{u}' : \nabla \mathbf{u}' \right] \rangle \tag{4.22}$$

The terms in Eq. (4.22) represent the diffusion due to molecular action and, as it has been done for the turbulence kinetic energy, the equation is modeled a standard gradient diffusion approach. Introducing the turbulent Prandtl number for dissipation it is possible to link the dissipation to the eddy viscosity. Finally the last terms are rewritten as:

$$\mu \nabla \left(\nabla \varepsilon \right) - 2\nu \langle \nabla \mathbf{u}' : \nabla \left(\nabla p' \right) \rangle - 2\mu \langle \mathbf{u}' \cdot \nabla \left[\nabla \mathbf{u}' : \nabla \mathbf{u}' \right] \rangle = \nabla \left[\left(\mu + \frac{\mu_t}{\sigma_\varepsilon} \right) \nabla \varepsilon \right] \tag{4.23}$$

where μ_t is the eddy viscosity and σ_ε.

To close the model an expression for the eddy viscosity is needed, since it is an unknown inside the k-equation and the ε-equation . To compute μ_T the dimensional analysis is used with the local equilibrium assumption: with this assumption one can say that turbulence and mean quantities are proportional and the ration between these two scales is the eddy viscosity.

$$\mu_T \approx \frac{\rho k_T^2}{\varepsilon} \quad \Rightarrow \quad \mu_T = C_\mu \frac{\rho k_T^2}{\varepsilon} \tag{4.24}$$

The final expression for ε-equation is:

$$\rho\frac{\partial\varepsilon}{\partial t}+\rho\bar{\mathbf{u}}\cdot\nabla\varepsilon=C_{\varepsilon1}\frac{\varepsilon}{k_T}\nabla\cdot(\langle\mathbf{u}'\mathbf{u}'\rangle:\nabla\bar{\mathbf{u}})-C_{\varepsilon2}\rho\frac{\varepsilon^2}{k_T}+\nabla\left[\left(\mu+\frac{\mu_t}{\sigma_\varepsilon}\right)\nabla\varepsilon\right] \tag{4.25}$$

where a minus has been put ahead the second term in the equation (4.25) RHS because it represents a dissipation for ε.

Finally the $k-\varepsilon$ model is:

$$\begin{cases}\frac{\partial k_T}{\partial t}+\bar{\mathbf{u}}\cdot\nabla k_T=-\nabla\cdot(\rho\langle\mathbf{u}'\mathbf{u}'\rangle\cdot\bar{\mathbf{u}})-\rho\varepsilon+\nabla\cdot\left[\left(\mu+\frac{\mu_t}{\sigma_k}\right)\nabla k_T\right]+\langle\mathbf{f}'\cdot\mathbf{u}\rangle\\ \rho\frac{\partial\varepsilon}{\partial t}+\rho\bar{\mathbf{u}}\cdot\nabla\varepsilon=C_{\varepsilon1}\frac{\varepsilon}{k_T}\nabla\cdot(\langle\mathbf{u}'\mathbf{u}'\rangle:\nabla\bar{\mathbf{u}})-C_{\varepsilon2}\rho\frac{\varepsilon^2}{k_T}+\nabla\cdot\left[\left(\mu+\frac{\mu_t}{\sigma_\varepsilon}\right)\nabla\varepsilon\right]\end{cases} \tag{4.26}$$

The final form for the model terminate the coefficients, also said *closure coefficients*, have to be evaluated. The determination of these coefficients is not rigorously established, since the model involve many assumptions and arguments based on physical reasoning, therefore the most popular approach is to set the values in such way that the model agrees with experimentally observed properties of turbulence.
The closure coefficient[19] are presented in the Tab. 4.1.

C_μ	$C_{\varepsilon1}$	$C_{\varepsilon2}$	σ_κ	σ_ε
0.09	1.44	1.92	1.0	1.3

Tab. 4.1: Values of constants in the $k-\varepsilon$ model.

Chapter 5

Turbulent mixing

Turbulent and laminar plane wake flows and their mixing characteristic have been a subject of research for more than a century and they are of fundamental relevance for many engineering design, such as the coolant mixing in the fuel bundle subchannels, mixing between fluid at different temperature in the pipe junction, the mixing between air and fuel in the combustion chamber and so on. Several works[9],[33],[20] have investigated the effects of the turbulent mixing in the nuclear reactor, indeed mixing of coolant flows with different properties, temperature and density, is of significant interest for nuclear safety. When there is an important difference between the properties of the two fluids and flows rate and velocity are important the mixture turbulent lead to fluctuations of temperatures. The temperature fluctuations induce oscillating thermal stresses at walls which can be damaged by fatigue and cracking. The consequences of thermal fatigue in the nuclear power plants are exemplified by the failure of the residual heat removal loop in one of the reactors of the Civaux plant, in France, an event investigated in [12]. The turbulent mixing understanding is a crucial aspect for the extension of the power plants up to 60 years in order to preserve the wall and junction integrity.

When two streams with a strong temperature difference mix a strong density gradient also exists. In normal condition the temperature differences can be as high as $160°C$ which results in a density difference of approximately 10%. Understanding how density interfaces affect the mixing of coolant streams is integral to predicting areas susceptible to thermal fatigue[7].

The Generic Mixing Experiment performed at the Paul Scherrer Institute focuses on the basic mechanism that promote or define mixing over a density interface.

5.1 The Generic Mixing Experiment

5.1.1 The facility

The **GE**niric **MI**xing e**X**periment(GEMIX) at the Paul Scherrer Insitute focus on the basic mechanisms of turbulent mixing in the presence of temperature and/or density gradients under isokinetic mixing conditions. To study the fundamental mixing phenomena, co-flow experiments were carried out in a square channel with Reynolds number covering the range of $Re = 5000$ to 60000 at various relative densities. In Fig. 5.1 a schematic of the test facility is shown where the flow direction is from left to right. The GEMIX flow channel is manufactured of acrylic glass to enable access for optical methods and only the last $80mm$ of the tapered splitter plate assembly are manufactured of stainless steel to maintain the precision requirements and avoid deformations. Both half-channels of the inlet, denoted as upper leg and lower leg, have constant rectangular cross sectional area of $25mm$ in the $y - direction$ and $50mm$ in the $z - direction$.

Two turbulent streams are initially separated in the inflow section(Fig. 5.2) by the splitter plate, which has an angle of 3°, in the inflow section the presence of honeycombs

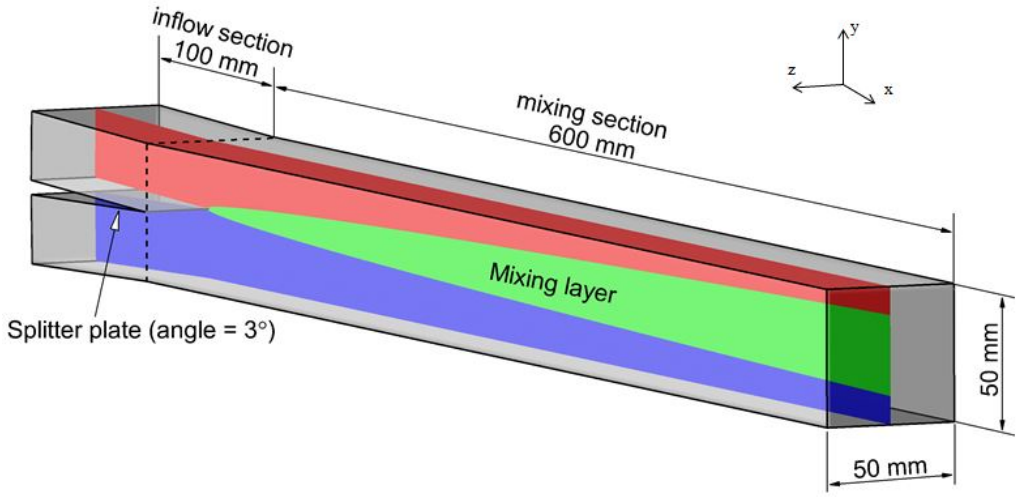

Fig. 5.1: Schematic of GEMIX experiment[4].

and grids allows to obtain velocity profiles equal for the two legs and the end of the splitter plate and free from rotational components. The last conditioning grid in both

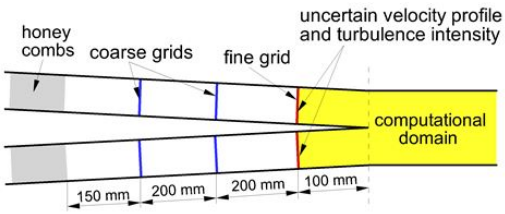

(a) Schematic of inflow section.

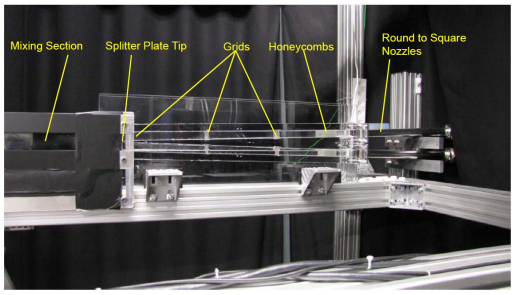

(b) Picture of inflow section.

Fig. 5.2: Inflow conditioning[4].

legs is located 100 mm upstream of the splitter plate tip, its wire diameter is 0.4 mm while the wire spacing is 1.25 mm. Downstream of the splitter plate tip both streams pass into the mixing section and start interacting to form the mixing zones. The mixing section has a square cross section of area $50 \times 50mm$ and both streams are having the same velocity,*i.e.*isokinetic conditions. The facility allows to modify the velocity between $0.2m/s$ and $1.2m/s$ that corresponds to the Reynolds number range mentioned before.

To generate a density difference of up to 1.5% between the fluids in the upper and lower legs the temperature of one of the streams was adjusted, while for higher densities, sucrose was added to one of the streams.

The development of the velocity field and concentration field downstream of the splitter plate is observed with three different flow measurement techniques, one intrusive and two optical flow measurement:

- **Particle Image Velocimetry**(PIV) has been used to determine the velocity field in flow direction in the plane $x - y$ in the center of the channel.
- **Wire-Mesh sensor**(WMS) has been installed to measure the concentration field in the cross sectional area, $y - z$ plane, for six downstream distances.
- **Laser Induced Fluorescence**(LIF) has been employed to measure the concentration field in flow direction in the center of the channel.

The measurement domain covers a range of $x = 50\ mm$ to $x = 550\ mm$ downstream from the splitter plate tip, downstream the measurement section is ad an additional straight channel section of approximately $1m$ length attached. The outlet sections consists of a rectangular box of $40l$ with a spillover weir that maintains a constant back pressure of $150mm$ a constant back pressure of 150 mm head in the channel for all flow rates.

Water supply to the flow channel is realized with a pumping station and two water storage tanks of $200l$ capacity each, one tank contain tap water and the second contains de-ionized water or a solution of de-ionized water and sucrose to increase the density. The latter tank is equipped with a propeller stirrer, Geppert CR-6, to increase the dissolution of the sucrose in the de-ionized water. The pumping station is composed of two nearly identical pumping lines, enabling separate conditioning for each stream, the only difference between the two pumping lines is that the de-ionized water one is equipped with a heater while the tap water pumping line has a cooler to adjust the temperatures. Each pumping line is equipped with a frequency controlled centrifugal inline pump(Grundfos CRNE 5-10), a Coriolis mass flow meter(Endress & Hauser Promass 83F), temperature and pressure transmitters and a water filter(Nussbaum 1810,50 Microns) to keep the flow channel free from undesired pollutants. Furthermore each pumping lines has a bypass immediately downstream of the pump, over which the water can pass through the heater/cooler and pumped back into the dedicated storage tank until a required temperature set point in each tank is adjusted.

As it has said before sucrose is added to altered the water density without a substantial change in the electrical conductance of the water and to avoid any problem it's added to the de-ionized water. The mass fraction of sucrose in conjunction with the temperature can be altered to set precise density differences between the two streams keeping the viscosity of the two streams similar. The isoviscosity is required to prevent significant differences in the Re number between the streams, which could affect the flow symmetry in the mixing region. The flow rates inside the channel are adjusted by a PID-controller which adjusts the rotational speed of the frequency controlled centrifugal pump.

The experimental results revealed that as one increases the density difference, the resulting stable stratification)lighter over heavier fluid) tends to suppress the turbulent mixing between the two streams which hinders the growth of the mixing layer.

For further details on GEMIX experiment the reader is referred to [11] and [9].

5.1.2 The instrumentation

Particle Image Velocimetry

The *Particle Image Velocimetry*(PIV)[30],[2] has been employed evaluate the velocity in the flow direction, that means in the $x - yplane$. This method is an optical non-intrusive technique, developed in the last 20 years, that can provide an quantitative measure of the instantaneous flow velocity field across a planar area of a flow field. To perform the measurement small seeding particles are injected in the flow, the particles are tiny, neutrally buoyant and they can be aerosol or solid depending of the nature of the flow. The velocity is measured indirectly with the displacement of the seeding particle in a given time interval within which the particle velocity variation is assumed to be linear.

A double pulsed laser is installed, it generates a planar light sheet, the laser light is scattered by the seeding particles and cameras record the scattered light. The cameras are typically positioned perpendicular to the plane of the light sheet. The double pulse is needed to generate two different images with a small time separation between. The record particle displacement field is measured locally across the whole field of view of the images, scaled by the image magnification and then divided by the known pulse separation to obtain flow velocity at each point. From the time delay between the two illuminations and the displacements of the tracers velocity can be calculated.

The PIV recording is divided in small subareas, called interrogation window, and using statistical correlation techniques one local displacement vector is determined for each interrogation window. The dimension of the interrogation window, then the number

of particles inside the interrogation window, is an important aspect in order to get good results. The interrogation window has to satisfy two requirements: first the interrogation window has to contain a minimum number of particles, indeed it has been proved that the signal improves with the amount of particles. Second the particles inside the interrogation window have to move homogeneously in the same direction and the same distance in order to be able to consider the velocity law linear.

The evaluation of the particle images depends on the way these images have been recorder by the used camera. One possibility is to record the scattered light of both illuminations in one frames and to evaluate the pictures using an autocorrelation technique. The other possibility is to record the scattered light from the illuminations in different frames and to analyze the images using a cross-correlation technique.

Wire Mesh Sensor

The WMS is a developing technique that replaces a conductance probe by measuring local conductance over the entire cross section of the channel with minimal solidity(10%) and in the GEMIX experiment has been used to measure the mixing process over the cross sectional area normal to the flow direction. The most common use of the WMS is the measuring of the conductance to map multiphase flows but by using conductive tap water and non conductive dissolution in each stream a similar conductance map for single phase flow can be obtained. The WMS used in the experiment facility consists

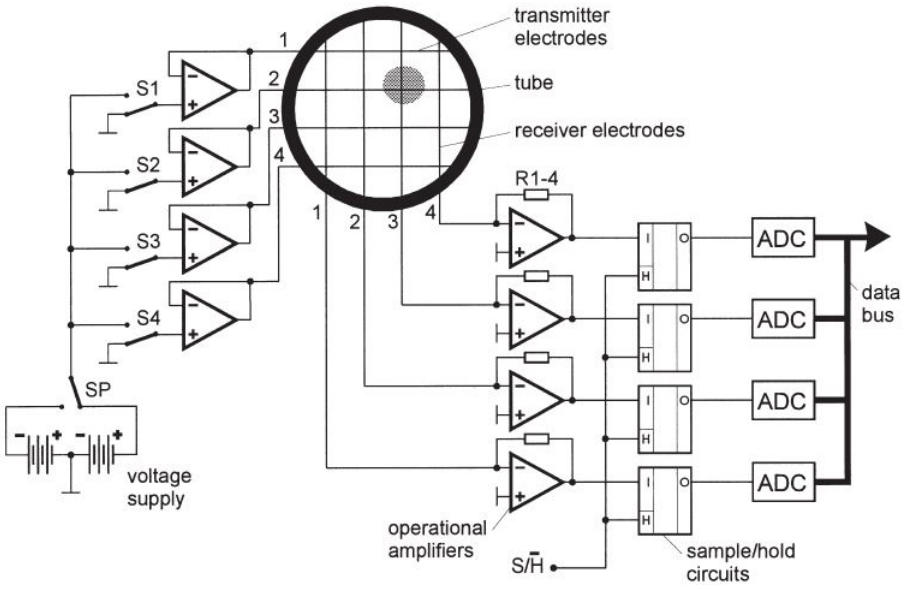

Fig. 5.3: Simplified scheme of the electrode-mesh device[23].

of two perpendicular arrays of 48 wires of diameter $0.05mm$ that are spaced $0.5mm$ from each other, where one plane acts as transmitter the other one as receiver plane. The results is a matrix in the cross section of 48×48 measurements nodes. During the measuring cycle the transmitter electrodes are activated by a multiplex circuit in a successive order. The multiplex procedure is illustrated in Fig. 5.3. The data acquisition is achieved by replacing the binary signal integration by an evaluation of the analogue current signal form the receiver electrodes. The currents are transformated into voltages by operational amplifiers and sampled by individual sample/hold circuits. After an analogue/digital conversion the signals are recorded by a data acquisition computer connected to AD converters. This procedure is repeated for all transmitter electrodes and after the last transmitter electrode activation a two-dimensional matrix of values of current is available that reflects the conductivities between all crossing points of the electrodes of the perpendicular planes. Finally the magnitude of the signal is proportional to

the conductance of the fluid at the given node. The WMS covers the entire cross section of $50mm^2$ spaced equidistantly, so achieves a resolution of $1.08mm$.

Further explanations about the measurement techniques are outlined in [23].

Laser Induced Fluorescence

The *Laser Induced Fluorescence*(LIS)[31] is an optical method that allows to visualize a fluid flow and to estimate its concentration in mixing phenomena. The idea is to introduce a dye tracer inside the fluid and to hit it with a laser in order to induce the fluorescence signal that is proportional to the local dye concentration. The fluorescence signal comes from the photon emission following the disexcitation of the dye electrons. A light source hits the dye causing an excitation of the electrons to higher energy level, coming back to the ground state a photon is emitted. The emitted photons hit a sensor from which photo electrons are emitted and converted into a signal. In Fig. 5.4 is shown the idea of the

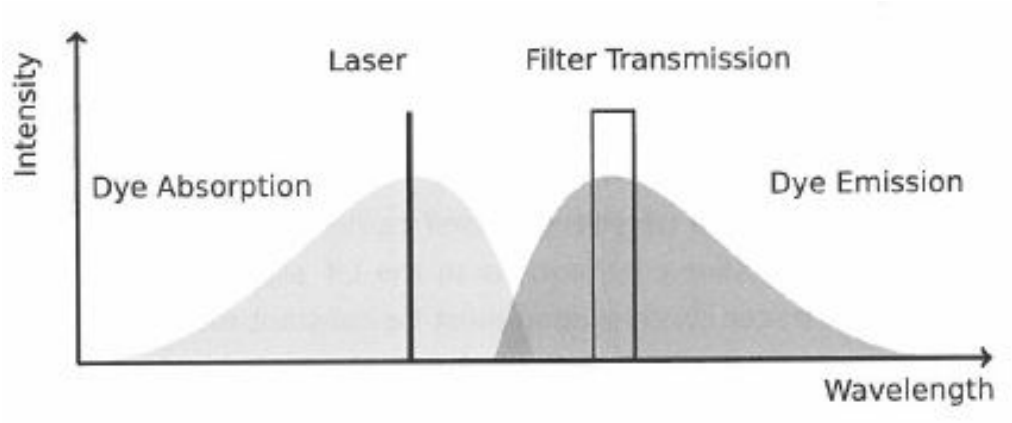

Fig. 5.4: Absorption and emission diagram for the tracers and filters[31].

method: a laser beam hit the dye tracer causing the excitation of the atomic electrons that after a disexcitation in the fundamental state emit light in a different spectrum with longer wavelength compared to the laser one. For the phenomenom of exciting photons it is important that the laser wavelength matches the excitation energy gap of the active tracer substance. If the energy step is known it is possible to calculate the wavelength of the emitted photons with Eq. (5.1).

$$\delta E = \frac{hc}{\lambda} \tag{5.1}$$

The emitted photons are in a longer wavelength than the laser one, then a band pass filter can be applied to the camera to calculate the wavelength of the emitted photons.

Since a whole flow field is enlightened with a laser beam the intensity of the laser beam is weakened and this effect increases with the total number of particles. The laser intensity depends on the length of the evaluated measurement section is given by the *Beer-Lambert* law:

$$I(x) = I_0 e^{-n_i \sigma x} \tag{5.2}$$

where I_0 is the initial intensity of the laser, n_i is the density of the tracer and σ is the absorption cross section.

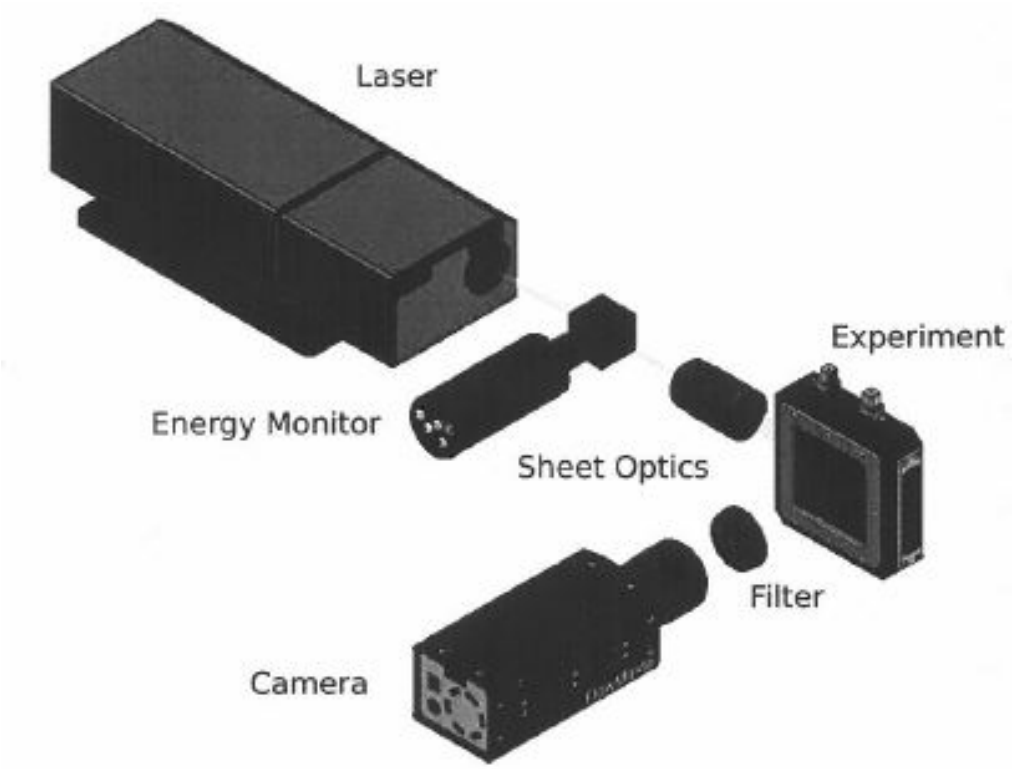

Fig. 5.5: Experimental setup[31].

Chapter 6

Uncertainty quantification

In this chapter the methods for Uncertainty Quantification(UQ) of Computational Fluid Dynamics simulation are presented. The framework where the Uncertainty Quantification is placed is explained. After the attention is focused on the Polynomial Chaos Expansion, a non-intrusive method used to evaluate the uncertainty propagation through a CFD simulation. Finally in the last section two Polynomial Chaos Expansion are described.

6.1 The Uncertainty Quantification

In engineering Virtual Prototypes(VP) have become a key technology to cope with the challenges in designing new products, satisfying environmental and cost constrains. All these objectives require a highly integrated computer-based design system relying on advanced massively parallel hardware, making the virtual product development and qualification process more achievable.

Virtual Prototyping involves all those fields in which the product conception is supported by a software utilization, it can be subdivided in three different sector[13]:

- **Computer-Aided Design(CAD)**: The use of computer systems to assist in the creation, modification analysis or optimization of a design in order to increase the conception productivity and the conception quality.
- **Computer-AUTOmated Design(CAutoD)**: It extends the idea of the CAD systems, the computer is not only a tool that helps during the conception phase but through opportune algorithms it allows to optimize the product conception.
- **Computer-Aided Engineering(CAE)**: The use of computer systems in order to analyze a physical system, these fields include Finite Elements Analysis, Multibody dynamics, optimization and also Computational Fluid Dynamics(CFD).

The need for computer simulations has become crucial in science and engineering, to minimize the need for costly physical experiments that may be even impossible during early design stages.

Computational Fluid Mechanics simulations are largely used not only to understand what we cannot see with our naked eyes or with the assistance of instrumentation, but also from our need to predict what will happen in future. However numerical simulations have to be carefully performed and verified to yield useful and reliable information regarding the system being studied. One of the key aspects in numerical simulation is level of confidence at the numerical results, in the boundary conditions, physical properties or model parameters,as they contains numerical errors and uncertainties. Thus, the understanding and quantification of these errors is critical aspect in order to provide the level of uncertainty in the CFD results.

In the *AIAA G-077-1998* guidelines a distinction between the concept of *uncertainty* and *error* is presented:

- **Uncertainty** is a potential deficiency in any phase or activity of the modeling process that is due to the *lack of knowledge*.
- **Error** is a recognizable deficiency in any phase or activity of the modeling process that is not due to the lack of knowledge.

Uncertainty Quantification(UQ) focuses on the study and quantification of how uncertainties propagates through a given system. In particular, physical models are often very complex and built on several assumptions resulting approximate and uncertain. Because of the complexity their solutions is performed through numerical method that involve other error and uncertainty, the UQ is applied on this case in order to build an universal tool that yields reliability and robustness to the numerical world.

The UQ approach considers the sources of uncertainties as random variables and, assigning them a probability density function, it computes the total uncertainty affecting the system response. In this approach *non-deterministic method* are applied and the physical system are described by *stochastic partial differential equations*. The deterministic solution of a system is substituted by a non deterministic representation thanks to which statistical quantities are computed.

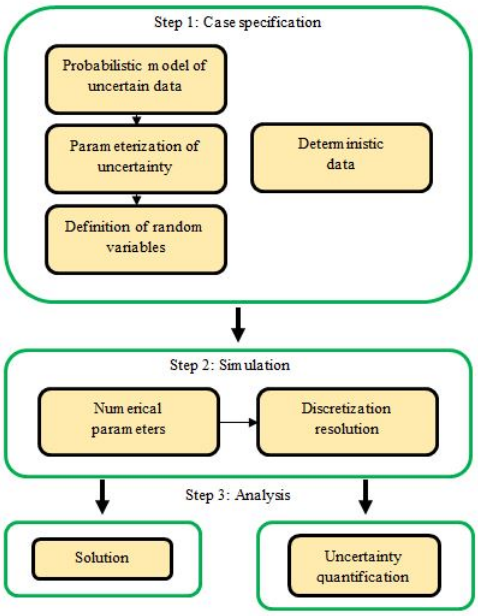

Fig. 6.1: Uncertainty Quantification strategy.

6.1.1 Source of uncertainties

The uncertainties have different causes but it is possible to make a simply distinction in three main category to reflect the usual pragmatic viewpoint of the industrial user and also the different difficulties associated with the management of each class met by the software developer:

- **Operational uncertainties**, uncertainties related to the operational issues.
- **Geometrical uncertainties**, uncertainties inside the system geometry, like geometrical tolerance due to the manufacturing of the system.
- **Numerical uncertainties**, it covers the uncertainties connected to the modeling issues and numerical errors.

The present work focuses in model uncertainties, *i.e.*all the discrepancies due to approximate or imprecise representation of the underlying model, input parameters boundary conditions and the numerical errors linked to the solution of the model.

6.1.2 Uncertainty classification

The uncertainties can be split in two sub-category basing on the degree to which they are inherent to the application or reflect a lack of knowledge[26]:

- **Aleatory Uncertainty**, known also as *irreducible uncertainty* or stochastic uncertainty, associated with inherent randomness of the modeled physical system and its environment. This kind of uncertainty is often naturally defined in probabilistic framework.
- **Epistemic Uncertainty**, known also as *reducible uncertainty*, caused by a lack of knowledge about a quantity whose true value exhibits no actual variability. These uncertainties are often biased and they are typically less defined in a probabilistic framework.

The epistemic uncertainties are considered as *reducible* since they could be reduced through increased understanding and research, or more relevant physical data, and are globally related to the lack of knowledge about the appropriate value to use for the considered quantity. The important consequence is that epistemic uncertainties have a fixed, but poorly known, value in the analysis. For instance the turbulent viscosity in a CFD simulation is known to be subject to the many approximations attached to the turbulence model chose.

On the other hand aleatory uncertainties are related to the inherent randomness of the system being analyzed, such as variability of operational conditions, geometrical randomness from manufacturing process, which cannot be reduced by further data.

Hence, *epistemic uncertainties* of a mathematical model represents the level of uncertainty in reproducing the real system, while the *aleatory uncertainties* are a strict property of the system being analyzed. This distinction is not always clear since lack of knowledge is relative and depends on current theory and experimental capabilities. One goal of uncertainty quantification is to reformulate epistemic uncertainties as aleatoric uncertainties where the probabilistic analysis is applicable.

6.1.3 Probabilistic framework

The Uncertainty Quantification needs of a properly probabilistic framework, since the uncertainties are treated as a probabilistic variables and the principal outcomes of the uncertainty quantification are statistical parameters. Depending on the operative viewpoint, parameters with epistemic uncertainty may or may not be handled in a probabilistic UQ context. This distinction has to do with the *Bayesian* framework versus the *frequentist* view of probability. In the frequentist viewpoint only a quantity that exhibits a stochastic interpretation can be treated as a random variable, since it's possible to associate a probability density function with it. The aleatoric uncertainty is defined in a frequentist framework.

This frequentist idea seems to be in contrast to the epistemic uncertainty, which, being defined as a lack of knowledge, is usually handed in a *Bayesian* framework. The main difference between these two probabilistic interpretation lays in the fact that in the Bayesian framework the probability is inherently the degree of belief in a proposition and it does not necessarily derive from sampling or observation. Therefore probabilities are considered to be a distribution rather than a single frequency value. Similarly, parameters are considered to be random variables with associated densities and the solution of the parameter estimation problem is the posterior probability density. The Bayesian perspective is thus natural for model uncertainty quantification since it provides densities can be propagated through models.

Therefore both epistemic and aleatoric uncertainties can be handled using probability theory in the Bayesian framework.

6.2 Approach to Uncertainty quantification

With these assumptions one can introduce the *Spectral Methods* and *Monte Carlo method*, two strategies used to propagate the uncertainties through models. In the spectral methods the idea is to write the solution as a sum of certain orthogonal basis. In this category the **Polynomial Chaos Expansion** is situated.

The fundamental idea of the Monte Carlo methods is a random sampling of the parameter space in order to construct a set of realization of the input data. At each realization corresponds a unique solution of the model. Starting from model realizations it is possible to estimate the statistics of the model.

6.2.1 Monte-Carlo method

Monte Carlo methods rely on a homogeneous random sampling of the parameter space, to determine the probability density function of a system. The advantage of this technique is its robustness, implementation simplicity and independence from the number of parameters used.

One of the main disadvantages is the large number of samples requires to achieve convergence. The Monte Carlo method is characterized by a slow convergence. The convergence rate is $\mathrm{O}(M^{-1/2})$ where M is the number of realizations. Hence the number of simulations has to be increased by a factor 100 to gain an additional place of accuracy. Therefore the Monte-Carlo method requires a large number of sampling points to determine the variability of the solution: for a specific realization of the model, one obtains a local information on the solution and the model domain must to be sampled with sufficiently resolution to determine the variability of the solution. Consequently one realizes that the local representation penalizes the research of a solution both in terms of efficiency and the limited analytical capability.

6.2.2 Spectral Methods

The spectral methods provide techniques for constructing surrogate models in the parameter space based on orthogonal expansions and to significantly reduce the number of deterministic model solution required to obtain statistical moments associated with a quantity of interest. The sampling based on spectral methods are characterized by convergence rates that are considerably faster that the Monte Carlo rates for low dimension parameter space.

The idea is based on reconstructing the response dependance of the solution on the independent random variables describing the input data, this functional dependance is expressed in terms of a series:

$$\mathbf{R}(\boldsymbol{\xi}) = \sum_{k=0}^{\infty} \mathbf{c}_k \boldsymbol{\Psi}_k(\boldsymbol{\xi}) \tag{6.1}$$

where $\mathbf{s}$ is the problem solution, $\boldsymbol{\Psi}_k$ are suitably selected orthogonal basis of the random variables and the $\mathbf{c}_k$ are the deterministic coefficients. The orthogonal basis used in Eq. (6.1) is non-zero on the whole domain, so the spectral methods represent a global approach and they are largely used because of their good accuracy, efficiency and fast convergence.

The *Polynomial Chaos Expansions*(*PCE*) is part of the spectral methods. It is a propagation technique that use spectral representation of the response in the probabilistic space. This representation is made in terms of *orthogonal polynomials bases* of the random variables. In the Eq. (6.1) the "basis function" $\boldsymbol{\Psi}_k$ is an orthogonal polynomial basis and

the computation of the coefficients $\mathbf{c}_k$ allow to estimate the statical quantity of the response $\mathbf{R}$.

6.3 Polynomial Chaos Expansion

The idea of Polynomial Chaos Expansion(PCE) is to project the solution on to independent directions represented by the random variables composing the parameter space. It is necessary to introduce a vector space in which an inner product can be defined. The PCE is defined in an *Hilbert space* H:

$$H = \left\{ \mathbf{x} \in \Omega \subseteq \Re^n : \|\mathbf{x}\|_{L^2(\Omega)} < \infty \right\} \tag{6.2}$$

In an Hilbert space it's possible to define the L^2 inner product as:

$$\mathbf{x}, \mathbf{y} \in H \quad \Rightarrow \quad \langle \mathbf{x}, \mathbf{y} \rangle = \int_\Omega \mathbf{x}\mathbf{y} dP \tag{6.3}$$

6.3.1 Polynomial Chaos

Consider a probability space consisted in:

- Ω, the sample space, which is the set of all possible outcomes.
- σ, the $\sigma - algebra$, a collection of events that generate the outcomes.
- P, the probability measure on (Ω, σ) that allows to specify each event's likelihood of happening.

Let $\{\xi_i(\omega)\}_{i=1}^{\infty}$ be a set of independent standard Gaussian variables on Ω, then it's possible to represent any random variables $U : \Omega \to \Re$ with finite variance,*i.e.*$U \in L^2(\Omega, P)$ as[21]:

$$R(\omega) = \sum_{i=0}^{\infty} c_i \Psi_i(\xi), \qquad \xi = \{\xi_1, \xi_2, \xi_3, \dots\} \tag{6.4}$$

where Ψ_i is a set of polynomials orthogonal to Ψ_{i-1}, that is called *Polynomial Chaos* of order i and the Eq. (6.4) is the Polynomials Chaos representation of the variable $R(\omega)$. The set of polynomials Ψ_i is a subspace of $L^2(\Omega, P)$ and it's called the *p-th Homogenous Chaos*, the word homogenous appears since the Eq. (6.4) is built using Gaussian random variables.The coefficients c_i are called Polynomial Chaos coefficients and Ψ_i are ordered with increasing polynomial order.

All the polynomials are mutually orthogonal with regards to the Gaussian measure associated to the random variables in $\{\xi_i\}_{i=1}^{\infty}$ and it's possible to express the expectation value of U:

$$E[R] = \int_\Omega U(\xi(\omega) dP(\omega) = \int R(\mathbf{x}) p_\xi(\mathbf{x}) d\mathbf{x} \equiv \langle U \rangle \tag{6.5}$$

where $R(\xi)$ is the Polynomial Chaos representation of $R(\omega)$ and p_ξ stands for the Gaussian probability density function:

$$p_\xi(\mathbf{x}) = \prod_{i=1}^{\infty} \frac{1}{\sqrt{2\pi}} exp\left(-\frac{x_i^2}{2}\right)$$

In the case of a multivariables system the Eq. (6.4) has to be modified and the polynomials Ψ_i must be changed. Consider a collection of N random independent Gaussian variables, $\xi = \{\xi_1, \dots, \xi_N\}$ where each random variable is independent from the others

the probability density for ξ can be written as the product of the probability density for each ξ_i:

$$\mathbf{p}_{\boldsymbol{\xi}}(\mathbf{x}) = \prod_{i=1}^{N} p_{\boldsymbol{\xi}}(x_i) \tag{6.6}$$

The statement of independent variable translates the maximal uncertainty situation in the model, indeed if two variables are correlated the degree of uncertainty is smaller because the degrees of freedom for the stochastic variables are smaller.

A polynomial basis has to be associated to each random variable, so each functional in equation (6.4) is the product between the different polynomial basis, that is let Ψ_k be the k-degree polynomial, it is equal to all the combination between the polynomial basis that generate a polynomial of degree k. Starting from now the index in Eq. (6.4) will be a vector of index stating the degree of the single polynomial. So Eq. (6.4) can be rewritten as following:

$$R(\omega) = \sum_{\mathbf{i}=\vec{0}}^{\infty} c_{\mathbf{i}} \Psi_{\mathbf{i}}(\boldsymbol{\xi}) \tag{6.7}$$

In Eq. (6.7) it has been noted that the index of the summation is a vector of indices, each vector component refers to the correspondent random variable and identifies the degree of the respective polynomial.

The equation (6.4) involve an infinite collection, $\boldsymbol{\xi}_i$, of random Gaussian variables, it appears that for a practical implementation of the methods the series has to be composed by a finite number of terms, so the collection $\boldsymbol{\xi}_i$ must be truncated as well as the series in Eq. (6.4). The number of terms retained in the expansion after the double truncation at N dimensions and order p is given by:

$$L - 1 = \frac{(N+p)!}{N!p!} \tag{6.8}$$

The truncated version of a random variable U can consequently be expressed as:

$$U(\omega) = \sum_{\mathbf{i}=\vec{0}}^{L-1} c_{\mathbf{i}} \Phi_{\mathbf{i}}(\boldsymbol{\xi}) \tag{6.9}$$

The Eq. (6.8) shows how for multi-dimension system the PC expansion needs of a high number of terms already truncating the polynomials to the second or third order. Indeed if a model is described in 6-dimension space the number of terms increase rapidly with the truncated degree of the polynomials.

p	N	L-1
1	6	7
2	6	28
3	6	84
4	6	128

p	N	L-1
3	1	4
3	2	10
3	3	20
3	4	35

Tab. 6.1: Evolution of the number of terms in the series (6.9).

The fast increasing of the terms number can represent a big problem in term of computationally cost, especially where the number of realization of the deterministic model has to be equal to the terms number inside the Eq. (6.9).

6.3.2 Generalized Polynomial Chaos

Until now the discussion has been limited to only random Gaussian variables. However it is possible to generalize the idea to any probability density distribution. One could construct the polynomial expansion using a measure corresponding to any probability

law. Knowing the probability density distribution of the input data it is possible to assign it the right polynomial basis in order to generate the Polynomial Chaos basis. In the Tab. 6.2 the polynomial basis for the most important probability distribution, either continuous or discrete, are shown with their definition supports. It's generally possible

	Distribution ξ	**Polynomial basis** $\psi_k(\xi)$	**Support**
Continuos RV	Gaussian	Hermite	$(-\infty;\infty)$
	Uniform	Legendre	$[-1;1]$
	γ	Laguerre	$(0;\infty)$
	β	Jacobi	$[-1;1]$
Discrete RV	Poisson	Charlier	$\{0,1,2,\ldots\}$
	Binomial	Krawtchouk	$\{0,1,2,\ldots,n\}$
	Negative Binomial	Meixner	$\{0,1,2,\ldots\}$
	Hypergeometric	Hahn	$\{0,1,2,\ldots,n\}$

Tab. 6.2: Orthogonal polynomial basis for different kinds of probability density.

to build a Polynomials basis for any probability density function following the Gram-Schmidt orthogonalization process.

It is important to note that the multidimensional PC is composed by one dimensional basis when the random variables are uncorrelated. In this case the multidimensional polynomial is the product of each one dimensional polynomial[3]. Such construction can be useful for the propagation of multiple uncertainties in complex models, with the various random variables are linked to different source of uncertainty having different probability laws.

6.3.3 Coefficients evaluation

As Polynomial Chaos Expansion relies on orthogonal polynomials, the coefficients of expansion can be directly estimated by taking the inner product of Eq. (6.9) and the orthogonal polynomials. So to evaluate the $i-th$ coefficient the inner product between the polynomial expansion and the $i-th$ degree polynomial is taken:

$$\langle R(\mathbf{X}), \Psi_i(\mathbf{X})\rangle = \langle \sum_{j=0}^{L-1} c_j \Psi_j(\mathbf{X}), \Psi_i(\mathbf{X})\rangle = \sum_{j=0}^{L-1} c_j \langle \Psi_j(\mathbf{X}), \Psi_i(\mathbf{X})\rangle = c_i \langle \Psi_i^2(\mathbf{X})\rangle$$

$$\Rightarrow c_i = \frac{\langle R(\mathbf{X}), \Psi_i(\mathbf{X})\rangle}{\langle \Psi_i^2(\mathbf{X})\rangle} \tag{6.10}$$

The integral to compute the Eq. (6.10) numerator is evaluated using a quadrature method where the inner product is approximated as a weighted sum of the function and the orthogonal polynomial evaluated at the quadrature points $\mathbf{z}_i$ with associated quadrature weights h_i in the following manner[4]:

$$\langle R(\mathbf{X}, \Psi_i(\mathbf{X})\rangle = \int_\Omega R(\mathbf{X}, \Psi_i(\mathbf{X}) p_{\mathbf{X}} d\mathbf{x} = \sum_{k=1}^{n} h_k y(\mathbf{z}_k) \Psi_i(\mathbf{z}_k) \tag{6.11}$$

The one dimensional quadrature input designs are the roots of classical orthogonal polynomials, for the multivariate case, the input design is the tensor product of the one dimensional designs. The total number of points in the input designs is therefore $n = i^d$ for an isotropic design, where i is the polynomial degree and d is the dimension of the random parameter space.

The method outlined above relies on the total knowledge of the response R. However, in the most part of the problems, like the CFD simulations, the response is known only in a few points, therefore Eq. (6.10) can not be applied.

If the response R is known only in a few points a linear system is solved using these points, called *sampling points* $\{\mathbf{X_i}\}_0^{N_samples}$, in which the model is evaluated. A grid of points is built depending from the number of independent variables used in the expansion and an algorithm is perform to sample the points. Once the points have been sampled the model is evaluated in the points and finally it's possible generate the following linear system:

$$\begin{bmatrix} \Psi_0(\mathbf{X}_0) & \dots & \Psi_{L-1}(\mathbf{X}_0) \\ \vdots & \ddots & \vdots \\ \Psi_0(\mathbf{X}_{N_{samples}}) & \dots & \Psi_{L-1}(\mathbf{X}_{N_{samples}}) \end{bmatrix} \begin{bmatrix} c_0 \\ \vdots \\ c_{L-1} \end{bmatrix} = \begin{bmatrix} R(\mathbf{X}_0) \\ \vdots \\ R(\mathbf{X}_{N_{samples}}) \end{bmatrix} \tag{6.12}$$

The number of model evaluation is given by the equation (6.8).

6.3.4 Sampling points

As it has been explain before a sampling points grid has to be built to solve the system (6.12) and compute the coefficients. To assure a robustness the coefficients of the PCE should be independent from the choice of the sampling points. In the last part of the chapter a practical example is given in order to show this independence of the method from the sampling points, here a mathematical proof is explained.

Let $\mathbf{R}_0$ and $\mathbf{R}_1$ two response for the same system referring to two different set of sampling points, the index 0 refers to the 0-grid while the index 1 to the 1-grid. According to the PCE theory it is possible to represent the system responses through the PC expansion. Therefore Eq. (6.12) can be written for each response vector:

$$\begin{cases} A_0\mathbf{c} = \mathbf{R}_0 \\ A_1\mathbf{c} = \mathbf{R}_1 \end{cases} \tag{6.13}$$

where A_0 and A_1 are the matrix generate evaluating the polynomial basis in the two set of sampling points. Because of the sampling points independence it can be possible to map a system to the other without losing any information, so it's possible to introduce an operator that acting on one system allows to pass to the other system.

Let M be a square matrix:

$$MA_0\mathbf{c} = M\mathbf{R}_0, \quad \text{with} : \begin{cases} A_1 = MA_0 \\ \mathbf{R}_1 = M\mathbf{R}_0 \end{cases} \quad \Rightarrow \quad M = A_1A_0^{-1} \tag{6.14}$$

The matrix $M = A_1A_0^{-1}$ allows to map the approximate response using the sampling points 0 to the approximate response for the sampling points 1.

6.3.5 Statistical parameters

Let U be a random variable belonging to $L^2(\Omega, \sigma, P)$ and the expression below:

$$R = \sum_{\mathbf{i}=\vec{0}}^{L-1} c_\mathbf{i}\Psi_\mathbf{i}(\boldsymbol{\xi}) \tag{6.15}$$

is its Polynomials Chaos expansion on the orthogonal basis $\{\Psi_0, \Psi_1, \dots, \Psi_{L-1}\}$ where $\Psi_0 = 1$. So using the definition for the inner product Eq. (6.3) and for the mean value Eq. (6.5) it's possible to evaluate the expectation value of U:

$$\langle R(\xi)\rangle = \langle \Psi_0, R(\xi)\rangle = \langle \sum_{\mathbf{i}=\vec{0}}^{L-1} c_\mathbf{i}\Psi_0\Psi_\mathbf{i}\rangle = \sum_{\mathbf{i}=\vec{0}}^{L-1} c_\mathbf{i}\langle \Psi_0, \Psi_\mathbf{i}\rangle \tag{6.16}$$

Using the orthogonality of the PC, *i.e.*$\langle \Psi_i, \Psi_j \rangle = \delta_{ij} \langle \Psi_i^2 \rangle$, the mean value is equal to:

$$\langle R(\xi) \rangle = c_{\vec{0}} \langle \Psi^2_{\vec{0}} \rangle = c_{\vec{0}} \tag{6.17}$$

Therefore the first coefficient of the PC expansion represent the mean value of the random variable U.

In the same way it's possible to compute the variance, and then the standard deviation taking the variance square root, of the random variable U, so starting from the variance definition it can be written:

$$\sigma_R^2 = E[(R - E[R])^2] = E\left[\left(\sum_{i=\vec{1}}^{L-1} c_{\mathbf{i}} \Psi_{\mathbf{i}}\right)^2\right] = \sum_{i=\vec{1}}^{L-1} c_{\mathbf{i}}^2 \langle \Psi_{\mathbf{i}}^2 \rangle \tag{6.18}$$

The variance of U is given as a weighted sum of its squared PC coefficients. Similar expressions can be derived for the higher order moments of U in terms of its PC coefficients.

Finally to evaluate the variance for the model the inner product has to be solved. For the "classical" polynomial basis analytical solutions are known , AppendixB. But if the analytical solution for the inner product is unknown an other way to compute the integral is necessary,*e.g.*quadrature methods, numerical methods,....

6.3.6 Output PDF

One of the objective of the Uncertainty Quantification is also the estimation of the probability density function for the model response, because in the most of cases it is unknown. With the PCE methods is not possible to get directly this probability density function but, being a representation of the model, it's possible in indirect way. Indeed through a MonteCarlo simulation the construction of the output PDF is feasible, the input probability densities are sampled and for each successful realization the PCE is evaluated, in that way the histogram, so the output PDF, is built.

6.4 PCE in Uncertainty Quantification

As it has been mentioned before the Polynomial Chaos Expansions is a spectral method that it may be used to evaluate the uncertainty propagation in a model with less computational cost compared to the Monte Carlo methods. There are two methods of Polynomial Chaos developed so far: *intrusive method*(IPCM) and *non-intrusive method*(NIPCM).

6.4.1 Intrusive method

The intrusive method is based on the *Galerkin projection* of the original model to compute the governing equations for the Polynomials Chaos. The Galerkin projection leads to introduced a stochastic partially difference equation for the coefficients. This method requires the construction of expectations or inner products no typically employed in the deterministic codes and hence they are called *intrusive* in the sense that the existing codes must be modified. The disadvantage is the large number of partially differential equation to solve, equal to the number of coefficients, but it's favorable for the time dependent problems because it demands a less computational cost.

6.4.2 Non-intrusive method

The basic principle of non-intrusive method is to generate a polynomial approximation for the solution in the parameter space knowing the values of the solution at particular points. Therefore this method relies on a set of deterministic model representation, corresponding to some specific values of the input random variables.

Along this line, a deterministic simulation code can be used as a black box, which associates to each realization of the input parameters the corresponding model output. This "black box" idea is the most attractive feature of the method, which require only a deterministic solver and no particular adaptation of existing codes to generate the outputs. In addition it's possible to plan the needed deterministic model simulations, so they can be distributed and performed in parallel.

However, the numerical cost of non-intrusive methods essentially scales with the number of deterministic model resolutions that has to be performed, so the method becomes disadvantageous if the model is expensive to solve. Consequently the reduction of the complexity in a non-intrusive methods plays a crucial role.

In this work only the non-intrusive method are applied to quantify the CFD model uncertainty where the CFD solver is repeatedly sampled without modification to the source code.

6.5 Two simple systems

In this paragraph two simple application of the Polynomial Chaos Expansion methods are presented. In both of the cases the objective is to study how the input uncertainty described by a normal distribution, its parameters are shown in the Tab. 6.3, propagates inside two different systems: the first system is characterized by a linear behavior while the second by an exponential behavior. According with the Tab. 6.2 the Hermite polynomial basis has been employed.

Mean value	**Standard deviation**
$\mu = 4$	$\sigma = 0.5$

Tab. 6.3: Parameters of the input normal distribution.

In certain cases, depending on the characteristics of the system, it is possible to compute the output probability density function in an analytically way through the *Distribution Function Technique*. Let $\mathbf{X}$ be a continuous random variable with a distribution on a subset $S \subseteq \Re^n$ and a generic probability density function f_X and let $\mathbf{Y} = u(\mathbf{X})$ be another continuous random variable with a distribution on the subset $T \subseteq \Re^m$. In this discussion u represents the system interested.

The scope is to find the probability density function for $\mathbf{Y}$. The schema is the following:

1. Finding the cumulative distribution function:

$$F_{\mathbf{Y}}(\mathbf{y}) = \mathbb{P}[\mathbf{Y} \leq \mathbf{y}]$$

2. Differentiating the cumulative distribution function to get the probability density function:

$$f_{\mathbf{Y}}(\mathbf{y}) = \frac{dF}{d\mathbf{y}}$$

To find the cumulative distribution function it's possible to write:

$$F_{\mathbf{Y}}(\mathbf{y}) = \mathbb{P}[\mathbf{Y} \leq \mathbf{y}] = \mathbb{P}[u(\mathbf{X}) \leq \mathbf{y}] = \mathbb{P}[\mathbf{X} = u^{-1}(\mathbf{y})] \tag{6.19}$$

so using the definition of cumulative distribution the (6.19) becomes:

$$F_{\mathbf{Y}}(\mathbf{y}) = \mathbb{P}[\mathbf{X} = u^{-1}(\mathbf{y})] = \int_{-\infty}^{u^{-1}(\mathbf{y})} \mathbf{X} d\mathbf{x} \tag{6.20}$$

so (6.20) represents the cumulative distribution function for the random variable $\mathbf{Y}$.

The second step is to get the probability density function, so applying the definition the pdf for $\mathbf{Y}$ is:

$$f_{\mathbf{Y}}(\mathbf{y}) = \frac{dF}{d\mathbf{y}} = \frac{d}{d\mathbf{y}} \int_{-\infty}^{u^{-1}(\mathbf{y})} \mathbf{X} d\mathbf{x} \tag{6.21}$$

using the *Leibniz Integral rule* the following relation is introduced in order to differentiate the integral in the (6.21):

$$\frac{\partial}{\partial y} \int_{a(y)}^{b(y)} f(x,y)dx = \int_{a(y}^{b(y)} \frac{\partial f}{\partial y} dx + f\left(b(y),y\right) \frac{\partial b}{\partial y} - f\left(a(y),y\right) \frac{\partial a}{\partial y} \tag{6.22}$$

with (6.22) the pdf for Y can be evaluated:

$$f_{\mathbf{Y}}(\mathbf{y}) = \mathbf{X}\left(u^{-1}(\mathbf{y})\right) \left| \frac{d}{d\mathbf{y}} u^{-1}(\mathbf{y}) \right| \tag{6.23}$$

where the first and the third term of the Eq. (6.22) vanish because X does not dependent on $\mathbf{y}$ and X valuated at $-\infty$ is zero by definition. The absolute value is introduced as a probability density function cannot be non-positive. Finally the probability density function for Y is equal to the expression in Eq. (6.23).

Until now none assumption has been made about the shape of the system u. The only requisite needed is the possibility to evaluated the function inverse of u and it is possible if and only if u is a bijective function, that means there is a one-to-one correspondence between the domain and the codomain of u. This assumption is quite strong since it restricts the possibilities to find the output pdf to a few cases, for instance not all the polynomials are bijective and then only for some polynomial is possible to compute the inverse function.

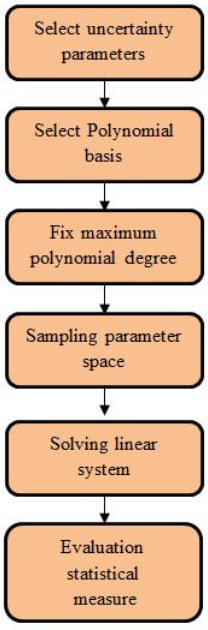

Fig. 6.2: Iterative procedure for non-intrusive PCE method.

In the next examples the equation Eq. (6.23) will be used to compute the analytical output pdf in order to compare it with the PCE results, the comparison will be done based on mean value, standard deviation and the output probability density function.

Starting from 1 the maximum degree of the polynomials have been varied up to 15 in a iterative way, for each iteration the mean value and the standard deviation have

been evaluated, so it has been possible to see the convergence rate of the method and the coefficients behavior too. In final step the output pdf's have been evaluated using a Monte Carlo method on the Polynomial Chaos Expansion.The operational schema is shown in Fig. 6.2.

For the sake of the reader the expression of the normal distribution is reminded:

$$f(x) = \frac{1}{\sigma\sqrt{2\pi}} \exp\left[-\frac{1}{2}\left(\frac{x-\mu}{\sigma}\right)^2\right] \tag{6.24}$$

6.5.1 Linear systems

The first case analyzed is a linear system described by the following equation:

$$y(x) = x \tag{6.25}$$

the system equation is bijective so applying the Eq. (6.23) the analytical solution is equal to:

$$\begin{cases} y = x \;\rightarrow\; x = y^{-1}(x) = y \\ \left|\frac{dx}{dy}\right| = 1 \end{cases} \Rightarrow\; g(y) = \frac{1}{\sigma\sqrt{2\pi}} \exp\left[-\frac{1}{2}\left(\frac{y-\mu}{\sigma}\right)^2\right]$$

In Fig. 6.3 the system behavior, the distribution of the input data and the distribution waited for the output data are represented and it's possible to see how in this case the output is only the reflection of the input data. Clearly this result is due to the linearity of the system.

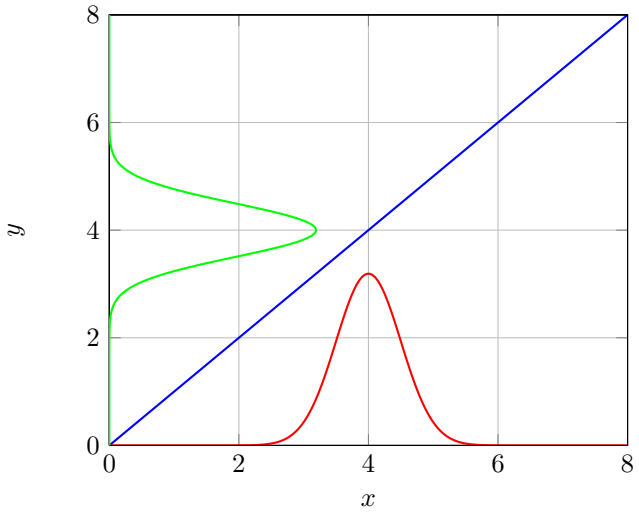

Fig. 6.3: Linear case: the system(blue), the input distribution(red) and the output distribution(green).

After choosing the polynomials basis following the procedure illustrated in Fig. 6.2 the maximum polynomial degree has been fixed as well as the sampling points. To perform the realization of the system the sampling points have been chosen in equidistant way within the support $[\mu - 1.5\sigma; \mu + 1.5\sigma]$.

Before to solve the linear system (6.12), the sampling points support must be shifted in the support interval where the orthogonality of the basis is verified. In this particular case the sampling points have to be shifted in the following support interval: $[-1; 1]$.

A Matlab script has been implemented to apply the PCE theory, the coefficients have been computed to get the mean value and the standard deviation.

The simulations have shown that at the first iteration, at which corresponds a maximum polynomial degree equal to one, the output distribution mean value and standard deviation are equal to the analytical solution. This is due to the linearity of the system.

For each iteration the output probability density function has been evaluated. To accomplish this step the PC expansion has been sampled with a simple Monte Carlo method. In Fig. 6.4 the PC expansion is plotted as well as the probability density function sampled from the PCE. The curves of the different PCE representations are

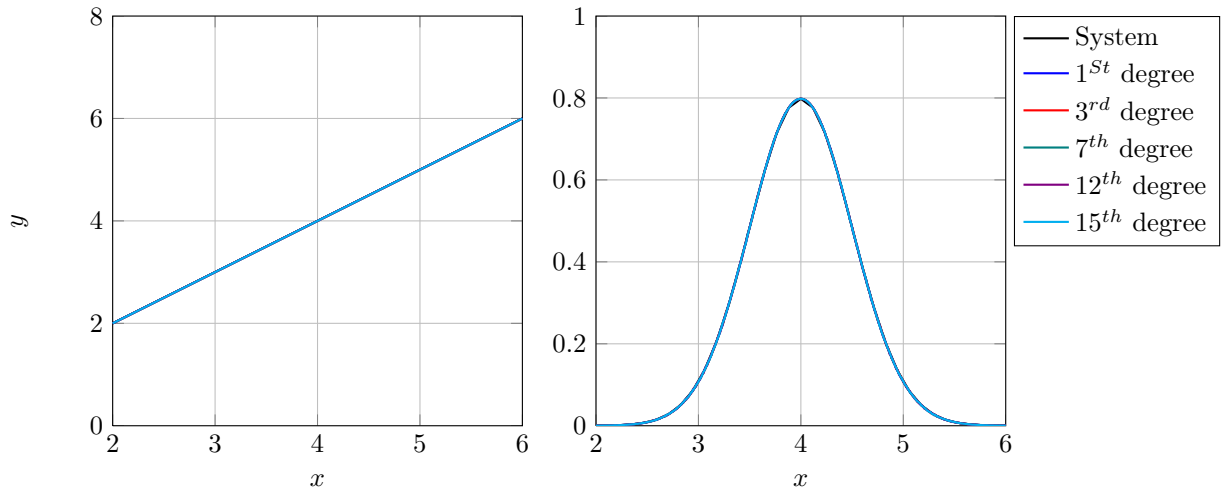

Fig. 6.4: PCE representation and PCE probability density function.

superimposed and they follow perfectly the system behavior, same remark can be made for the probability density function obtained sampling the PCE representation.

These considerations are strongly confirmed by the relative error related to the difference between analytical and PCE mean value/standard deviation. In Fig. 6.5 the relative errors are plotted in terms of percentage. The relative error is always equal to zero except

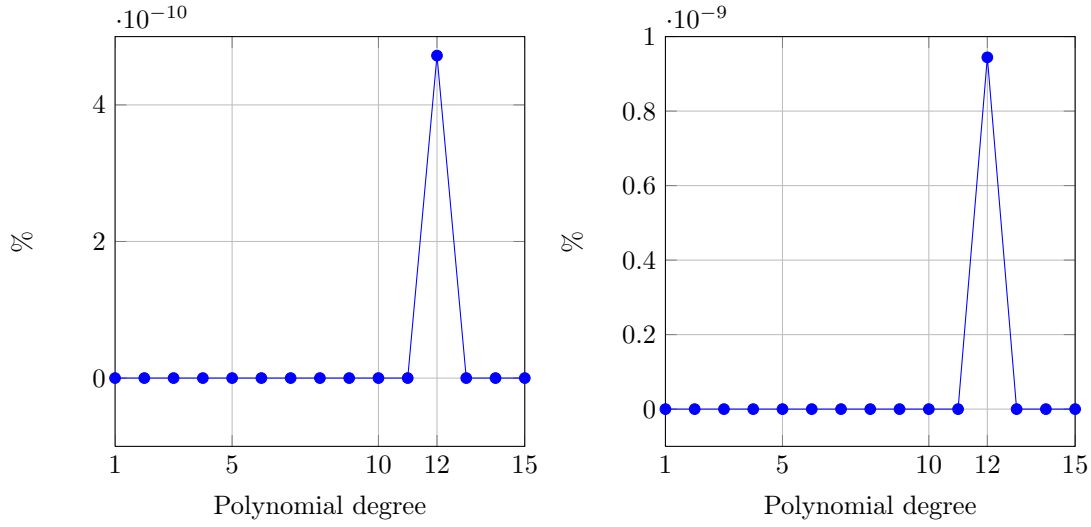

Fig. 6.5: Relative error for the PCE mean value and PCE standard deviation.

in one point but very small due to numerical issue in the coefficient computational, so it's possible to assert that the Polynomial Chaos Expansion is capable to represent a linear system without any errors.

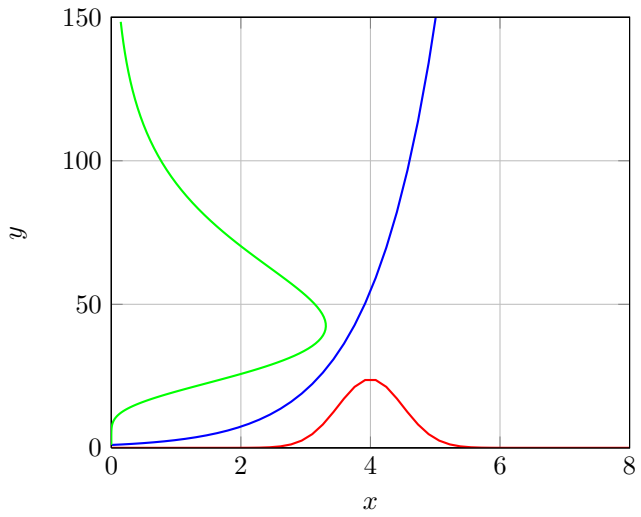

Fig. 6.6: Exponential system: the system(blue), the input distribution(red) and the output distribution(green).

6.5.2 Exponential system

The second case analyzed concerns an exponential system described by the following equation:

$$y = e^x \tag{6.26}$$

As in the linear case the system equation is bijective so the analytical solution has been computed using the (6.23):

$$\begin{cases} y = e^x \;\rightarrow\; x = y^{-1}(x) = ln(y) \\ \left|\frac{dx}{dy}\right| = \frac{1}{y} \end{cases} \quad \Rightarrow \; g(y) = \frac{1}{y\sigma\sqrt{2\pi}} \exp\left[-\frac{1}{2}\left(\frac{ln(y)-\mu}{\sigma}\right)^2\right]$$

The output distribution follows a lognormal distribution thus it has been possible to evaluate the analytical expression for the mean value and the standard deviation. In the Fig. 6.6 The applied procedure has been the same as the linear system, but this time three different cases have been performed using three different sampling points distribution in order to show the PCE independence from the sampling points:

1. Equidistant points with $\Delta x = const.$ in the symmetric support $[\mu - 1.5\sigma, \mu + 1.5\sigma]$.
2. Hermite polynomial roots as sampling points.
3. Equidistant points with $\Delta x = const.$ in the asymmetric support $[\mu - 1.5\sigma, \mu]$.

In Fig. 6.7 the mean value and standard deviation evolution are displayed for all of the three case:

The three different trends show that all of the cases reach the analytical solution, the only difference is the velocity to reach the analytical solution, indeed the asymmetric case is the slowest that reach the solution only with a maximum polynomial degree equal to 5. The other two case exhibit a faster trend and they reach the analytical solution already at the degree 2.

Such a consideration is more remarkable in the relative error plotted in the Fig. 6.8. The relative error shows the faster convergence using the polynomials roots as sampling points, anyway the relative error are very small for the three set of sampling points used and it decreases quite fast. An interesting trend is shown, increasing the maximum polynomial degree improves the relative error up to about the eleven degree, after the relative error increases because of the shape of polynomials. The Hermite polynomials become

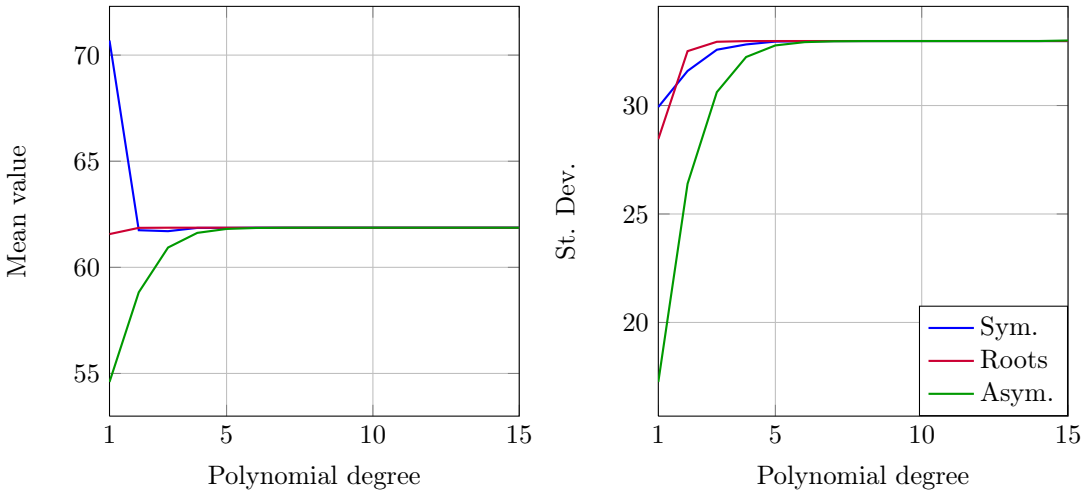

Fig. 6.7: Mean value and standard deviation trend as a function of the polynomial degree.

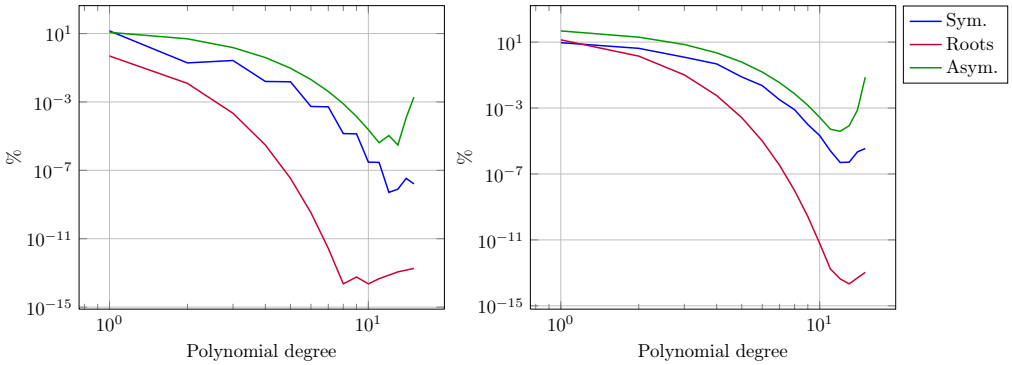

Fig. 6.8: Relative error for the mean value and standard deviation evaluated with PCE.

very oscillating at the higher degree therefore small changes in the random variables can be generate big changes in the response.

An important parameter for the stability of the solution is the *condition number* of the polynomials matrix, this indicates how much the output value of a function can change for a small change in the input argument. A big condition number means that a small change in output parameter causes a big variation of the output response. Its expression is:

$$\kappa(A) = \left\|A^{-1}\right\| \cdot \|A\| \tag{6.27}$$

The plot in Fig. 6.9 shows how the system evaluated in a asymmetric grid is more unstable compared to the other tow grids. For all the grids the conditioning number increases with the degree of the polynomials and this is due to the oscillating behavior of the polynomials that increases with the degree. Increasing the maximum polynomial degree also the oscillations of the polynomial increase, especially far away of the origin.

One of the scope of this example is to show also the independence of the PCE from the sampling points choice. Before a matrix operator has been derived, Eq. (6.14), that allows to map one response into the other using the polynomial matrix computed with the sampling points, following that idea two matrix have been computed using equation (6.14):

1. $M_{s\to r} = A_r A_s^{-1}$, this matrix maps the response of the symmetric grid, subscript s, into the response obtained with the polynomial roots, subscript r.

2. $M_{r\to a} = A_a A_r^{-1}$, this matrix maps the response of the polynomial roots, subscript

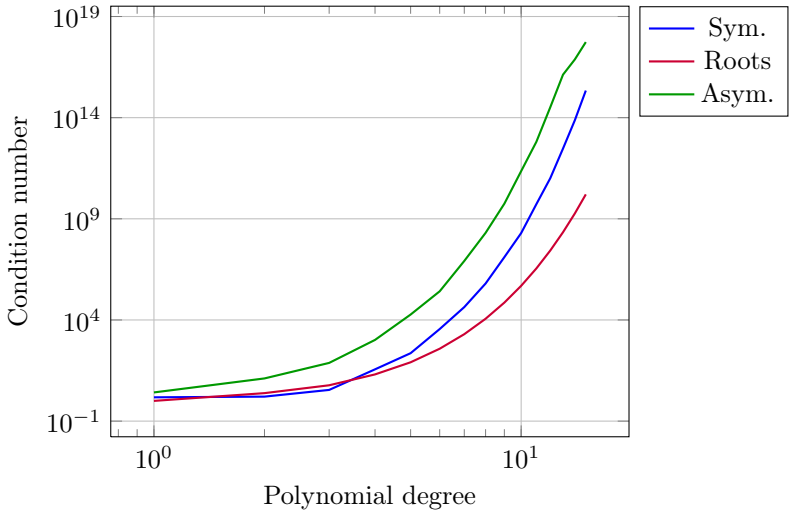

Fig. 6.9: Condition number for the three sampling grids.

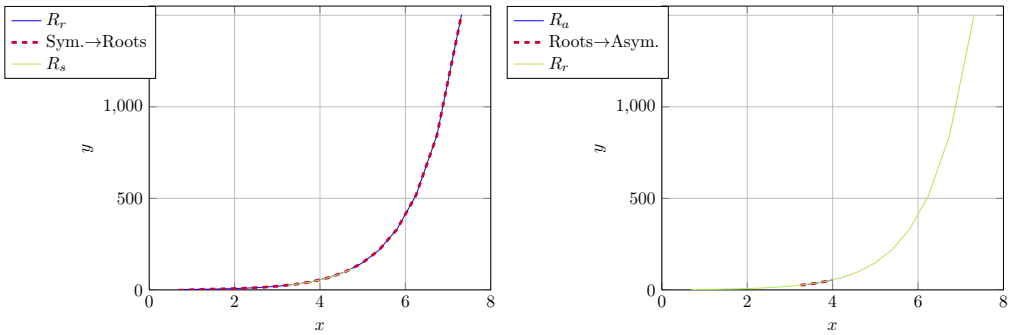

Fig. 6.10: Matrix operator M application: the green system is mapped into the red system.

r, into the response obtained with the asymmetric grid, subscript a.

As it has been done for the linear system the output pdf has been computed and the system reconstruction by Polynomial Chaos expansion too. Below the reconstruction and the output pdf are plotted for the case computed with a symmetric grid. The model reconstruction shows how improving the polynomial degree the PCE is capable to reproduce almost the exact behavior of the system, indeed using a maximum polynomial degree equals to 4 the system is completely captured by the expansion method. The same considerations can be done for the output pdf, right plot in Fig. 6.11, the amelioration in the output pdf gives to the improving of the biggest polynomial degree is remarkable, the 4^{th} degree reproduces an almost perfect lognormal distribution.

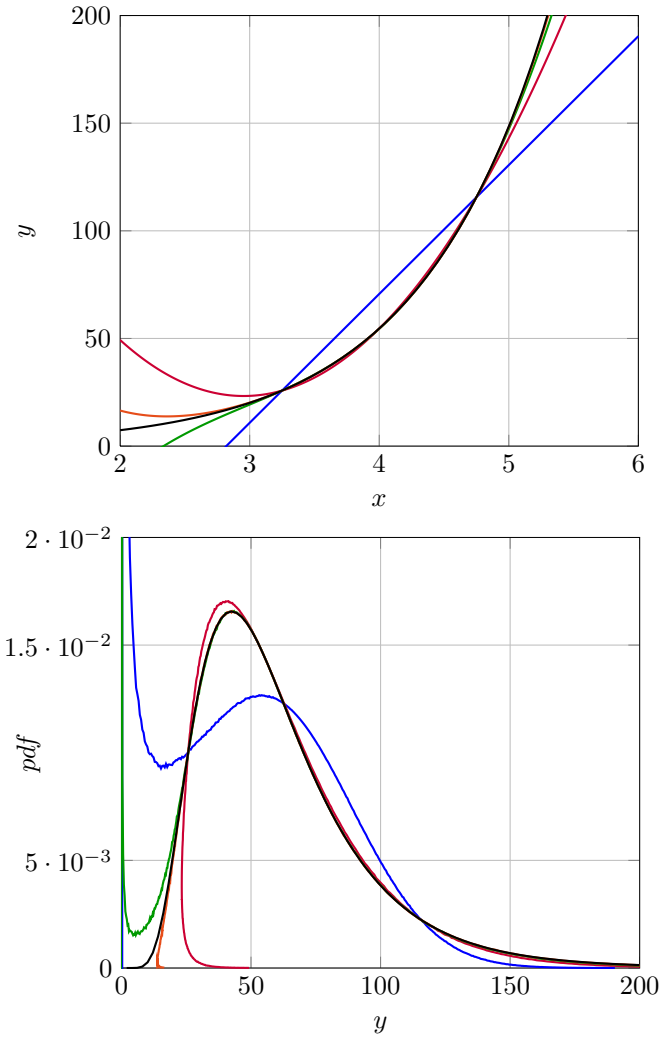

Fig. 6.11: System reconstruction and output pdf for the exponential system.

Chapter 7

Uncertainty quantification of the CFD simulations of the GEMIX test by Polynomial Chaos Expansion

In this chapter the application of the PCE method to the GEMIX experiment is presented. The first section is dedicated to the CFD simulations where the CFD mesh and simulation parameters are presented. The second section focuses on the Polynomial Chaos Expansion method, where the stochastic variables are introduced together with the Latin Hypercube sampling method, used to generate the sampling points grid. Finally in the last section the sensitivity indices, based on the Sobol indices, are introduced to conduct a sensitivity analysis of the output variables.

The CFD grid was generated using ICEM-CFD©V.15.0, a commercial software developed by ANSYS©. The CFD simulation have been performed on ANSYS FLUENT©V.14. while PCE method on a script in MATLAB©R2014a.

7.1 Computational Fluid Dynamic simulation

7.1.1 The geometry

Fig. 7.1 shows the geometry used to represent a portion of the GEMIX test. It considers $100mm$ of the conditioning section and $600mm$ of the mixing channel. Only $600mm$ length for the mixing zone has been simulated because the experimental measurement range goes from $50mm$ to $550mm$ and to avoid possible influence in the simulation from the outlet section.

7.1.2 The CFD mesh

The grid is uniform in the $x-direction$ and $z-direction$ but in $y-direction$ direction a Spline has been used to generate the grid. The peculiarity of a Spline is to generate a finer grid in specific zones in order to improve the accuracy of the numerical solution. In the case of GEMIX, turbulent mixing phenomena is more relevant in the center of the channel along the $y-direction$. For that reason a grid finer near the center line is necessary. The profile of the spline used is shown in Fig. 7.2.

The simulation results have to be independent of the grid chose so several simulation with different grids configurations have been performed in order to find the independent one, that means find the smallest grid for which increasing the number of nodes doesn't change the numerical results. All the grids used during this phase vary in the number of

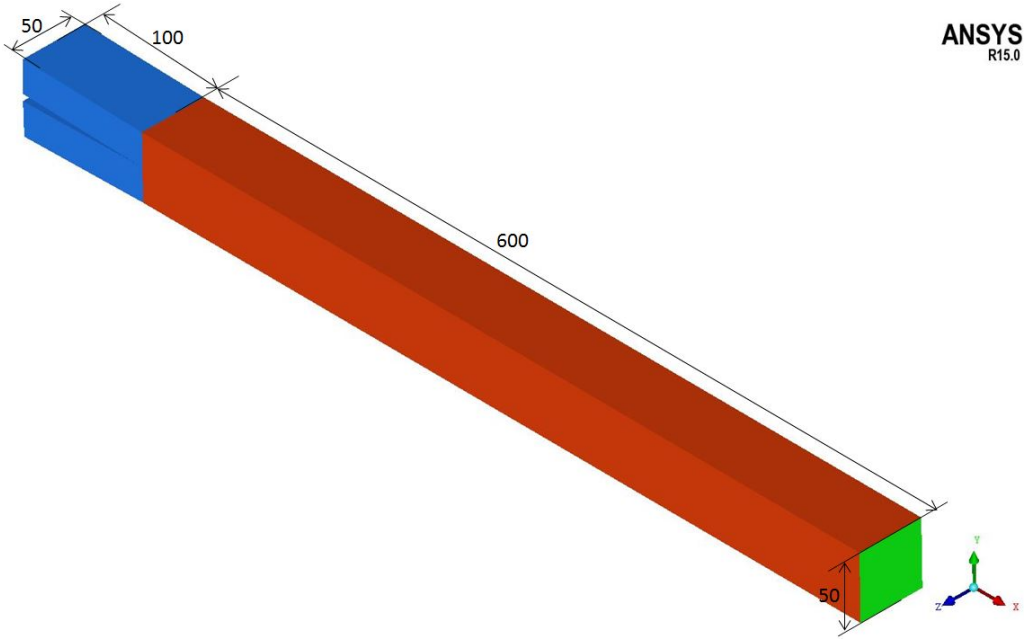

Fig. 7.1: CFD geometry for the GEMIX facility. Dimension in mm.

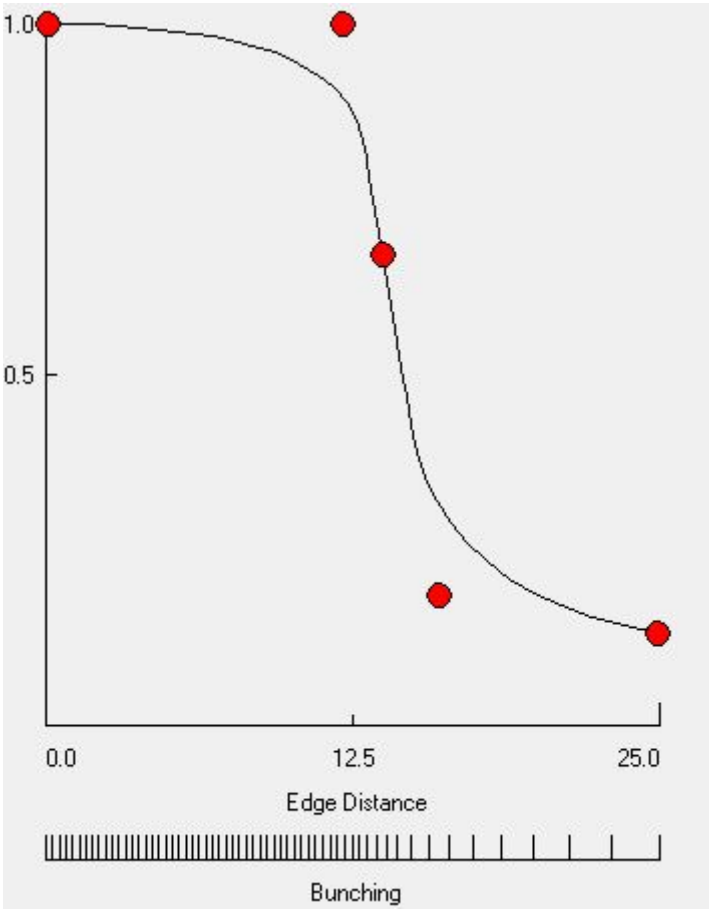

Fig. 7.2: Profile Spline for $y-direction$. The picture is a screen capture directly from ICEM-CFD

nodes in only one direction, in order to identify the most sensible one. In the Tab. 7.1 all the configurations used are summarized. For the $x - direction$ two number of nodes are given,the first one refers to the conditioning section while the second one to the mixing section. In the figures below the profile along $y - direction$ for the velocity magnitude

Simulation number	Nodes x-direction	Nodes y-direction	Nodes z-direction
I	10 50	120	30
II	20 100	120	30
III	40 150	120	30
IV	20 100	60	30
V	20 100	120	30
VI	20 100	180	30
VII	20 100	120	15
VIII	20 100	120	30
IX	20 100	120	60

Tab. 7.1: Mesh configurations used to show the grid independence.

and the turbulent kinetic energy are plotted. Two points have been chosen, one point near the splitter plate located a $x = 30mm$ and $z = 0mm$ and the second one located at $x = 400mm$ and $z = 12.5mm$. The second point has been chosen outside the midplane in order to see the influence of the grid density along the $z - direction$.

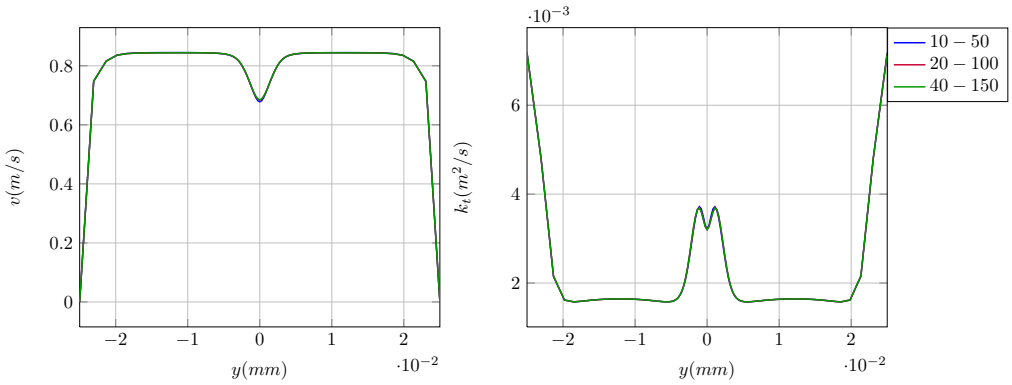

Fig. 7.3: Velocity profile and turbulent kinetic energy profile for different grids in $x-direction$ at $x = 30mm$ and $z = 0mm$

It was identified that the $y-direction$ is the most sensible to the grid density especially near the splitter plate. Nevertheless the profiles are quite close each other, the profile with 60 nodes and with 90 are practically identical, it is possible to see a very small difference near the walls but it is negligible since the difference is less than 0.1%.

The final grid has the following configuration: 120 nodes in the y-direction, 30 in the z-direction and 20-100 in the x-direction; thus it contains 425'400 nodes. That choice has been done since a lower number of nodes doesn't allow to capture properly the mixing zone. In addition a higher number of nodes increases the computational time without generating a better solution.

7.1.3 Boundary conditions

Before to start the simulations, appropriate boundary conditions must be defined to represent in a proper way the experimental conditions. In the GEMIX experiment the only

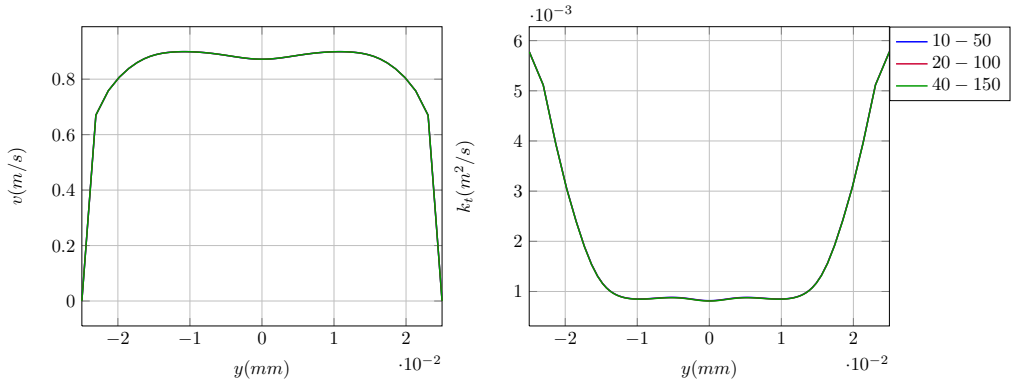

Fig. 7.4: Velocity and turbulent kinetic energy profiles for different grid sizes in $x-direction$ at $x = 400mm$ and $z = 12.5mm$

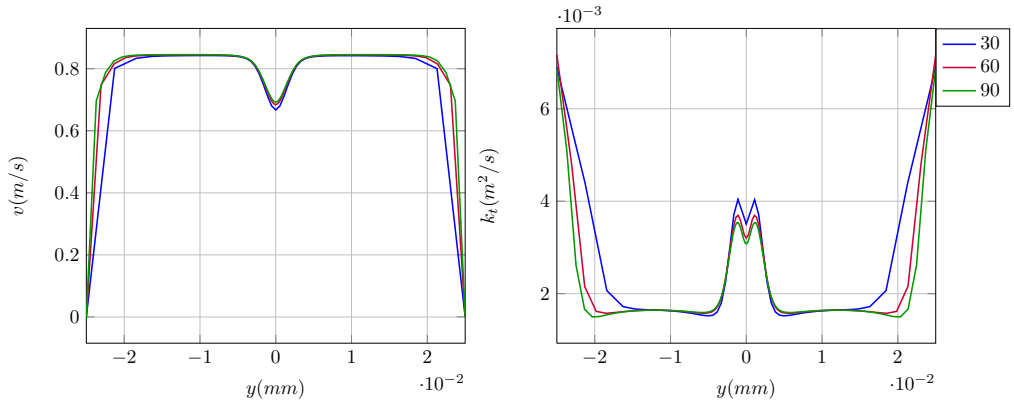

Fig. 7.5: Velocity and turbulent kinetic energy profiles for different grid sizes in $y-direction$ at $x = 30mm$ and $z = 0mm$

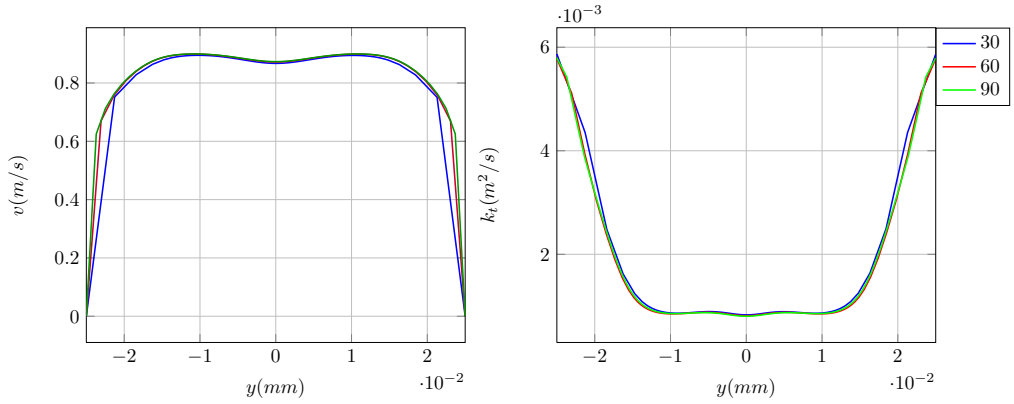

Fig. 7.6: Velocity and turbulent kinetic energy profiles for different grid sizes in $y-direction$ at $x = 400mm$ and $z = 12.5mm$

quantity known is the mass flow rate which is equal to $1kg/s$ for the present study. The presence of honey combs and grids in the conditioning section of the facility doesn't allow to know the inlet velocity profile with high accuracy, which can vary from uniform profile to fully developed turbulent flow. Because of this lack of knowledge about the

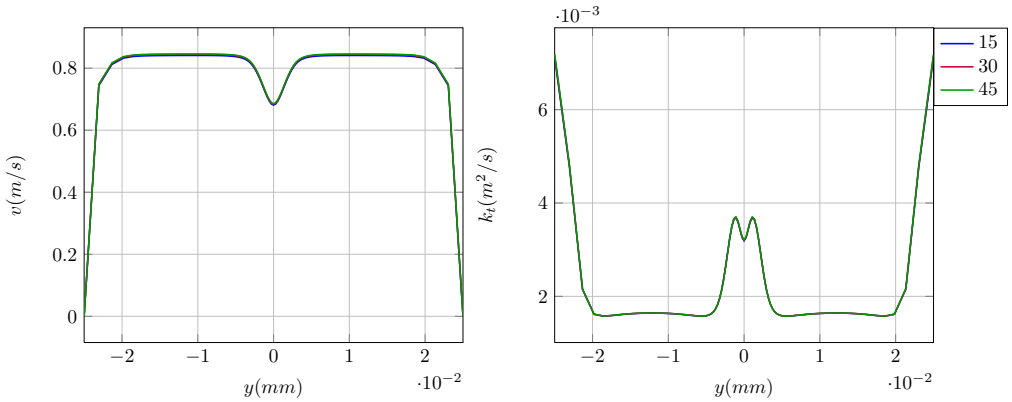

Fig. 7.7: Velocity and turbulent kinetic energy profiles for different grid sizes in $z-direction$ at $x = 30mm$ and $z = 0mm$

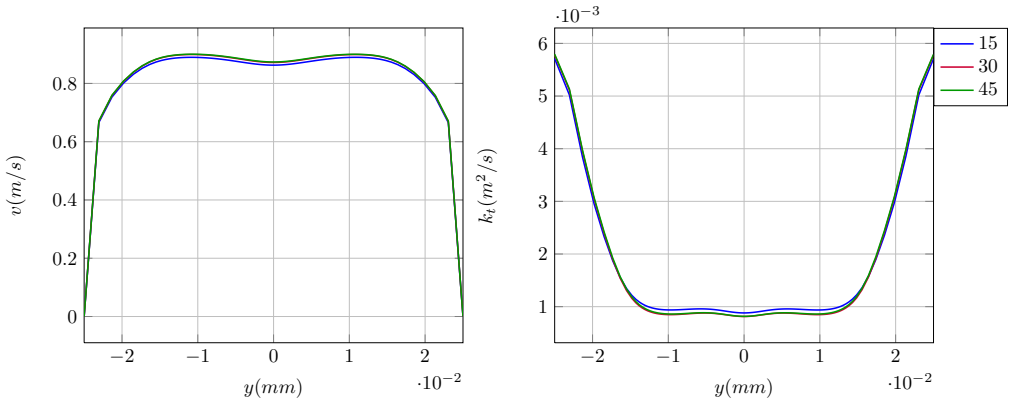

Fig. 7.8: Velocity and turbulent kinetic energy profiles for different grid sizes in $z-direction$ at $x = 400mm$ and $z = 12.5mm$

inlet boundary condition, the inlet velocity profile has been interpreted as a stochastic variable. This will be further clarified in the subsequent section.

The inlet velocity is a stochastic variable, an inlet profile velocity has to be supplied to the software to perform the simulation. The idea is to build a fully develop profile in the conditioning section using periodic boundary conditions. For this purpose a new geometry has been built representing the conditioning section upstream the inlet section of the geometry in Fig. 7.1. The upper leg has been extruded along the inlet surface normal axis for a length twice as long as the conditioning section. The extrusion has to be done also for the grid because the extruded part has to have the same grid of the principal geometry in order to be consistent in the simulation. The final geometry for the inlet condition is show in Fig. 7.9: Once the grid has been defined, the simulation with ANSYS FLUENT©V.14 is carried out and the inlet profile velocity is computed. The 3-D view of the velocity profile is shown in Fig. 7.10.

7.1.4 Scalable wall function

The behavior and structure of turbulent flows near solid wall are considerably different from those in free streams. Due to the wall presence the mean velocity is affected because the no-slip condition has to be satisfied at the wall but also the fluctuations, the turbulent kinetic energy and all the other parameters describing the turbulence. Therefore the implementation of the turbulent models close to the walls represents an important

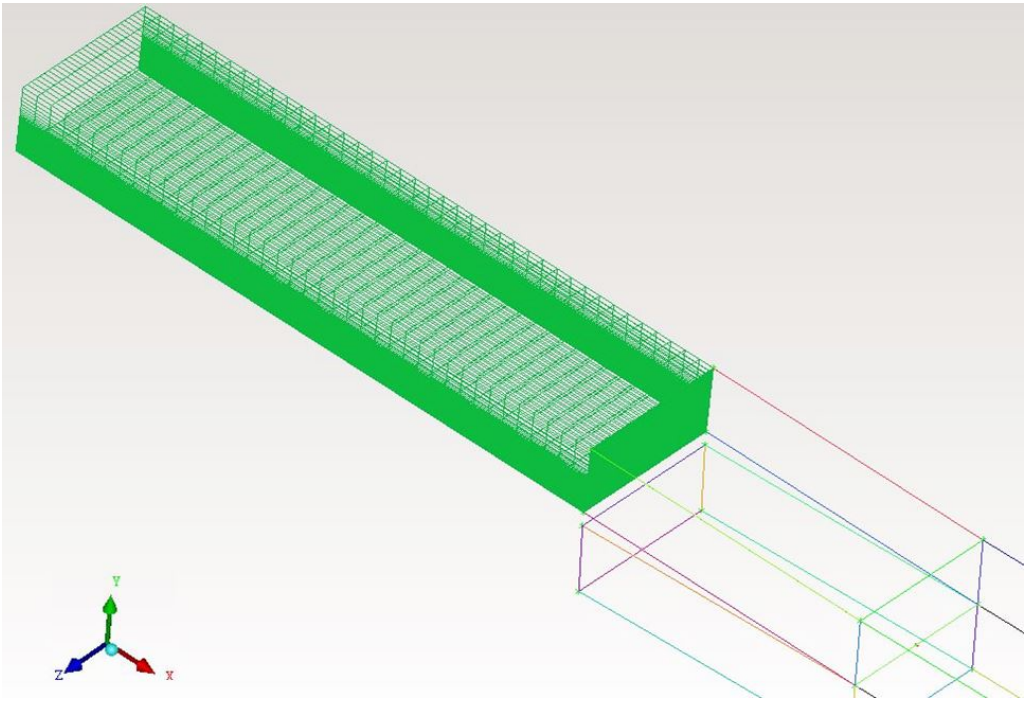

Fig. 7.9: Computational mesh used to set the inlet velocity profile.

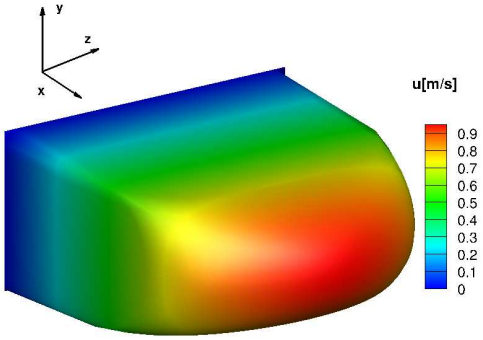

Fig. 7.10: Inlet velocity profile.

challenge.

Let us consider the flow through an horizontal pipe where the mean flow is predominantly in the axial direction and the mean velocity varying in the cross stream. Let us consider the Re number, that is the ration between the inertia forces and the viscous forces. If a Re number is formed based on a distance y away from the wall it is possible identify different situation that occur in the flow. As long as y is in the same order of L, main scale length, the Re is big a the inertia forces dominate the flow far away from the wall. Approaching to the wall the Re number based on y decrease and before that it reaches 0, on the wall, there is a zone in which the Re number is around 1. In this zone the viscous forces are equal in magnitude to the inertia forces. This zone is called *boundary layer*.

Inside the boundary layer, the viscosity and the wall shear stress are important parameters and the the velocity profile depends upon the Re number. Starting from these

quantity is possible define viscous scales for the velocity and for the lengths:

$$u_\tau = \sqrt{\frac{\tau_w}{\rho}} \tag{7.1a}$$

$$u^+ = \frac{\langle u \rangle}{u_\tau} \tag{7.1b}$$

$$y^+ = \frac{\rho u_\tau y}{\mu} \tag{7.1c}$$

Eq. (7.1a) is called *friction velocity* and it is a function of the wall shear stress. The variable y^+ is dimensionless distance from the wall, defined as a local Re number, its magnitude can reveal the relative importance of viscous forces for a given distance from the wall. In [14] a comparison between the viscous stresses and Reynolds stresses is made in function of y^+. The results show that for $y^+ = 0$ the wall shear stresses representing the total shear stress applied on the fluid and moving out from the wall the fraction of viscous stresses quickly decreases with consequent raised of the Reynolds stresses. Therefore inside the boundary layer two zone can be distinguished, the first for $y^+ < 50$ where the molecular viscosity acts on the shear stress, the second for $y^+ > 50$ where the shear stress is due mostly to the Reynolds stresses. Therefore a law that links the two zones is necessary. This bridge is realized by using a *wall function*:

$$u^+ = f_w(y^+) \tag{7.2}$$

The first region, $y^+ < 50$, can be subdivided into others three zone following the importance of the wall shear stress on the total shear stress:

- **Viscous sublayer**, $y^+ < 5$: in this region the mean velocity profile is determined by the viscous scales. In this zone the wall function is:

  $$u^+ = y^+ \tag{7.3}$$

  This function is an excellent approximation until $y^+ < 12$, after this limit the departures from the linear relation are significant.

- **Buffer layer**, $5 < y^+ < 30$: it identifies the transition zone between the viscosity dominated and the turbulence dominate parts of the flows.

- **Log-law region**, $y^+ > 30$: in this zone the Reynolds stresses start to be prevalent on the wall stresses. In this region the wall function is given by:

  $$u^+ = \frac{1}{\kappa} \ln(y^+) + B \tag{7.4}$$

Equation (7.4) is called *log law* and it is due to von Karman[32], where $\kappa = 0.41$ is the Von Karman constant and a constant equal to 5.2.

In the simulations performed in this work a *Scalable Wall function* has been used, this approach doesn't solve the turbulent model in the viscous sublayer and buffer layer but, using the log-law, it builds a link between the wall and the fully turbulent region. The scalable wall function avoid the deterioration of standard wall functions under grid refinement below $y^+ < 11$. The purpose of this function is to force the usage of the log law in conjunction with the standard wall function approach. This is achieved by introducing a new definition for y^+[10]:

$$y^{+^*} = max(y^+, y^+_{limit}), \quad \text{with } y^+_{limit} = 11.225 \tag{7.5}$$

Using the wall function approach avoid to modify the turbulent model because near the wall where the model $k - \varepsilon$ loses its validity due to the low Re number. Furthermore the wall function makes the velocity profile symmetric in the inlet flow section, without the scalable wall function the profile would be asymmetric because of the different size of the grid between the zone near the splitter plate and the zone near the wall.

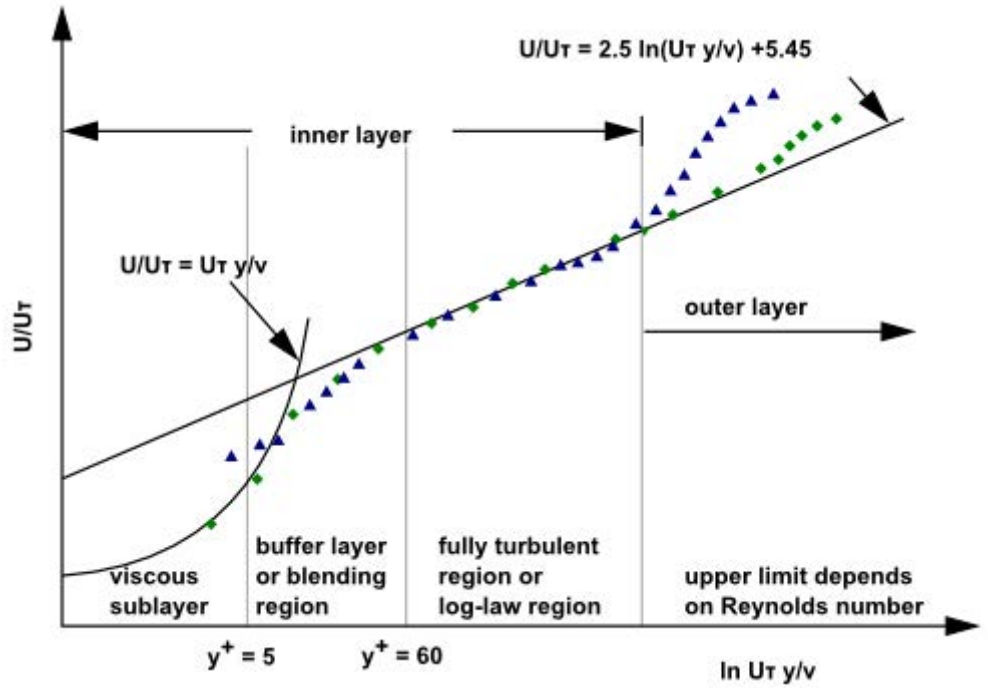

Fig. 7.11: Subdivision of near wall region[10].

7.1.5 Simulation model

All the simulations have been performed using ANSYS FLUENT©V.14, a commercial CFD package using the standard $k-\varepsilon$ turbulence model. The model coefficients have been treated as stochastic variables in order to evaluate the uncertainty simulation coming from the turbulent model. In addition a scalable wall functions were used to calculate the velocity field at the splitter plate where y^+ is around 10. The SIMPLE algorithm has been used for linking the momentum and the mass conservations equations and to calculate the advection terms for all the variables a second order upwind scheme has been used. Water at 23° and with density equal to $992kg/m^3$ has been considered for both of inlet legs.

One of the variables of interest is the concentration of the water in the mixing zone, therefore an equation for the species concentration has to be solved, together with the turbulent model. The turbulent transport of the concentration field is controlled by the *Turbulent Schmidt Number* defined as the ratio between the eddy viscosity and the eddy diffusivity of the fluid. This parameter was also considered as stochastic variable.

7.1.6 Concentration equation

In turbulent mixing one of the crucial parameters is the species concentration within the mixing zone, for that reason one of the goals of the GEMIX experiment is to measure the concentration field and elucidate its turbulent transport mechanism. To reproduce in a proper way the experimental results, a concentration equation has to be solved to get the concentration field inside the mixing channel.

Starting from the continuity equation an equation for the species concentration can be derived. The continuity equation in according with the experiment condition states:

$$\frac{\partial \rho}{\partial t} + \nabla \cdot \mathbf{J} = 0 \tag{7.6}$$

where $\mathbf{J}$ represents the species flux across the control surfaces and it can be expressed as:

$$\mathbf{J} = \rho \mathbf{u} + \mathbf{J}_D \tag{7.7}$$

therefore the continuity equation becomes:

$$\frac{\partial \rho}{\partial t} + \nabla \cdot (\rho \mathbf{u}) = -\mathbf{J}_D \tag{7.8}$$

The term $\mathbf{J}_D$ is the diffusive flux.

The density is considered to a be a function of:

$$\rho = \rho(\mathbf{x}, t, T, p, c_1, c_2, \cdots, c_i, \cdots, c_N)$$

where c_i identifies the i-th specie concentration. If the density only changes with the concentration then the time and spatial density derivative can be rewritten for the i-th specie:

$$\frac{\partial \rho}{\partial t} = \frac{d\rho}{dc_i}\frac{\partial c_i}{\partial t} \tag{7.9a}$$

$$\nabla \rho = \frac{\partial \rho}{\partial c_i}\nabla c_i \tag{7.9b}$$

Introducing Eq. (7.9a) and (7.9b) inside the equation (7.8) one gets the following equation:

$$\frac{\partial \rho}{\partial c_i}\frac{\partial c_i}{\partial t} + \rho \nabla \cdot \mathbf{u} + \mathbf{u} \cdot \frac{\partial \rho}{\partial c_i}\nabla c_i = \nabla \cdot \mathbf{J}_{D_i} \tag{7.10}$$

Using the incompressibility assumption, that means $\nabla \cdot \mathbf{u} = 0$, and developing all the mathematical steps the final shape of equation (7.10) is:

$$\frac{\partial c_i}{\partial t} + \mathbf{u} \cdot \nabla c_i = -\frac{1}{d\rho/dc_i}\nabla \cdot \mathbf{J}_{D_i} \tag{7.11}$$

Therefore one obtains a system of partial differential equations, one for each species in the fluid, where the concentration must satisfy:

$$\sum_i^N c_i = 1 \tag{7.12}$$

Using the Fick's law is possible to write an expression for the diffusion flux:

$$\mathbf{J}_{D_i} = -D\nabla c_i \tag{7.13}$$

substituting Eq. (7.13) inside equation (7.11) and applying the Reynolds average, defined in RANS equations, the diffusion flux becomes:

$$\mathbf{J}_{D_i} = -\left(D_i + \frac{\nu_T}{Sc_T}\right)\nabla c_i \tag{7.14}$$

In the equation (7.14) two diffusion coefficient appear, D_i is the mass diffusion coefficient, while ν_T/Sc_T represents the turbulent diffusivity, the diffusion fluctuation. In the latter term the *Schmidt number* has been introduced, which is defined as the of the eddy viscosity ν_T and the mass diffusivity. This number can reveal which phenomenon among mass diffusivity or turbulence prevails. In Fig. 7.12 the concentration fields for different Sc_T numbers are plotted. An important remark is that the turbulent mixing layer thickness is inversely proportional to Sc_T.

7.2 PCE application

The aim of this work is to quantify the uncertainty in CFD simulations of turbulent mixing. The sources of uncertainty include the boundary conditions and the coefficients of the $k - \varepsilon$ turbulent model. The Polynomial Chaos Expansion has been applied to three variables, concentration, turbulent kinetic energy and the velocity $x - component$, to evaluate their final uncertainty. For each variable of interest a mean value and a standard deviation is computed in each mesh nodes allowing the building of mean values profile and, through the standard deviations, error bars.

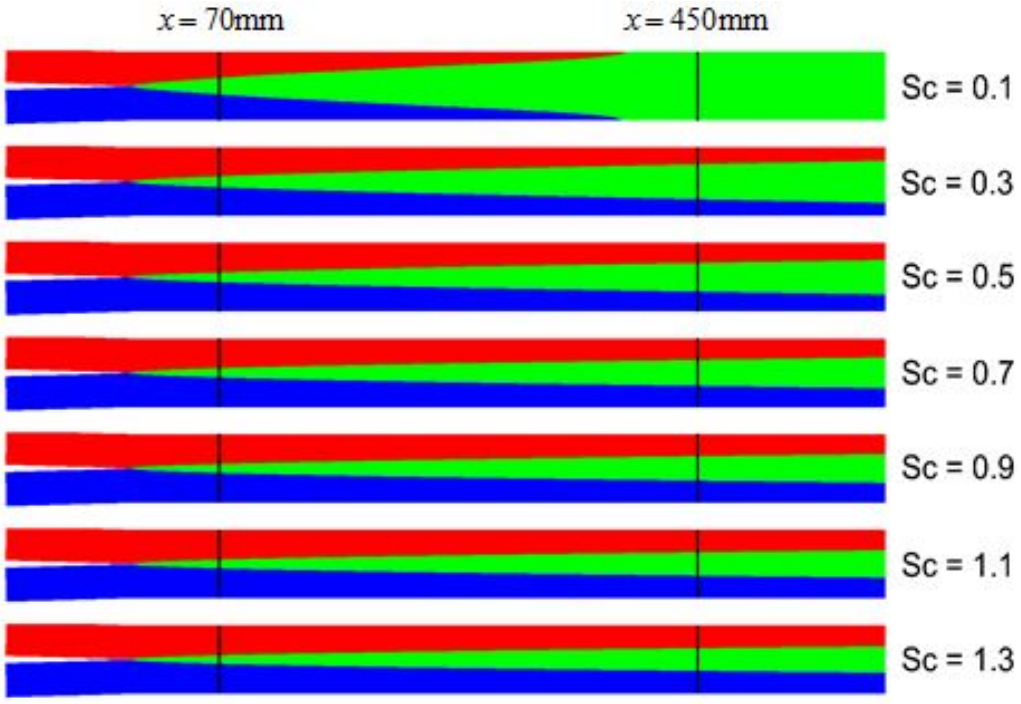

Fig. 7.12: Influence of the Sc_T number on the shape of the mixing layer[3].

7.2.1 Stochastic variables

In order to apply the Polynomial Chaos Expansion, seven quantities have been chosen as stochastic variables, two coming from the boundary conditions and two coming from the turbulence model. For each stochastic variable a probability density function has been associated.

The first variable analyzed is the inlet boundary condition. None information about the shape of the profile is known. The presence of grids and honey comb in the conditioning section makes the shape of velocity profile uncertain at the location selected as inlet in the present work. For this reason the velocity profile has been parametrized and assumed to be in between a fully turbulent developed and a uniform velocity profile. The shape of the velocity profile is given by the combination of a uniform u_u and a fully developed turbulent u_d profile in the following manner:

$$u(y,\alpha) = \left(\frac{\alpha}{u_d(y)} - \frac{1-\alpha}{u_u} \right)^{-1} \tag{7.15}$$

where α is a random parameter that varies from 0 and 1. The shape of the velocity profile for $\alpha = 1$ and for $\alpha = 0$ is shown in Fig. 7.13. A *uniform probability density* distribution has been assigned to the parameter α, this choice reflects the lack of information about the inlet velocity profile, through this probability density function is assumed that all the velocity profiles are possible. The second variable analyzed concerns the inlet boundary conditions too, it is the turbulent intensity. The turbulent intensity is defined as:

$$\beta = \sqrt{\frac{2k_T}{3\bar{\mathbf{u}}}} \tag{7.16}$$

where k_T is the turbulent kinetic energy while $\bar{\mathbf{u}}$ is the velocity mean value.

This quantity at the inlet of the GEMX experiment depends on how the honey combs and grids are arrayed in the inlet channels. From a mathematical point of few this variable is bounded to the interval $[0; +\infty)$ but experimental values higher than 20% are unlikely

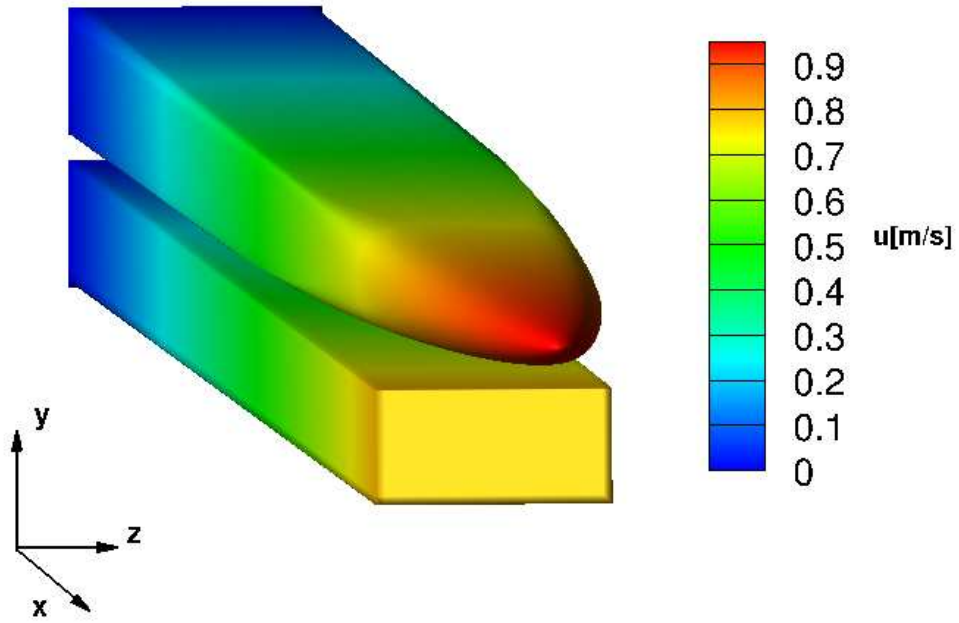

Fig. 7.13: Velocity profile for $\alpha = 1$(upper leg) and for $\alpha = 0$(bottom leg)

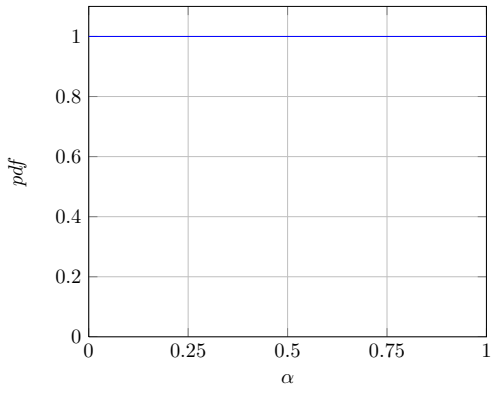

Fig. 7.14: Uniform distribution for α.

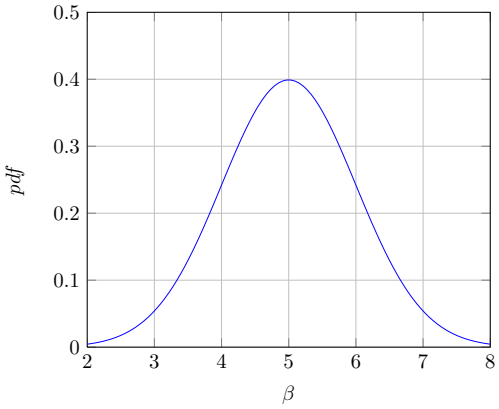

Fig. 7.15: Normal distribution for β.

for this type of confined flows. To estimate its value, an empirical correlation given for pipe flows has been used:

$$\beta = 0.16Re^{-1/8} \tag{7.17}$$

The Reynolds number for the current flow conditions is $Re = 40000$. This leads to a value for $\beta = 5\%$, which is consistent with the measured values in the mixing section. However, the precise value for β id not known at the inlet of the simulation domain and consequently, a probability density function has also been assigned to this parameter to account for its uncertainty in the simulation. The turbulent intensity has been mapped with a normal distribution centered in a mean value $\mu = 5\%$ and a standard deviation $\sigma = 1$. The choice of the distribution and its parameters translates the confidence in the value given by Eq. (7.17).

The other stochastic variables chose are the empirical coefficients used in the $k - \varepsilon$ model. The model presents five empirical coefficients($C_\mu, C_{\varepsilon 1}, C_{\varepsilon 2}, \sigma_\kappa$ and σ_ε) but only four of them have been considered stochastic variables. The $C_{\varepsilon 1}$ coefficient can be expressed as a function of $C_{\varepsilon 2}$[22]:

$$C_{\varepsilon 1} = \frac{C_{\varepsilon 2}}{2.1} + \frac{1.1}{2.1} \tag{7.18}$$

Equation (7.18) expresses a linear relation between $C_{\varepsilon 1}$ and $C_{\varepsilon 2}$. Therefore only $C_{\varepsilon 2}$ was considered to be a random variable. Nevertheless when sampling $C_{\varepsilon 2}$, $C_{\varepsilon 1}$ was varied according equation (7.18).

In [17] the values for the model coefficients are indicated and these values have been used in the probability density function for the coefficients. For each coefficient a normal distribution centered in the conventional values have been assigned while for the standard deviation for C_μ, $C_{\varepsilon 2}$ and σ_κ are taken from [8].

The last coefficient analyzed was σ_ε, the *Turbulent Prandtl Number* for the dissipation ε. It contributes to compute the total diffusion coefficient for the turbulent kinetic dissipation in the $k - \varepsilon$ model. As it appears as a consequence of the Reynolds average, it engulfs the fluctuation velocity correlation of order higher than two. In [25] and [22] σ_ε is written as a function of the others coefficients:

$$\sigma_\varepsilon = \frac{\kappa^2}{\sqrt{C_\mu}(C_{\varepsilon 2} - C_{\varepsilon 1})} \tag{7.19}$$

then σ_ε is a function of two stochastic variables,σ_κ and $C_{\varepsilon 2}$, being κ the von Karman constant, set to 0.4187 in FLUENT. Following Eq. (7.19) the coefficient σ_ε varies non-linearly with C_μ and $C_{\varepsilon 2}$. Plotting σ_ε as a function of C_μ and $C_{\varepsilon 2}$,Fig. 7.16, one sees that within the support interval for C_μ and $C_{\varepsilon 2}$, σ_ε behaves almost linearly. The linear relation allows to state that σ_ε varies following the same distribution of C_μ and $C_{\varepsilon 2}$,

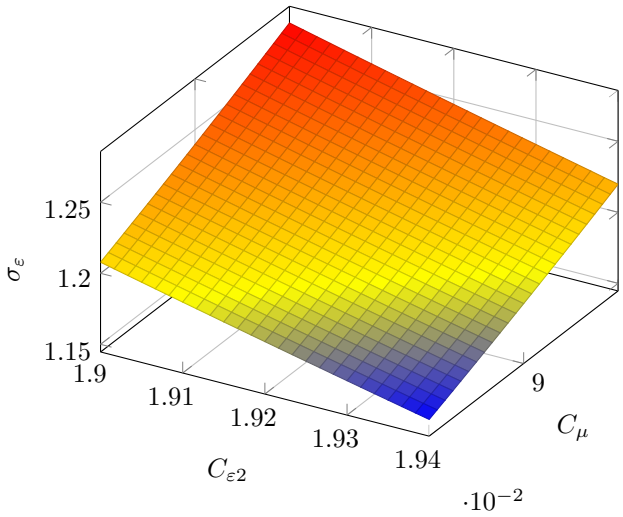

Fig. 7.16: σ_ε response surface for Eq. (7.19)

therefore it has assumed that σ_ε is described by a normal distribution. To understand which parameter introduces more uncertainty, a distribution for C_μ and $C_{\varepsilon 2}$ has been constructed using the following relations:

$$C_\mu = f_1(\langle C_{\varepsilon 2}\rangle, \sigma_\varepsilon) = \frac{\kappa^4}{\sigma_\varepsilon^2 \left(\frac{1.1}{2.1}\right)^2 (\langle C_{\varepsilon 2}\rangle - 1)^2} \tag{7.20a}$$

$$C_{\varepsilon 2} = f_2(\langle C_\mu\rangle, \sigma_\varepsilon) = 1 + \frac{\kappa^2}{\sigma_\varepsilon \sqrt{\langle C_\mu\rangle} \frac{1.1}{2.1}} \tag{7.20b}$$

where $\langle C_{\varepsilon 2}\rangle$ and $\langle C_\mu\rangle$ are the respective mean value. In Fig. 7.17 the two distributions

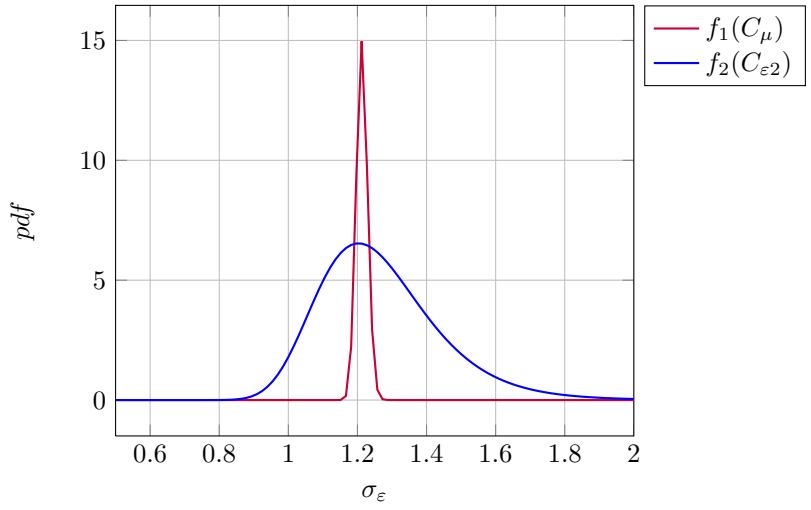

Fig. 7.17: Distributions for σ_ε.

show a mean value almost equal but a shape quite different. Indeed the distribution f_1 is sharper than f_2, that means smaller standard deviation, than f_2, then one can argue that varying σ_ε with f_1 implies less uncertainty compared to f_2. Therefore in a conservative spirit the distribution $f2$ has been associated to σ_ε.

The last stochastic variable is the Turbulent Schmidt number. For this dimensionless

number, there is no information coming from the experiment. The most conventional value found in literature for water is 0.7, also in FLUENT the standard value is 0.7[10]. A normal distribution with mean value of 0.7 and standard deviation of 0.1 has been attributed to this parameter. Finally there are an amount of seven stochastic variables, all of them are used to realized the polynomial chaos expansion for the concentration. For turbulent kinetic energy and the velocity the Sc_T number has not been employed since it concerns only the concentration and it would be unphysical taking account of it for kinetic energy and velocity . In the Tab. 7.2 the stochastic variables used are summarized with their probability density distribution and the respective Polynomial Chaos basis.

Uncertain unknown	**Probability distribution**	**Distribution parameters**	**Polynomial basis**
α	Uniform	$\mu = 0.5$, $\sigma = 8.33 \times 10^{-2}$	Legendre
β	Normal	$\mu = 5$, $\sigma = 1$	Hermite
C_μ	Normal	$\mu = 0.09$, $\sigma = 2.4 \times 10^{-3}$	Hermite
$C_{\varepsilon 2}$	Normal	$\mu = 1.92$, $\sigma = 1.174 \times 10^{-1}$	Hermite
σ_κ	Normal	$\mu = 1$, $\sigma = 1.67 \times 10^{-2}$	Hermite
σ_ε	Normal	$\mu = 1.23$, $\sigma = 0.1661$	Hermite
Sc_T	Normal	$\mu = 0.7$, $\sigma = 0.1$	Hermite

Tab. 7.2: Random variables with their probability density distribution.

7.2.2 PCE model

Once defined the stochastic variables, we must select the highest polynomial degree in the PC expansion. In the present work a degree equals to 3 has been taken as the maximum degree of the expansion. This choice seems reasonable after the results for the exponential case shown in the chapter 6. In fact, expansion truncated at the third order shows a good agreement with the analytical solution. Since the non-linearity of the exponential function is higher than the one expected from the CFD simulations, an expansion truncated at the third order provides a good compromise between computational cost and numerical accuracy.

The last step to compose the summation in Eq. (6.9) is determining the number of terms needed to compose it. Using the equation (6.8) it comes out that for the concentration 120 terms while for the turbulent kinetic energy and the velocity only 84 terms are required. This discrepancy of terms number is due to the different random variable numbers used to describe each variable of interest. Indeed for turbulent kinetic energy and velocity the Turbulent Schmidt number is not required, since this parameter describes a concentration diffusion therefore it is completely uncorrelated with the turbulent kinetic energy and the velocity.

Finally three algebraic system, as which one in equation (6.12) are generate:

$$\mathbf{R}_c(\mathbf{x}_s) = A_1 \mathbf{c}_c \tag{7.21a}$$

$$\mathbf{R}_{TKE}(\mathbf{x}_s) = A_2 \mathbf{c}_{TKE} \tag{7.21b}$$

$$\mathbf{R}_u(\mathbf{x}_s) = A_2 \mathbf{c}_u \tag{7.21c}$$

where the three vectors $\mathbf{R}_c$,$\mathbf{R}_{TKE}$,$\mathbf{R}_u$ are the deterministic FLUENT simulations, the vectors $\mathbf{c}_c$,$\mathbf{c}_{TKE}$ and $\mathbf{c}_u$ are the coefficients vectors for each output variable and the two matrix A_1 and A_2 are built using the polynomial basis evaluated in the sampling points. The two matrix are different, indeed A_1 is a square matrix 120×120, number of simulations times the number of terms, while A_2 is a rectangular matrix 120×84. Therefore a determined algebraic system is solved for the concentration while one overdetermined algebraic system is solved for turbulent kinetic energy and an other one for the velocity.

Before to build the polynomial matrix the sampling points have to be rescaled in the orthogonal space in which each polynomial basis is defined.

7.2.3 Sampling points via Latin Hypercube simulation

To sample the parameter space the *Latin Hyepercube Sampling* method(LHS) has been employed. Although the sampling points can be generated with other methods, *e.g.*collocation method, uniformo distribution,..., the LHS technique enables to sample the parameter space homogeneously.

The LHS method is the generalization of a *Latin square* to an arbitrary number of dimensions. A Latin square is a $n \times n$ array filled with n different values, each occurring exactly once in each row and exactly once in each column. Therefore in a Latin Hypercube each sample appears once in each hyperplane containing it. The big advantage of this method is that the sample space is sampled in a homogeneous way and each sampling point is completely uncorrelated from all the others.

Before to show how the method has been applied, a simple two dimensional example is presented to clarify the main ideas of the LHS method. Let be x_1 and x_2 two random variables defining the sample space where each variable is described by a uniform distribution. Let assume that the variables are bounded, $x_1 \in [0; 1]$ and $x_2 \in [3; 4]$, then the support interval is $[0; 1] \times [3; 4]$. To generate 11 sampling points in the parameter space, 11 points for each variable are considered. The points chosen belong to the probability law associated to the parameter. In this case being uniform law 11 equidistant points are considered. A sampling points is defined by two coordinates, thus applying the idea that a coordinate can be used only one time the sampling points grid is generated.In Fig. 7.18 in the left plot the sample space is shown while in the right plot the sampling points generated are shown, the random points covers almost the whole space and especially there is no superposition of the points so each point captures a different portion of the space.

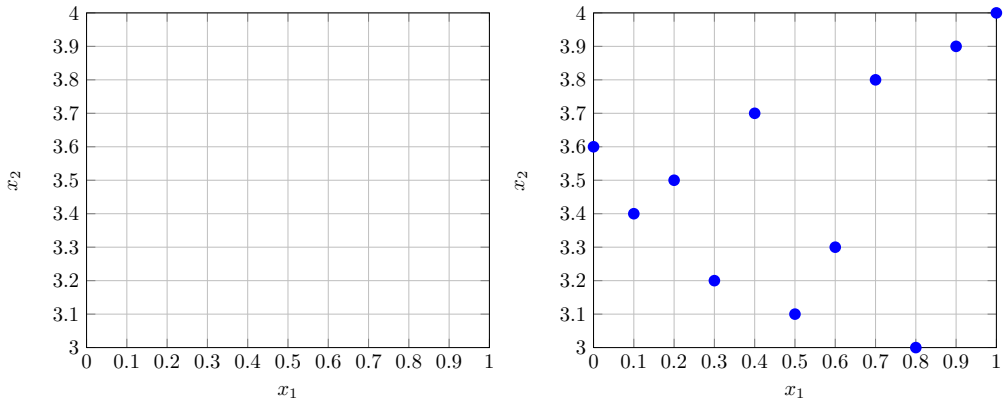

Fig. 7.18: Sample space(left) and sampling points(right).

As mentioned in the previous section at least 120 sampling points are required. In order to show the independence of the PCE from the sampling points choice two grids of points have been built, one symmetric and an other asymmetric:

- **Symmetric distribution**: for each random variable 120 points have been considered in a symmetric support respect to the mean value. The support is defined as $[\mu - 1.5\sigma; \mu + 1.5\sigma]$.
- **Asymmetric distribution**: for each random variable 120 points have been considered in the following support $[\mu - 1.5\sigma; \mu]$.

In Fig. 7.19 and Fig. 7.20 the symmetric and asymmetric grids are shown. In the asymmetric grid the fact that only the distribution below the mean value has been sampled

is well visible.

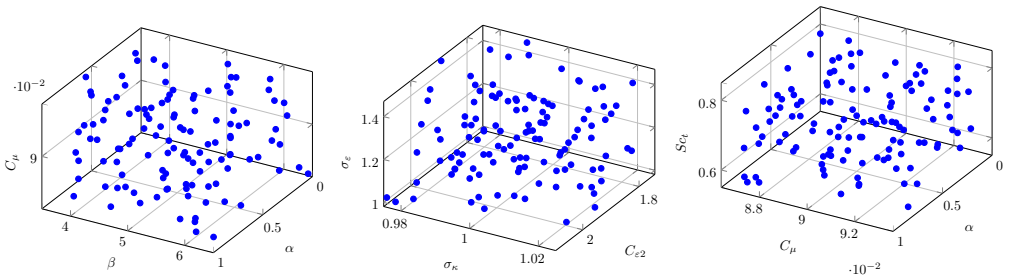

Fig. 7.19: LHS for the symmetric grid.

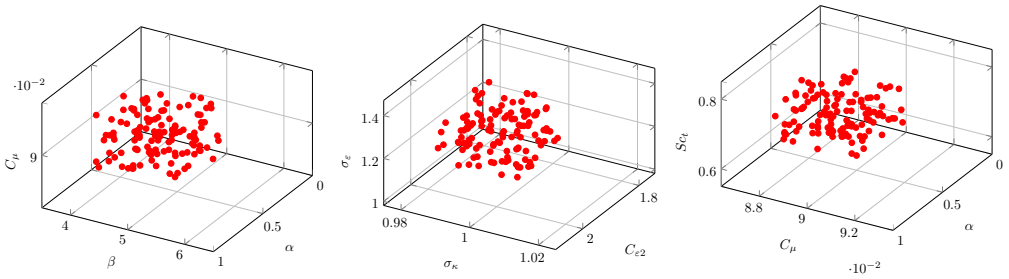

Fig. 7.20: LHS for the asymmetric grid.

7.3 Sensitivity analysis

The objective of sensitivity analysis is to identify the relative contribution of individual random variables to the global uncertainty.

In this work a sensitivity analysis is carried out to establish the dominant random variable, α, β, C_μ,..., on the total variance. To accomplish this the Sobol decomposition is employed. This technique is a variance method decomposition which computes sensitivity indices for each output parameter measuring the influence of an specific input parameter on the output parameter.

7.3.1 Sobol Indices

Considering a model represented by:

$$\mathbf{R} = f(\mathbf{X}) \tag{7.22}$$

where $\mathbf{R}$ is the model response and $\mathbf{X}$ is the input vector variables. The model response $\mathbf{R}$ can be represented by a Polynomial Chaos Expansion:

$$\mathbf{R} = \sum_{\mathbf{k}=\bar{0}}^{L-1} c_{\mathbf{k}} \mathbf{\Psi}_{\mathbf{k}} \tag{7.23}$$

and its variance can be written as:

$$D = \sum_{\mathbf{k}=\bar{1}}^{L-1} c_{\mathbf{k}}^2 \langle \Psi_{\mathbf{k}}^2 \rangle \tag{7.24}$$

It is possible to regroup the summation terms in Eq. (7.23) using a *Sobol Decomposition*[27],[28]

$$\mathbf{R} = \mathbf{R}_0 + \sum_{\mathbf{k}=\bar{1}}^{n} c_{\mathbf{k}} \mathbf{\Psi}_{\mathbf{k}} + \sum_{\bar{1} \leq \mathbf{k} < \mathbf{j} \leq n} c_{\mathbf{kj}} \mathbf{\Psi}_{\mathbf{kj}} \tag{7.25}$$

where the single index in Eq. (7.25) means the single order correlation between the polynomials $\mathbf{\Psi}_{\mathbf{k}}$ while the double index identify the higher order correlation between the polynomials. The equation (7.25) is called *ANOVA, Analysis Of Variance, Decomposition* if[27]:

$$\int_{\Omega} \mathbf{R}(\mathbf{X}) d\mathbf{X} = 0 \tag{7.26}$$

where the vector $\mathbf{X}$ is the random variable set, $d\mathbf{X}$ is the measure function for each random variables and Ω is the sample space. The total variance, Eq. (7.24), can be decomposed in a sum of relative variance:

$$D = \sum_{i=1}^{n} D_i + \sum_{1 \leq i < j \leq n} D_{ij} + \cdots + D_{12\ldots n} \tag{7.27}$$

where each single term is the relative variance linked to a random parameter, therefore *i.e.*the term D_{ij} is the relive variance generates from the combination effect of the random variables i and j.

For instance let consider a PCE expansion defined for two random variables a and b which two polynomial basis Ψ and Φ are assigned:

$$\mathbf{R} = c_{00} + c_{10}\mathbf{\Psi}_1 + c_{01}\mathbf{\Phi}_1 + c_{20}\mathbf{\Psi}_2 + c_{02}\mathbf{\Phi}_2 + c_{11}\mathbf{\Psi}_1\mathbf{\Phi}_1 \tag{7.28}$$

and let write its variance:

$$D = c_{10}^2\langle\mathbf{\Psi}_1^2\rangle + c_{01}^2\langle\mathbf{\Phi}_1^2\rangle + c_{20}^2\langle\mathbf{\Psi}_2^2\rangle + c_{02}^2\langle\mathbf{\Phi}_2^2\rangle + c_{11}^2\langle\mathbf{\Psi}_1\mathbf{\Phi}_1\rangle \tag{7.29}$$

Using the decomposition shows in Eq. (7.27) one can write:

$$\begin{cases} D_a = c_{10}^2\langle\mathbf{\Psi}_1^2\rangle + c_{20}^2\langle\mathbf{\Psi}_2^2\rangle \\ D_b = c_{02}^2\langle\mathbf{\Phi}_1^2\rangle + c_{02}^2\langle\mathbf{\Phi}_2^2\rangle \\ D_{ab} = c_{11}^2\langle\mathbf{\Psi}_1\mathbf{\Phi}_1\rangle \end{cases} \tag{7.30}$$

It is possible to define the *Sobol indices*[28] as:

$$S_i = \frac{D_i}{D} \quad , \quad S_{ij} = \frac{D_{ij}}{D} \ , i, j = 1, \ldots, n \tag{7.31}$$

moreover by definition they satisfy:

$$\sum_i S_i + \sum_{1 \leq i < j \leq n} S_{ij} = 1 \tag{7.32}$$

These indices represent the effect of each input parameter on the output variable. The Sobol indices are used to evaluate the *Total sensitivity indices*:

$$S_{T_i} = S_i + \sum_{j=1}^{n} S_{ij} \tag{7.33}$$

The sum of the indices defined in Eq. (7.33) is grater than one, since the higher order correlation terms,S_{ij}, are taken account for each random parameter. Because of this the interpretation of the sensitivity indices can be mislead. Those indices have to represent how the output variable variance is shared among the different input variable, therefore the indices can not be grater than one.

These considerations about the Sobol indeces have led to reformulate the sensitivity indices introduced. In order to analyze the contribution of each input to the variance the cross term have been equally split between the variables interested, that is a sensitivity index is defined as:

$$Sa_i = S_i + \sum_{1 \leq i < j \leq n} \frac{1}{2} S_{ij} + \sum_{1 \leq i < j < k \leq n} \frac{1}{3} S_{ijk} \tag{7.34}$$

The indices defined in Eq. (7.34) are evaluated for concentration, turbulent kinetic energy and velocity, an index for each random independent variable describing the output quantity, therefore 7 indices for the concentration and 6 for kinetic energy and velocity.

Chapter 8

Results

In this chapter the results coming from the PCE application are shown. First, we present the results in terms of mean field and standard deviation for the two sampling distributions. After, the comparison with the experimental results is made. The comparison is based on experimental profiles and fields measured in the GEMIX experiment. Finally a sensitivity analysis is carried out in order to show which are the most important input variables.

8.1 Polynomial Chaos results

In Fig. 8.1 and 8.2 the results for Polynomial Chaos Expansion are shown, the mean value and standard deviation fields for concentration, turbulence kinetic energy and the $x-component$ of velocity are displayed at the center plane of the computational domain. In all the contours the effect of the uncertainty parameters are symmetric about the $y = 0\ mm$ axis.

In the mean concentration field, the mixing zone is observable in the center of the plane, starting from the system origin, the end of the split plate. The thickness of the mixing zone increases along the flow direction. The standard deviation along the stream axis is zero, that means the concentration alongside the axis does not change. Concerning the concentration field evaluated with the asymmetric sampling point distribution there is an expected asymmetry in the standard deviation, which does not appear using the symmetric sampling points distribution. Two symmetrical location with respect to the flow axis have been chosen to analyze this asymmetry, they are located at $x = 587mm$ and $y = \pm 9.84mm$. For those points the concentration value for every one of the deterministic simulations is plotted in Fig. 8.3. In both of case a small difference appears between the response of the two points, this gap between the two response could affect the coefficients even if they look very symmetric in Fig. 8.4. The problem could be a numerical issue, since the coefficient are very small except the first one that is the mean value, a small variation can propagate through all the mathematical step and generates an observable difference in the output.

Turbulence kinetic energy mean value and standard deviation are symmetric in both of cases and also the contours are equals. The mean value decreases along the flow, this is an expected result, since the turbulence kinetic energy is dissipated along the axis and the flow is more homogenous thanks also to the mixing process that takes place. The standard deviation field shows how the inlet conditions influences the flow, indeed the standard deviation is very high in the inlet section and it decays as the flow becomes more developed.

Same considerations can be made for the velocity, analyzing the velocity standard deviation the first remark is the influence of the inlet conditions. Also for the velocity the standard deviation is high at the inlet and it decays along the channel. In Fig. 8.5, 8.6 and 8.7 5 mean value and standard deviation profiles are shown for each output

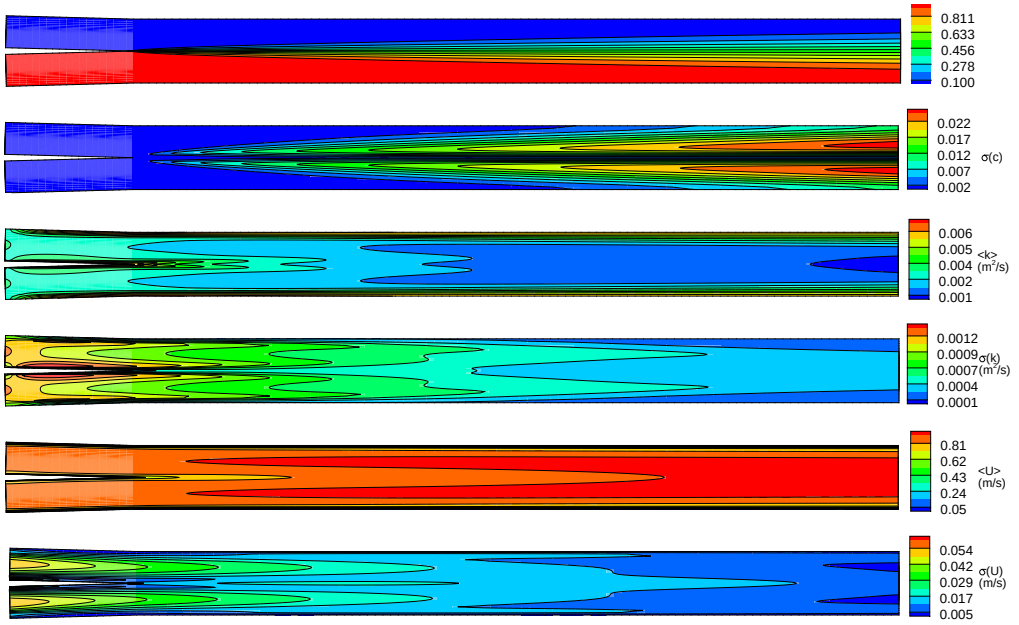

Fig. 8.1: CFD results for turbulent mixing using the symmetric grid. Mean values and standard deviation are shown for concentration,turbulence kinetic energy and velocity.

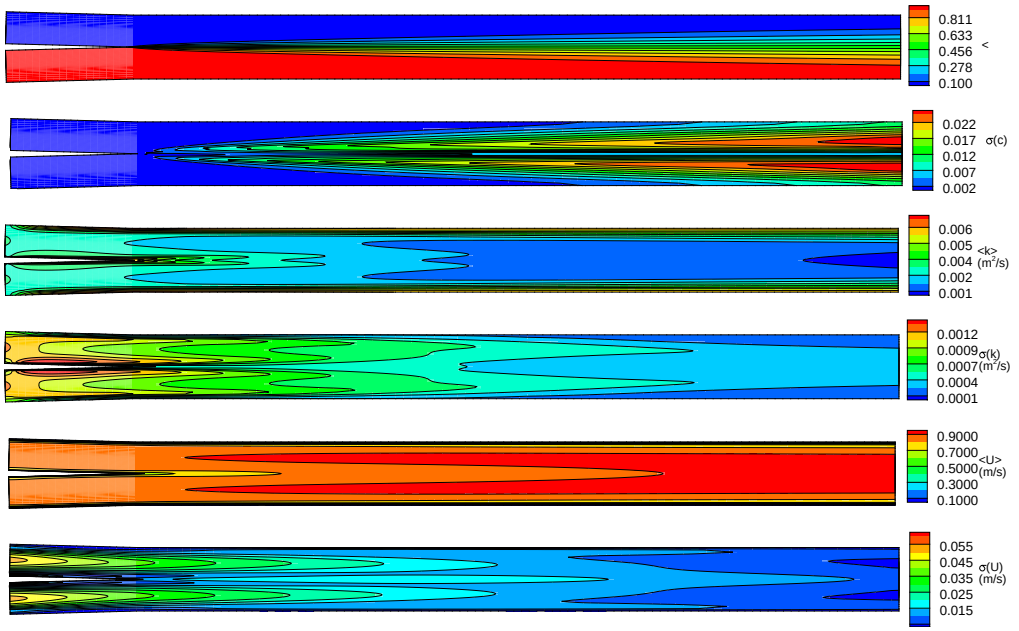

Fig. 8.2: CFD results for turbulent mixing using the asymmetric grid. Mean values and standard deviation are shown for concentration,turbulence kinetic energy and velocity.

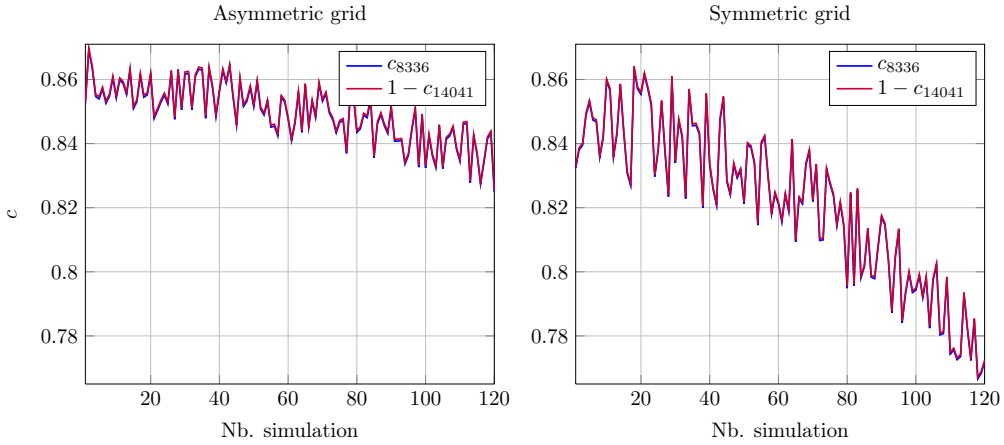

Fig. 8.3: Deterministic response comparison for two specular location,$x = 587mm$ and $y = \pm 9.84mm$, in function of the simulation number.

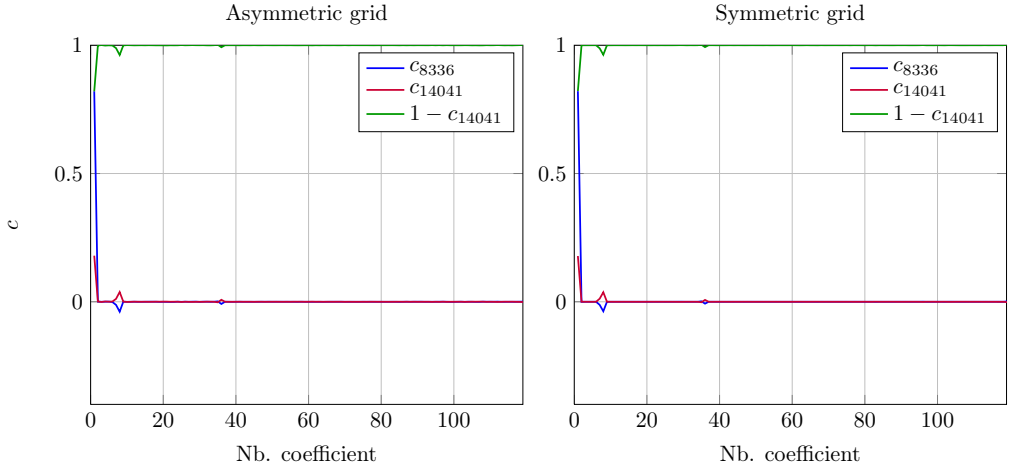

Fig. 8.4: Coefficient comparison for two locations: $x = 587mm$ and $y = \pm 9.84mm$.

variable. The profile positions coincide with the measurement positions and these profile are compared with the experimental results in the next section. In all mean value profiles, the results using PCE with symmetric and asymmetric sampling points distributions are superimposed. The concentration mean value is always equal to 0.5 for $y = 0mm$, this is the point where the concentration does not change along the entire length of the mixing channel. Since this value is constant, the standard deviation associated to $y = 0mm$, along the channel, is zero.

The turbulence kinetic energy and velocity profile exhibit the same behavior as much for the symmetric as asymmetric case, the development of the flow is well clear in both parameters, the profiles become flatter along the channel. The standard deviation decreases for the kinetic energy and for the velocity, this is due to the lower influence of the inlet section, where higher uncertainty exists.

In Fig. 8.8 and 8.9 a comparison is made between the coefficients computed with a symmetric sampling points distribution and with an asymmetric sampling points distribution. The coefficients are almost equals, indeed the two lines in both of the plots are superimposed. These plots give two important information, the first is about the independence of the PCE results by the selection of the distribution of the sampling points, where the coefficients are the sames independent of sampling points distribution. The second information is about the weight of the polynomial, indeed in the plots few peaks can be seen. Clearly after the first coefficient, and the most part of coefficients are equal

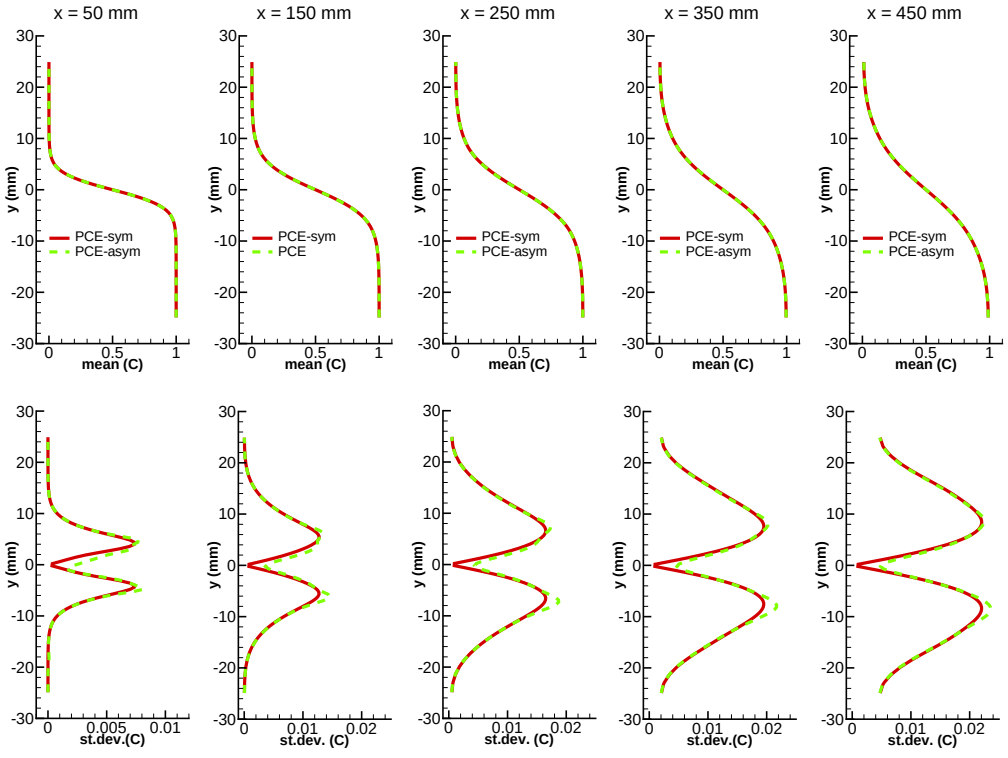

Fig. 8.5: Comparison between the mean value(top) and standard deviation(bottom) values for the concentration calculated with symmetric sampling points grid and asymmetric sampling points grid.

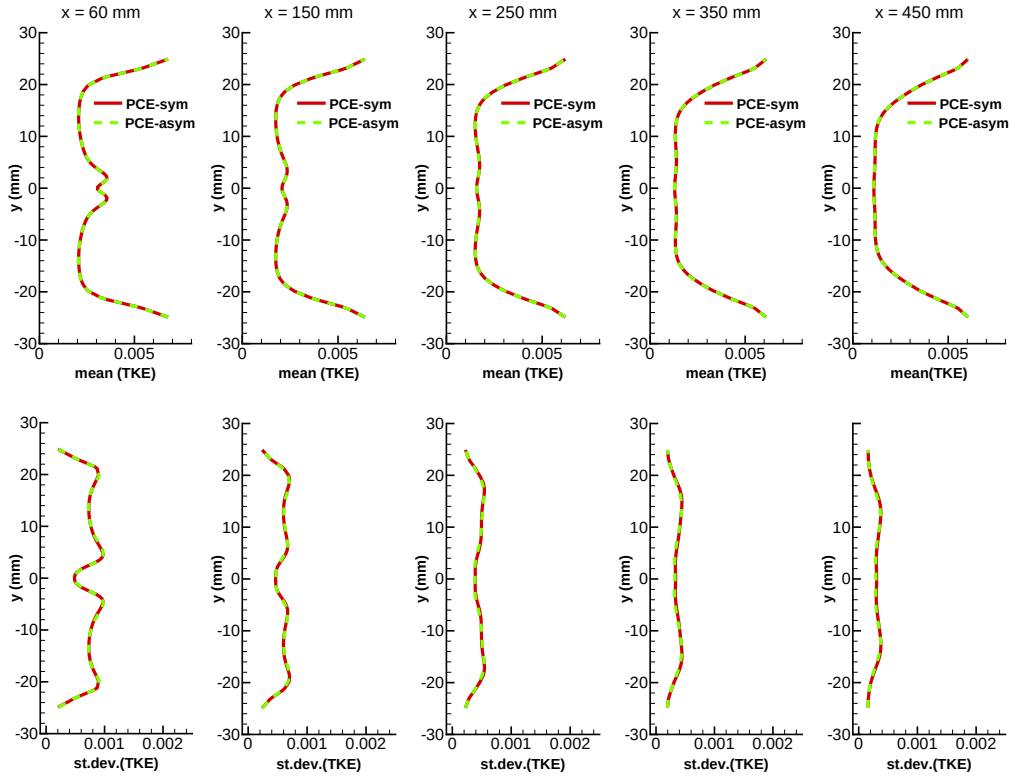

Fig. 8.6: Comparison between the mean value(top) and standard deviation(bottom) values for the turbulence kinetic energy calculated with symmetric sampling points grid and asymmetric sampling points grid.

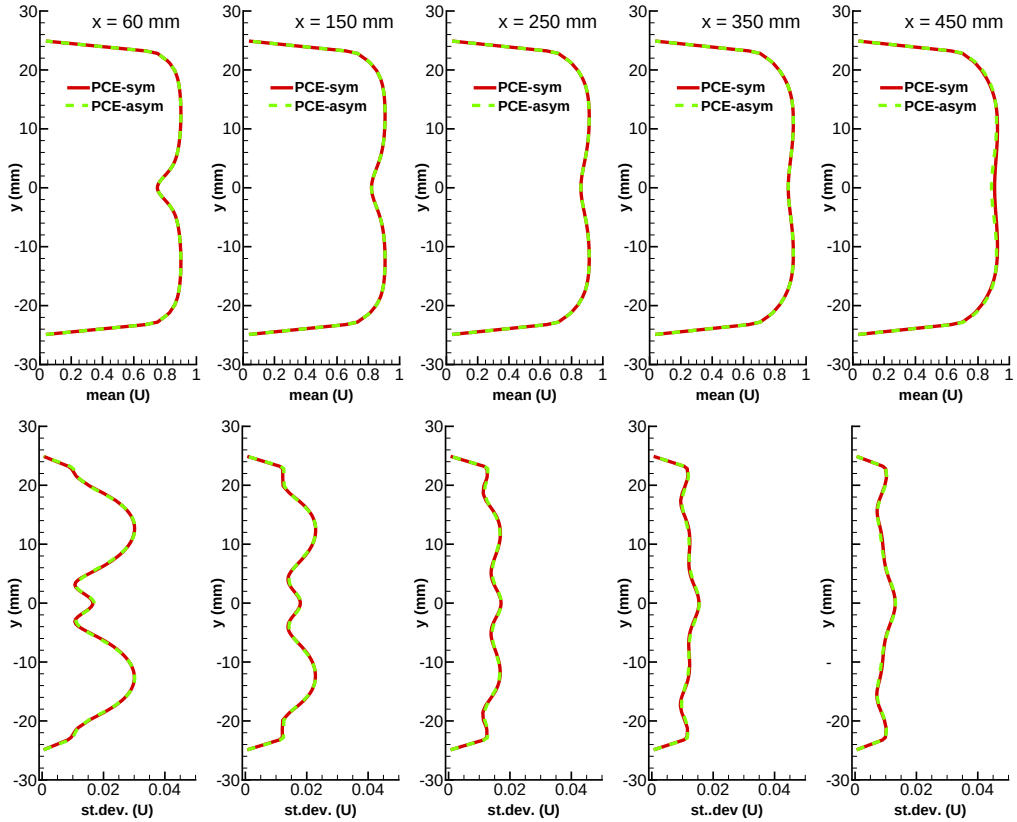

Fig. 8.7: Comparison between the mean value(top) and standard deviation(bottom) values for the $x - component$ velocity calculated with symmetric sampling points grid and asymmetric sampling points grid.

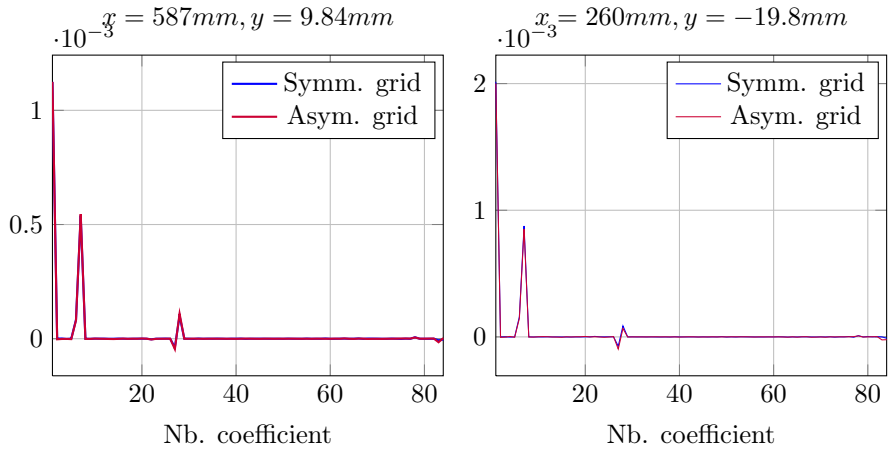

Fig. 8.8: Turbulence kinetic energy coefficients: comparison between asymmetric and symmetric grid for two locations.

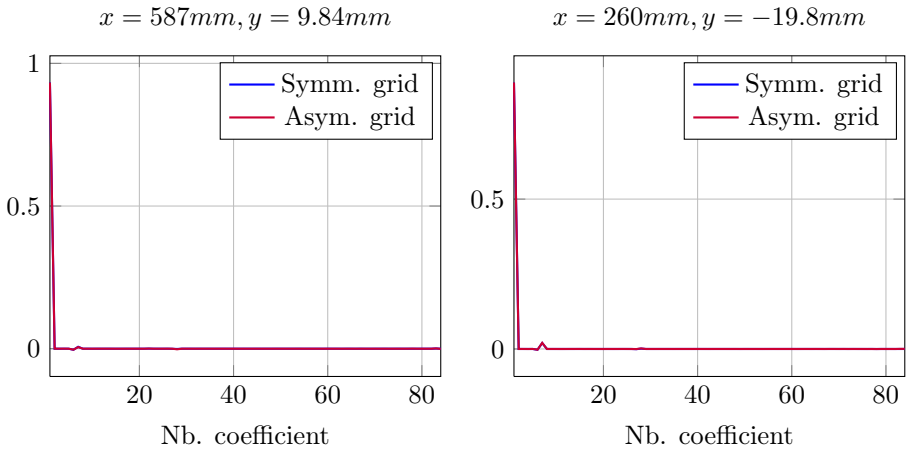

Fig. 8.9: $x-component$ velocity coefficients: comparison between asymmetric and symmetric grid for two locations.

to zero. It means that the highest polynomial degree play a small role in the mean value and the standard deviation because their effect is dumped by the small coefficient magnitude. Furthermore the highest coefficients are found for α and β polynomials, therefore in the statistical computation these polynomials play a more important role than other polynomials. This is an other evidence of the impact of the inlet uncertainty on the total output uncertainty.

To confirm the independence of the results by the sampling grid points, the application of an operator M defined iby equation (6.14) in Chapter6 is employed, in this particular case the response of the asymmetric case have been mapped into the symmetric case response through the operator M defined as:

$$M_{a\to s} = A_s A_a^{-1} \tag{8.1}$$

where the subscript a identifies the asymmetric case while s identifies the symmetric case and the mapping operation has been applied in one point located in the middle plane at $x = 587mm$ and $y = 9.84mm$. The operator $M_{a\to s}$ has been applied to the asymmetric response and the outcome is shown in Fig. 8.10. The deterministic representation for concentration, TKE and velocity are plotted against the simulation number, therefore Fig. 8.10 shows the variation of the response for each simulation. The action of $M_{a\to s}$ is represented by the green line, it change the asymmetric signal, red line, into the symmetric signal, blue line. This operation has been applied to all the output variables. The mapped signal fits quite well the symmetric signal for all the variables. Given any sampling grid points the polynomial matrix of equation (6.12) can be generated and therefore the M operator defined in (8.1) can be evaluated. Using this operator it is possible to find the deterministic response of any given sampling grid distribution without performing any simulation.

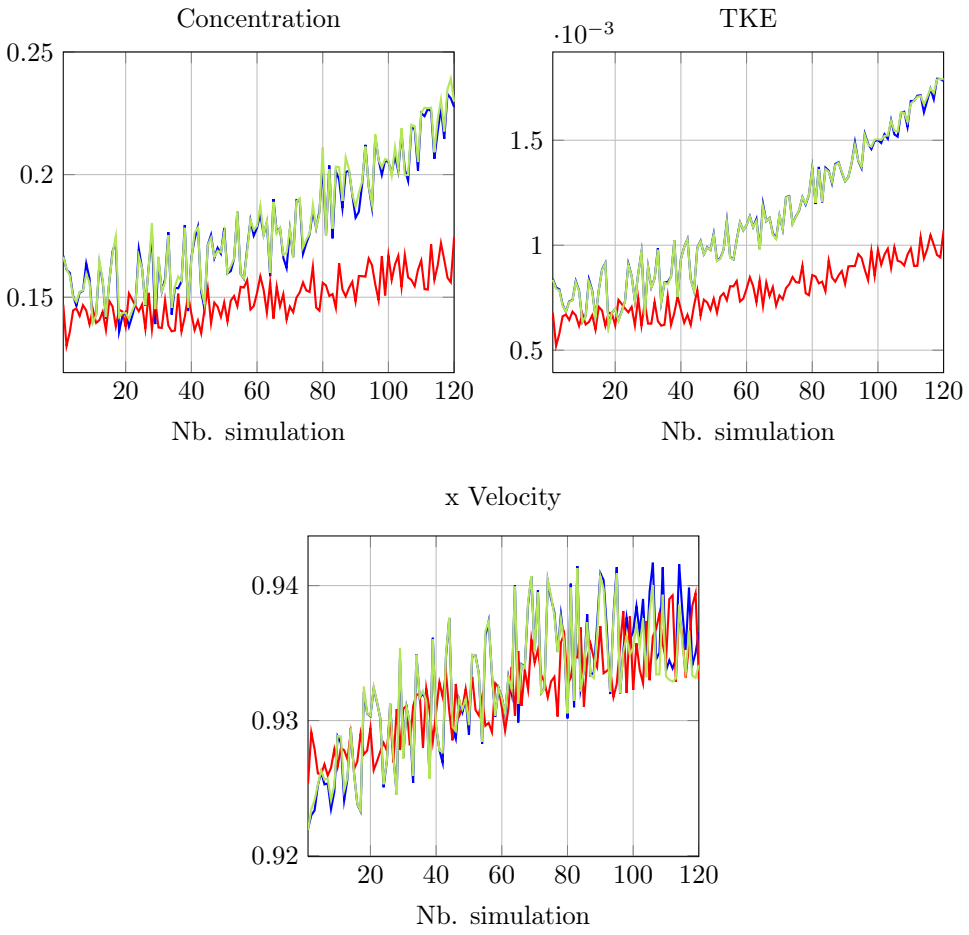

Fig. 8.10: Asymmetric response mapping:the blue line is the symmetric response, the red is the asymmetric response. The green line is the result of the $M_{a \to s}$ operator action to the asymmetric response.

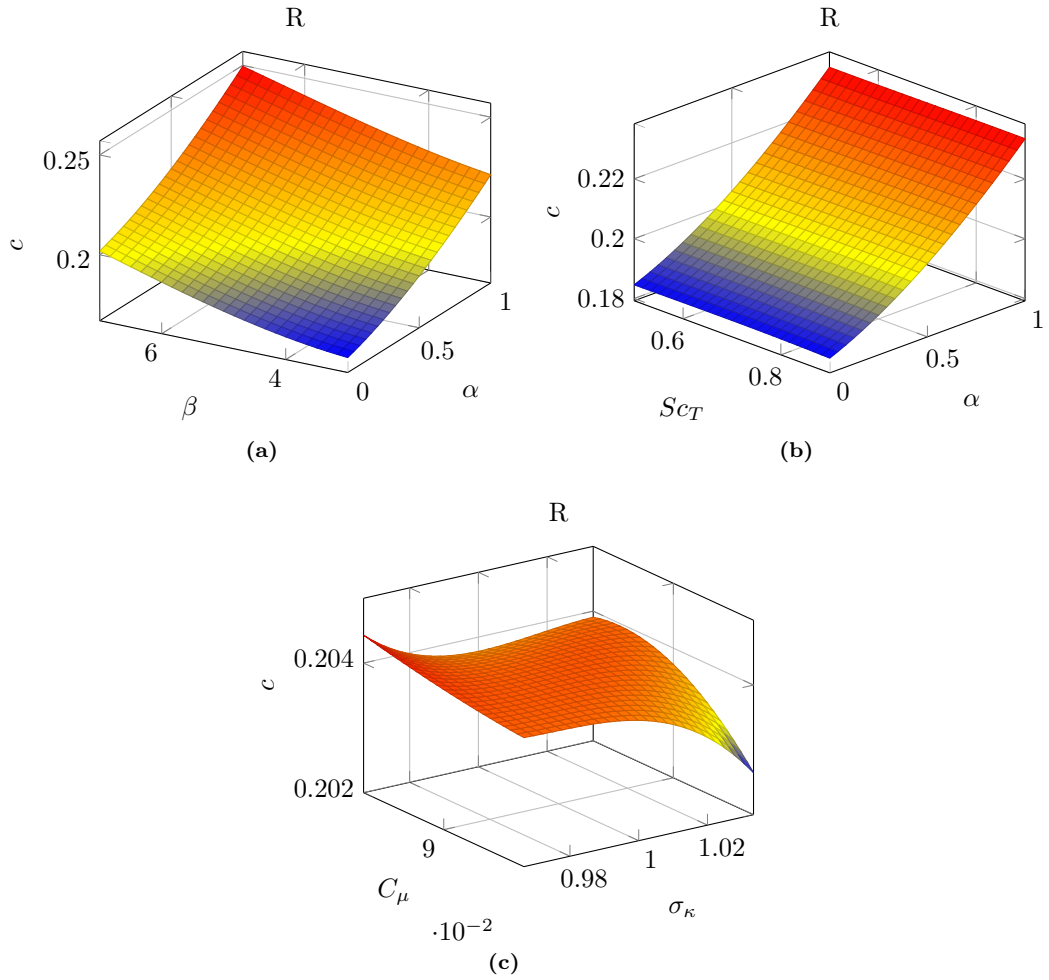

Fig. 8.11: Concnetrnation response surface for three output variables at $x = 260mm$ & $y = 5mm$.

The response surface of the variables of interest are shown in Figures 8.11, 8.12 and 8.13 for a selected point located in the middle plane at $x = 260mm$ and $y = 5mm$. The response surfaces are plotted as a function of uncertainty parameter couple, for all the variables of interest a surface depending by α and β is generated as these parameters have the biggest impact of the total output uncertainty. Furthermore based on the sensitivity indices analysis other parameters have been considered.

The response surface for α and β 8.11a shows a monotonic response and almost linear for β while for α is slightly non-linear, approaching the fully developed regime the concentration grows in a quadratic way. This is an excepted result, indeed the fully developed regime promotes the mixing and consequently the concentration increases. In Fig. 8.11b the surface shows how the variation of the inlet condition is predominant compared to the turbulent parameters, the relation between the concentration and the Sc_T number is constant, that is the turbulent diffusivity doesn't affect the concentration of the fluid. Finally in Fig. 8.11c the relation of the concentration with the $k - \varepsilon$ model parameters is plotted. The surface is very flat in the middle, the zone around the coefficient empirical values, but the response stop to be constant far away of the empirical values and it becomes monotonic non linear.

Concerning turbulence kinetic energy and velocity similar considerations can be made, in both of case there is a monotonic and linear relation between the response and the variables α and β, furthermore the predominance of α is well clear. Other aspect in

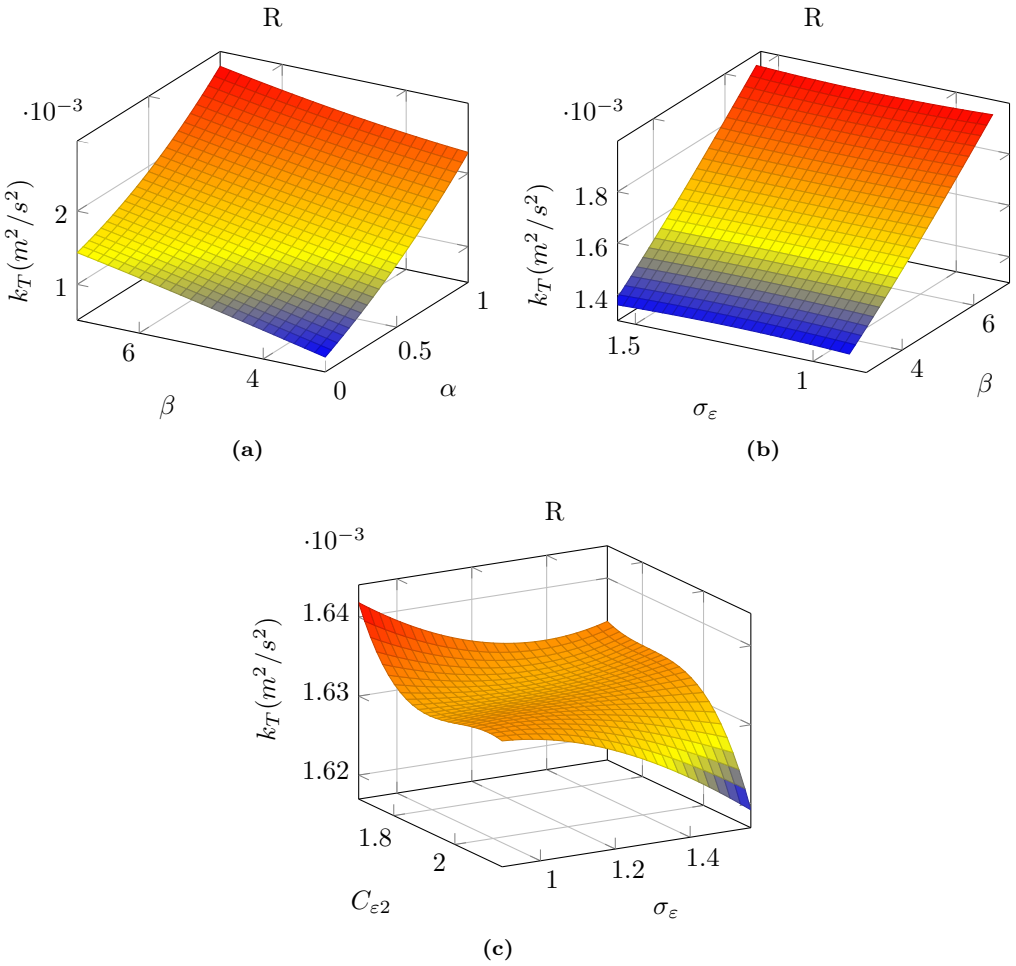

Fig. 8.12: Turbulence kinetic energy response surface for three output variables at $x = 260mm$ & $y = 5mm$.

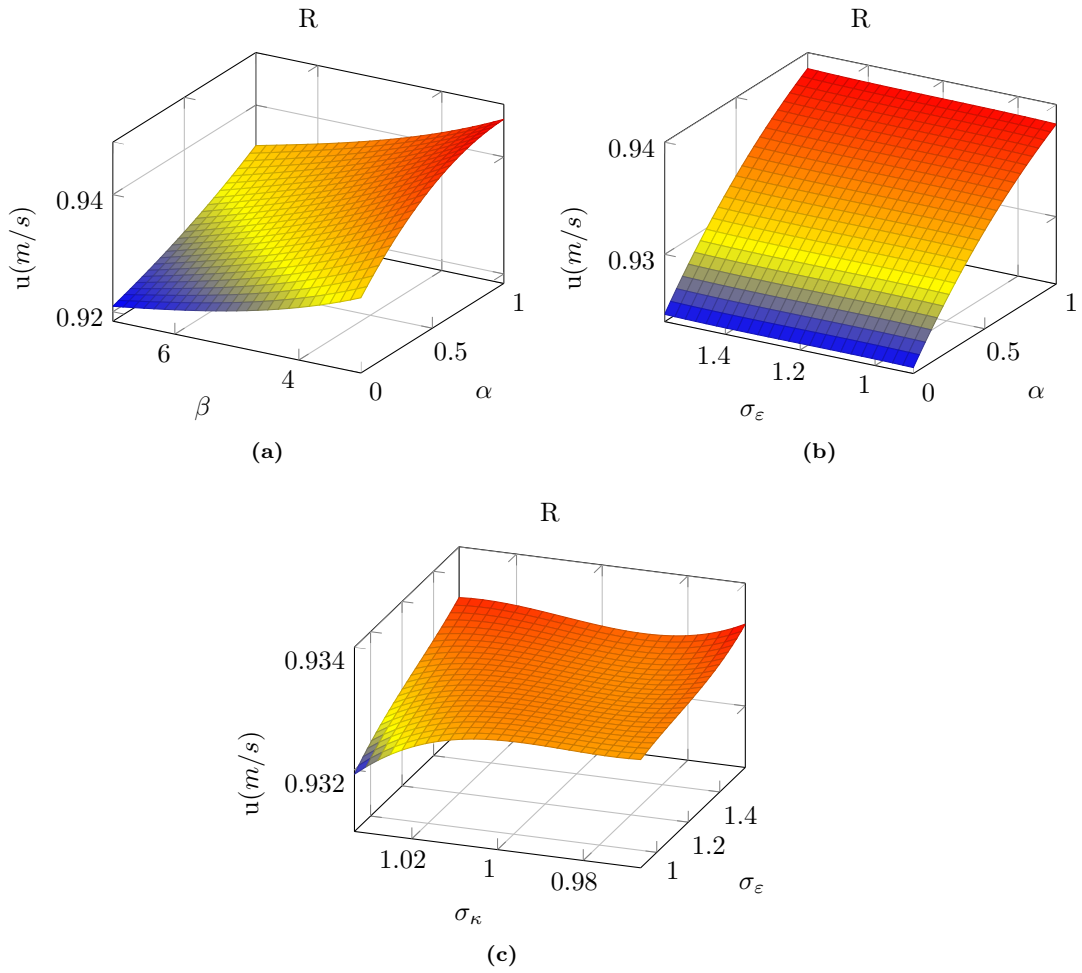

Fig. 8.13: Velocity response surface for three output variables at $x = 260mm$ & $y = 5mm$.

common is the dominance of the inlet conditions over the other parameters, in Fig. 8.12b and Fig. 8.13b the response grows monotonic with β and α while is practically constant with respect to the turbulent parameters. This is a further evidence of the big impact of the inlet conditions on the final output.
The two figures 8.12c and 8.13c show the influence of the turbulent model coefficients on the final response for turbulence kinetic energy and velocity. The same behavior, observed in concentration surfaces, can be found in these figure. Around the turbulent model coefficients empirical values, the mean values chose for the random variables, the response is constant, it means that a small change in the empirical values doesn't affect the final output. However far away from the mean values, near the tail of the variables distribution, the response changes a lot and in a non-linear way.

8.2 Comparison with experiment

8.2.1 Experimental profiles

The comparison with the experimental results is presented in this section. The PCE mean $+/-$ two standard deviation(errors bars) as well as the mean experimental ones are plotted for c, k_T and u at several location along the mixing channel in Fig. 8.14,8.15 and 8.16 respectively. The error bars for the PCE mean value have been evaluated as $+/-$ two standard deviation. For the present work the choice of $\pm 2\sigma$ has been selected in a heuristically way, but further analysis is needed to identify the most appropriate value to cover 95% of the tolerance interval of a multivariate probability density function. For the experimental results no error bars are available at the moment. The comparison with the experimental results is presented in this section. The PCE mean $+/-$ two standard deviation(errors bars) as well as the mean experimental ones are plotted for c, k_T and u at several location along the mixing channel in Fig. 8.14,8.15 and 8.16 respectively. The error bars for the PCE mean value have been evaluated as $+/-$ two standard deviation. For the present work the choice of $\pm 2\sigma$ has been selected in a heuristically way, but further analysis is needed to identify the most appropriate value to cover 95% of the tolerance interval of a multivariate probability density function. For the experimental results no error bars are available at the moment.

The experimental concentration profile were obtained with two independent measuring technique. Fig. 8.14 shows in red and in green the results from Wire Mesh Sensor(WMS) and Laser Induced Fluorescence(LIF) measurements respectively. The two techniques are explained in Chapter 5. The measured LIF profiles presents a small shift from the WMS measurements, which might be attributed to a slight misplacement of the Wire Mesh Sensor in the mixing section. Despite of the difference in the results of these two techniques the shape of the mixing layer is not altered but just shifted. The PCE results overpredict the mixing layer thickness along the entire mixing channel except at $x = 50mm$ where the PCE mean fits the experimental plot given by LIF measurements. Nonetheless the PCE profile shape follows the evolution that it is possible to see in the experimental profiles, there is a stretching of the profile at the inflection point position always located at $y = 0mm$ and $c = 0.5$. The error bars for the PCE profiles are quite small but they touch the experimental results in all the locations measured. The magnitude of PCE error bars indicates that the uncertainty parameter used doesn't affect much the concentration. The turbulence kinetic energy and the velocity experimental profile were obtained using the Particle Image Velocimetry. The comparison with the PCE profiles shows that the matching among PCE and experimental results is quite good. The PCE velocity mean reproduces very well the experimental results along the entire mixing section, moreover the PCE error bars cover almost all the experimental results. The error bars magnitude decreases along the channel since the effect of the inlet conditions becomes less important and it doesn't influence the velocity mean value.

Concerning the turbulence kinetic energy the PCE mean value reproduces well the experimental results, especially in the first profiles, and the error bars cover the experi-

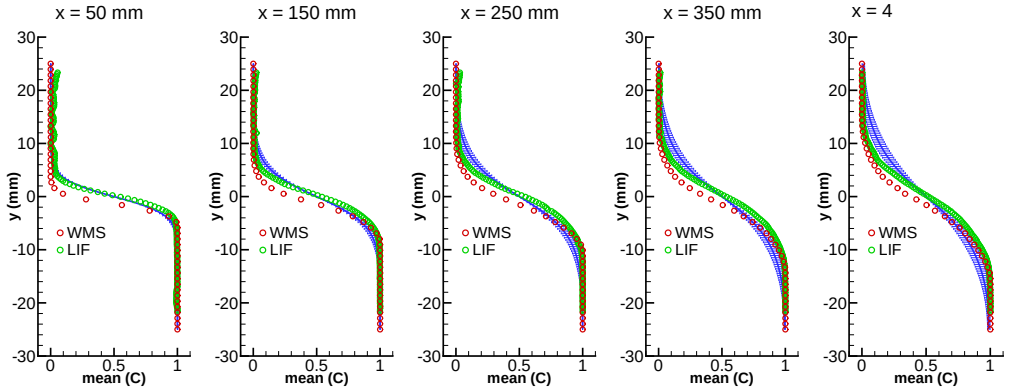

Fig. 8.14: Comparison between the experimental(green and red dots) and PCE mean concentration +/− two standard deviation(blue line).

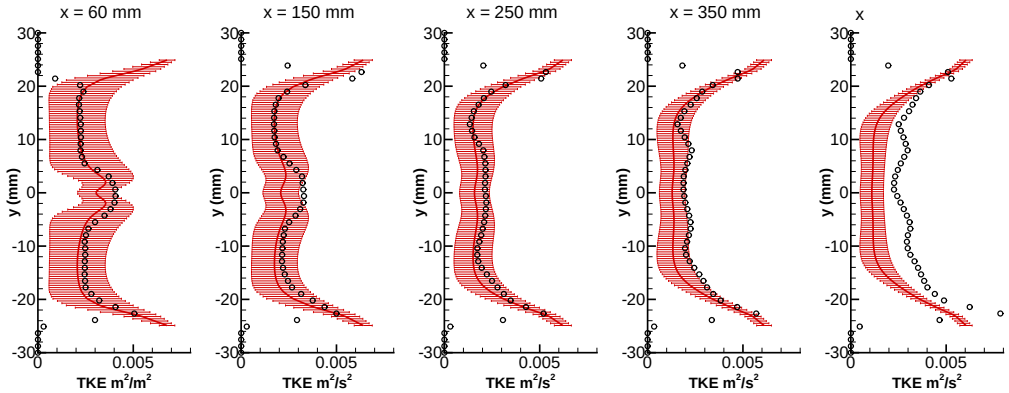

Fig. 8.15: Comparison between the experimental(black dots) and PCE mean turbulence kinetic energy +/− two standard deviation(blue line).

mental results also in the center line where the gap between the PCE and experimental value is bigger. In the last section, $x = 450mm$ the experimental results are outside the error bars. However the experimental results in the last measurement show some problems, indeed the profile stops to be symmetric but, especially, the turbulence kinetic energy is higher than the previous measurements. This is completely unphysical because the flow is developing along the channel and therefore the turbulence kinetic energy should be decreasing along the channel.

8.2.2 Experimental contours

The PIV allows for generating contour profile. The PCE contours shown in Fig. 8.1 are compared with experimental contours in Fig. 8.17, turbulence kinetic energy, and in8.18, velocity.

The comparison is very good for the velocity where there is a strong resemblance among the two pictures, clearly the experimental one is less sharp caused by the camera resolution, nevertheless the contours shape and their magnitude is almost the same in the mixing zones. Some differences between the experimental and PCE results appear in the turbulence kinetic energy pictures. However, the uncertainty of the measured values are necessary to make a better assessment of the PCE results.

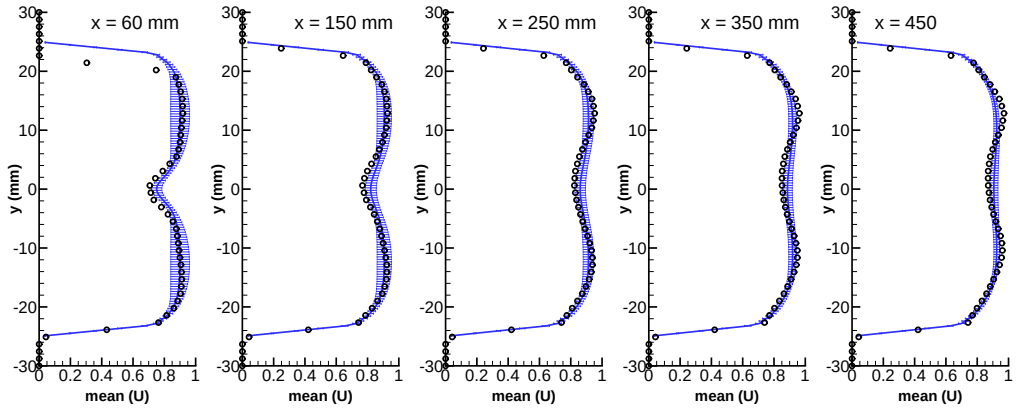

Fig. 8.16: Comparison between the experimental(black dots) and PCE mean velocity +/− two standard deviation(blue line).

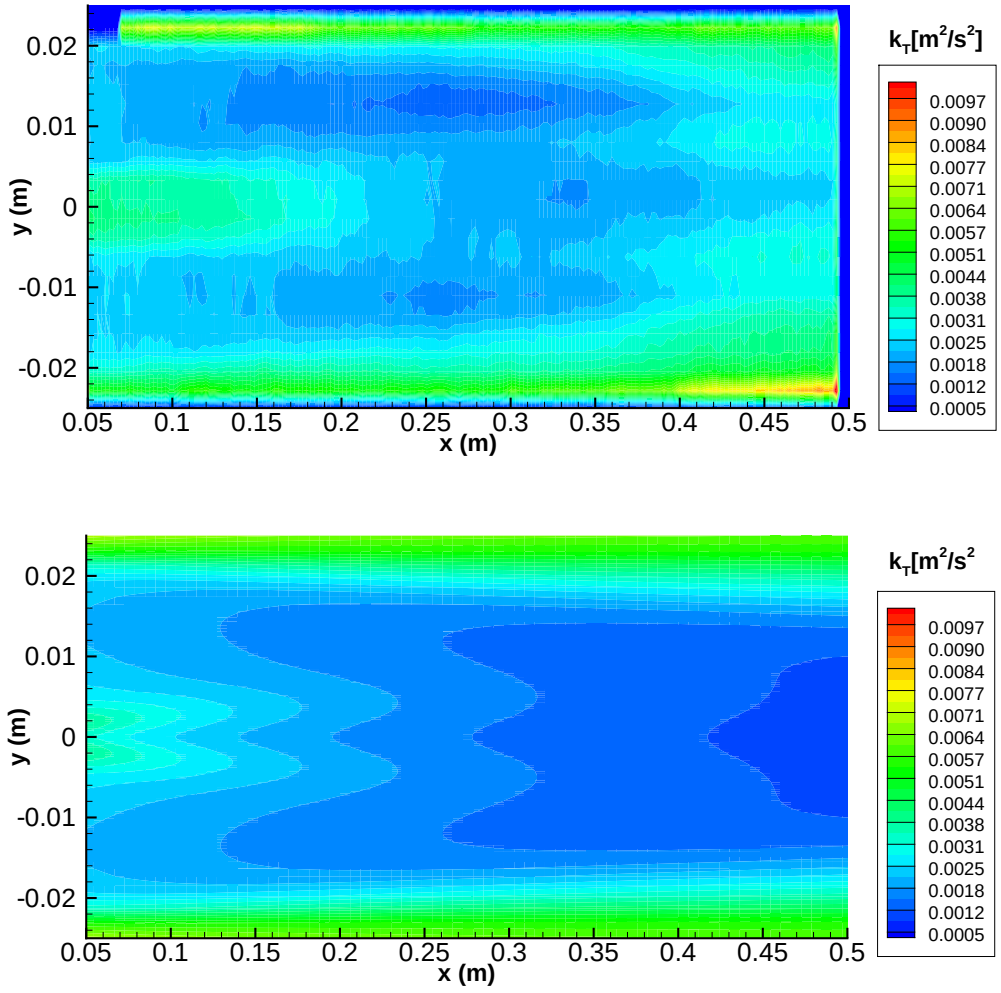

Fig. 8.17: Comparison between the experimental(top) and PCE(above) contours for the turbulence kinetic energy.

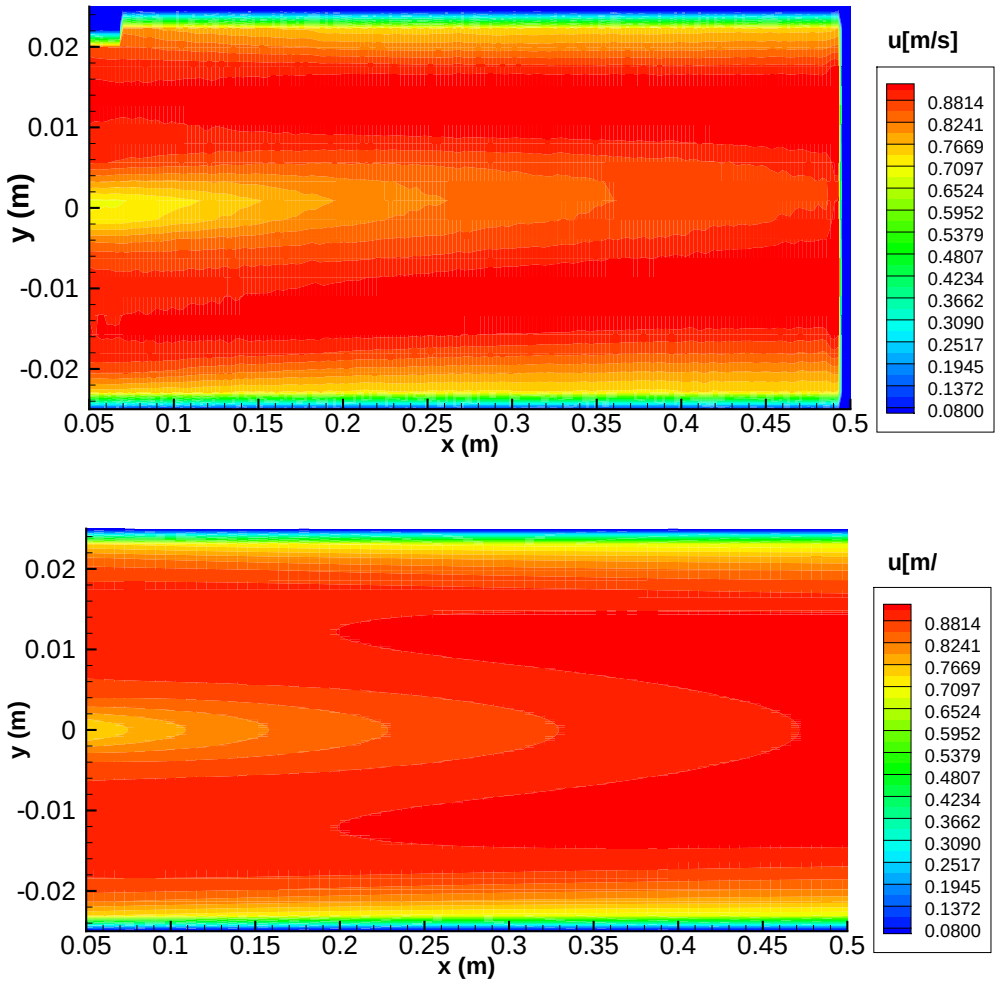

Fig. 8.18: Comparison between the experimental(top) and PCE(above) contours for the velocity.

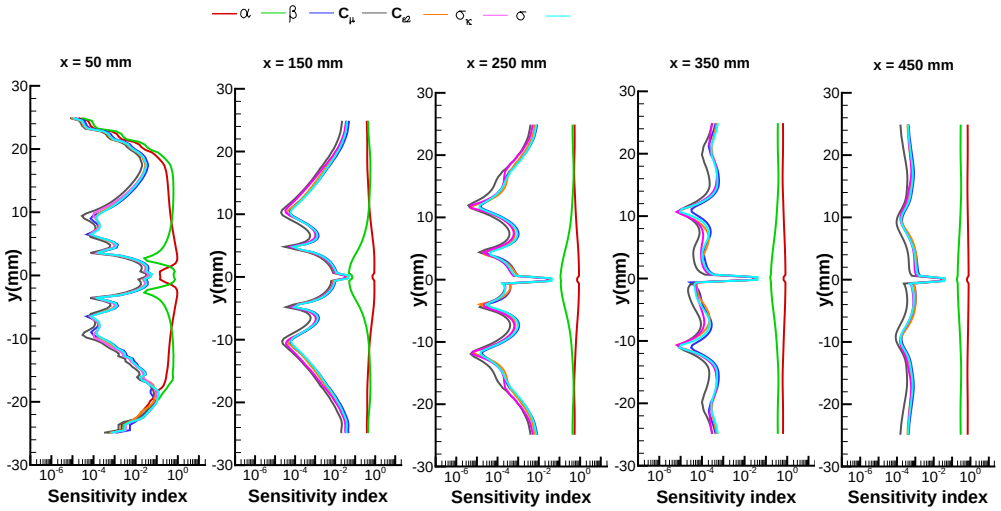

Fig. 8.19: Concentration sensitivity indices.

8.3 Sensitivity indices

As explained in Sec.7.3 a global sensitivity analysis has been carried out in order to understand which parameters affect mostly the final response. In Fig. 8.19,8.20 and 8.21 the sensitivity indices computed with equation (7.34) are plotted for concentration, turbulence kinetic energy and velocity respectively.

It stands out as the inlet velocity profile and the turbulence intensity are the predominant indices for all the three variable of interest, concentration, turbulence kinetic energy and velocity. The sensitivity indices for α and β are much higher than those associated to the coefficients of the turbulence model. Their value is almost equal to one and it is three and even four order of magnitude bigger than the turbulent model coefficients. The uncertainty in the variable of interest comes mostly from these two parameters, α and β, while the uncertainty links to the turbulent model is very small, almost negligible if compared to which introduced by the inlet conditions. The distribution associated to each parameter play a fundamental role in the output uncertainty. At α, due to the total lack of knowledge about the inlet velocity profile, an uniform distribution has been associated, therefore an important amount of uncertainty has been introduced already in this choice. About β using the correlation $I = 0.16Re^{-1/8}$ one gets a value of 4.2% that is not so far from the 5% chosen as mean value in the probability density function of β, but additional information is needed to construct more appropriate probability density functions.

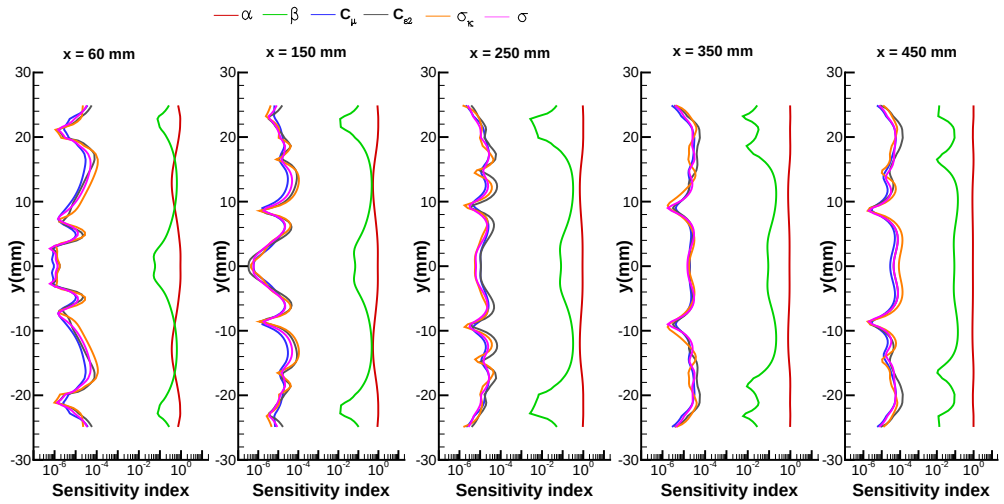

Fig. 8.20: The turbulence kinetic energy sensitivity indices.

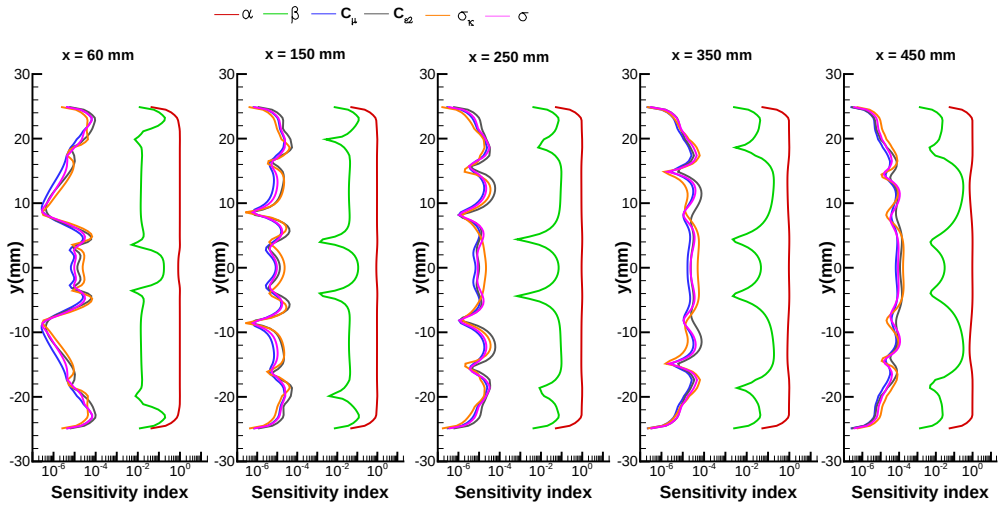

Fig. 8.21: Velocity sensitivity indices.

Chapter 9

Discussion and Conclusion

In this study the non-intrusive Polynomial Chaos (PC) expansion has been used to quantify the uncertainty of CFD simulations of the GEMIX experiment. Stochastic variables have been introduced to handle uncertain boundary conditions and the phenomenological coefficients in the $k - \varepsilon$ turbulence model, two describing the inlet conditions and five concerning the turbulent model. The PC expansion allows to approximate the response of a system in terms of series of orthogonal polynomials. The orthogonality of the polynomials in the PC expansion, enable us to obtain mean values and standard deviations, which were used to compute uncertainty bands for concentration, turbulence kinetic energy and velocity in the central plane of the GEMIX test rig.

The influence of the distribution of sampling points (used to sample the parameter space) and the convergence of the PCE results on the polynomial degree, was investigated thoroughly for the one dimensional exponential system. There, three set of sampling points has been used to compute the PC expansion (symmetrical distribution, asymmetrical distribution, roots of the polynomials) and to show its independent from the sampling points distribution. For each sampling points distribution the truncated polynomial degree has been increased in order to analyze the convergence rate of PCE. The analysis has highlighted how already at the third degree the analytical solution was reached by all the PC expansions. The only difference displayed by the three PCE is the convergence rate, indeed the asymmetric sampling points distribution is the lowest expansion to reach the analytical solution. Starting from the convergence results for the exponential system the truncated polynomial degree, for the PCE representing the CFD simulation, has been chosen equal to three.

The independence of the PCE results from the sampling points is guaranteed, if the response of one sampling points distribution can be perfectly mapped onto the response of a different set of sampling points. The symmetric response was mapped onto the roots polynomial case and the roots polynomial case was mapped onto the asymmetric case. In both cases showed a perfect match between the mapped and mapping distribution.

To investigate the influence of the distribution of the points used to sample the parameter space, we use the Latin-Hypercube sampling method to generate the sampling points, where two distributions were generated to assess their influence on the final PCE results. One distribution considered a symmetric distribution of points around the mean values, whereas the second one was generated only considering a half of the support interval in every random direction. The PCE results show that mean and standard deviation for the velocity and turbulence kinetic energy are independent from the sampling point distribution. However, an small asymmetry in the standard deviation field for the concentration is observed respect to center line, which might find an explanation on numerical errors in the solution of the linear system–associated to the PCE coefficients–or to a numerical error in the CFD simulation. To further clarify the reason of this asymmetry, the response of two CFD nodes located at the same distance from the center line (mirror

points), was plotted and a slight difference was observed. This difference in the response of the two mirrored CFD points was also observed when using the other set of sampling points, but no asymmetry in the standard deviation field of the concentration was seen. The independence of the PCE results from the sampling points is guaranteed, if the CFD response of one sampling points distribution can be perfectly mapped onto the response of a different set of sampling points. It was seen that a very close match was achieved when mapping the CFD response of the asymmetric case onto the symmetric one, which is reflected in the identical mean values for all the variables (velocity, turbulence kinetic energy and concentration).

To compare PCE mean values with experimental measurements, we have selected five vertical profiles at different locations along the mixing section. The PCE results plus error bars based heuristically on $\pm 2\sigma$, which for a one dimensional Gaussian distribution corresponds to a 95% tolerance interval. Most of the experimental data lay within the estimated error bars. About the velocity field in all the measured profile the experimental data lay in the error bars. The turbulent kinetic energy and the concentration display a progressive departure of the experimental data from the error bars. Although most of the experimental results are contained withing the error bars, this is not the main objective of UQ applied to CFD simulations. The experimental results are used only as a guidance to assess the correct physical prediction of the CFD model.

For velocity and turbulent kinetic energy it has been seen that the uncertainty decreases along the channel, this is due to the developing of the flow which becomes more and more developed along the channel. The concentration uncertainty increases along the channel, indeed the highest standard deviation is localized at the outlet of the channel. This behavior can be explained in terms of the residence time of the fluid inside the channel and the variability of the turbulent kinetic energy. Since the turbulent diffusion coefficient is related to the the turbulent kinetic energy through the Schmidt number and the eddy viscosity, the variability in the turbulent kinetic energy induces variability in the diffusion time along the channel. Therefore the longer the residence time inside the mixing region, the higher the standard deviation in the distribution of the mixing scalar.

At the moment, the calculation of the experimental uncertainty for the GEMIX database is undergoing and, therefore, further considerations about the comparison with the experimental data can not be made.

The sensitivity analysis carried out in the present work through the definition of sensitivity indices based on the Sobol decomposition. Three indices sets, one for each variable of interest, have been computed, each set is composed by the indices related to the input random variables. Finally 19 sensitivity indices have been evaluated. Each index represents the partial variance of the random variable, therefore the indices state the contribution of each random variable to the total variance and they indicate which random variables brings more uncertainty in the total uncertainty.

The indices reveal that the biggest sources of uncertainty in the response of the system are the inlet conditions, the inlet velocity profile and the turbulent intensity. The indices related to these variables are three, even four, order of magnitude bigger than the indices related to the turbulence model coefficients. One can argue that the most part of the response uncertainty comes from the inlet conditions. In particular the index connected to α, inlet velocity shape coefficient, is the biggest. This outcome has not to surprise because there were no information about the inlet condition provided by the experimental, indeed if for β, the turbulent intensity, an empirical correlation gives a rough estimation about the magnitude of the value, the inlet velocity profile was totally unknown. Further the presence of honey comb and grids in the conditioning section of the GEMIX does not allow to define somehow the inlet velocity profile.

The sensitivity analysis has disclosed that the turbulence model contributes in very little part to the final uncertainty.

The Polynomial Chaos Expansion is a propagation method, thus the final uncertainty

will depend on the probability density functions assigned to the input variables. Fixing the characteristic of each pdf expresses how much one trust in the parameter values, the pdfs state the degree of belief in the parameter accuracy. Therefore the pdfs assignment plays a crucial role in the estimation of the final uncertainty in the CFD simulation, since more uncertainty is introduced in the input parameter more will be the output uncertainty. In this work the inlet conditions were characterized with the biggest uncertainty, indeed the ratio σ/μ for α and β is the highest among the random variables. The inlet conditions uncertainty comes from a lack of knowledge in the experiment and it can be decreased through additional experimental measurement. A new experimental campaign has been realized to carry out additional measurement for the GEMIX test rig in order to decrease the level of uncertainty from α and β.

The sensitivity indices have underlined how the uncertainty introduced by the turbulence model is very low, almost zero if compared with the inlet uncertainty. This behavior is also due to the choice of the probability density functions assigned to the turbulence model coefficients. All the distributions, associated to the random variables, are characterized by a small ratio standard deviation over mean value, that implies a narrow distribution shape near the empirical value. In the $k-\varepsilon$ turbulence model The empirical coefficients have been evaluated in order to get good agreement with the experimental results and their values are largely used. On the other hand none information are provided by the literature about the statistic concerning the computational of these coefficients, therefore additional research about the probability density functions describing the model coefficients is needed. A better definition of the coefficients pdfs could give more information about the uncertainty introduced by the model in the CFD simulations.

In the present work has been shown that PCE is a robust technique to quantify the uncertainty in CFD simulations introduced by random variables. In addition to uncertainty quantification, this propagation method enables us to determine the dominant random variables through the sensitivity analysis based on the Sobol decompostion. By the sensitivity analysis is determined that the inlet conditions introduced the highest uncertainty inside the CFD simulations. Therefore further tests are needed to decreases the uncertainty linked to the inlet velocity profile and the turbulent intensity.

Appendix A

Vector identities

In this Appendix the vector identities used in all the chapter to the equations derivation are listed.
For all the equations the following notation is used: $\mathbf{a}$ and $\mathbf{b}$ are first order vector, $\underline{\underline{T}}$ and $\underline{\underline{S}}$ are tensors, and α is a scalar.

$$\nabla \mathbf{a} = \begin{bmatrix} \frac{\partial a_x}{\partial x} & \frac{\partial a_x}{\partial y} & \frac{\partial a_x}{\partial z} \\ \frac{\partial a_y}{\partial x} & \frac{\partial a_y}{\partial y} & \frac{\partial a_y}{\partial z} \\ \frac{\partial a_z}{\partial x} & \frac{\partial a_z}{\partial y} & \frac{\partial a_z}{\partial z} \end{bmatrix} \tag{A.1}$$

$$\nabla \cdot (\mathbf{ab}) = (\nabla \cdot \mathbf{a})\mathbf{b} + (\mathbf{a} \cdot \nabla)\mathbf{b} \tag{A.2}$$

$$\nabla \cdot (\alpha \mathbf{a}) = \alpha \nabla \cdot \mathbf{a} + \mathbf{a} \cdot \nabla \alpha \tag{A.3}$$

$$\mathbf{a}(\mathbf{a} \cdot \mathbf{b}) = \mathbf{a}(\mathbf{b} \cdot \mathbf{a}) = \mathbf{aa} \cdot \mathbf{b} \tag{A.4}$$

$$\langle \mathbf{a}(\mathbf{a} \cdot \mathbf{b}) \rangle = \langle \mathbf{aa} \rangle \cdot \mathbf{b} \tag{A.5}$$

$$\nabla \cdot \left(\nabla \mathbf{a}^T \right) = \nabla (\nabla \cdot \mathbf{a}) \tag{A.6}$$

$$\nabla (\mathbf{a} \cdot \underline{\underline{T}}) = \nabla \mathbf{a} \odot \underline{\underline{T}} + (\mathbf{a} \cdot \nabla)\underline{\underline{T}}, \quad \text{the symbol } \odot \text{ means the matrix product.} \tag{A.7}$$

$$\underline{\underline{T}} : \underline{\underline{S}} = \sum_i \sum_j T_{ij} S ij \tag{A.8}$$

$$\nabla \nabla^2 \mathbf{a} = \nabla^2 \nabla \mathbf{a} \tag{A.9}$$

Appendix B

Polynomial Basis

Given a system of orthogonal polynomials a set $\{P_n(x)\}_{n=1}^{\infty}$, where $P_n(x)$ is a polynomial of degree n. The polynomials are ortohognal in the sense that the following inner product vanishes when $n \neq m$:

$$\langle P_n, P_m \rangle = A\delta_{nm}, A = constant \tag{B.1}$$

where A is a constant because of the basis is just orthogonal and not orthonormal. The variable x may be continuous or discrete, in the former case the inner product becames:

$$\langle P_n, P_m \rangle = \int_a^b P_n(x)P_m(x)w(x)dx \tag{B.2}$$

while in the latter case it is given by:

$$\langle P_n, P_m \rangle = \sum_{i=1}^{M} P_n(x_i)P_m(x_i)w(x_i) \tag{B.3}$$

In both cases, $w(x)$ is a weight function and the limits of the integral and the sum can be either finite or infinite. The attention is focused on those orthogonal families of polynomials that form a basis of the function space $L_w^2 = \{f : \langle ff \rangle < \infty\}$. In this appendix the principal Polynomial basis, used in the Polynomial Chaos Expansion, are presented. In this work only the Hermite basis and Legendre basis have been used but for the sake of the reader also the other basis being in the table 6.2 on page 47 are shown.

B.1 Hermite polynomials

There are two widespread definitions of the Hermite polynomials, according to whether the weight functions are given by[1]:

$$w(x) = \frac{1}{\sqrt{2\pi}} \exp(-\frac{x^2}{2}) \tag{B.4}$$

or:

$$w(x) = \frac{1}{\sqrt{\pi}} \exp(-x^2) \tag{B.5}$$

In both cases the support interval in which x is defined is $[-\infty; +\infty]$. The function (B.4) is used in this work in Polynomial Chaos Expansion since it's the standard normal distribution and only the basis orthogonal to that distribution is presented. Applying a simple variable change is possible to obtain the other orthogonal basis.
The Hermite polynomials can be evaluated using the following recursive formula:

$$He_n(x) = xHe_{n-1}(x) - Hen - 1(x)' \quad \text{with} \quad He_0(x) = 1 \tag{B.6}$$

Using the (B.6) it's possible to evaluate the square norm of the Hermite polynomials He_n:

$$\langle He_n, He_n \rangle = \int_{-\infty}^{+\infty} He_n^2(x) w(x) dx = n! \tag{B.7}$$

According to (B.6) the first 6 Hermite polynomials are:

$$\begin{aligned} H_0(x) &= 1 \\ H_1(x) &= x \\ H_2(x) &= x^2 - 1 \\ H_3(x) &= x^3 - 3x \\ H_4(x) &= x^4 - 6x^2 + 3 \\ H_5(x) &= x^5 - 10x^3 + 15x \end{aligned}$$

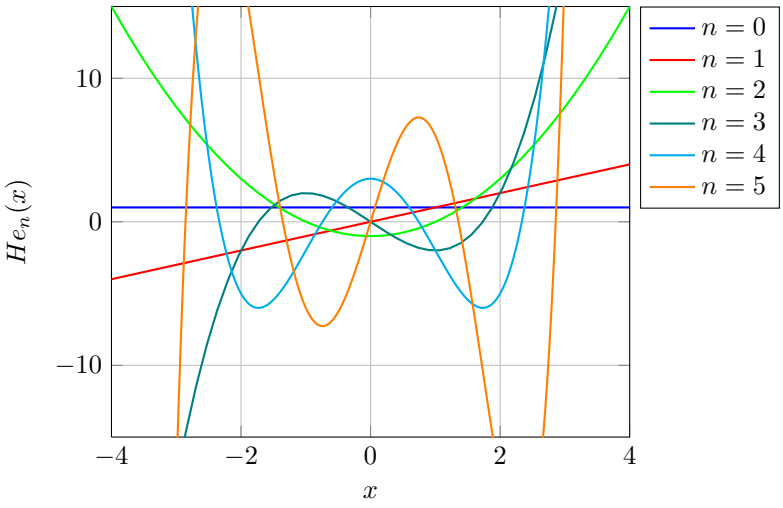

Fig. B.1: Representation of the first 6 Hermite Polynomials.

B.2 Legendre polynomials

Legendre polynomials are an orthogonal basis of $L^2_w[-1;1]$ with respect to the weight function $w(x) = 1/2$ for all $x \in [-1;1]$. The Legendre polynomials satisfy the following recurrence relation[1]:

$$L_n(x) = \frac{2n-1}{n} x L_{n-1}(x) - \frac{n-1}{n} L_{n-2}(x), \quad \text{with} \quad L_0(x) = 1 \tag{B.8}$$

So according the (B.8) the square norm of the Legendre polynomials basis is equal to:

$$\langle L_n, L_n \rangle = \int_{-1}^{+1} L_n^2(x) dx = \frac{1}{2n+1} \tag{B.9}$$

Using the (B.8) the first 6 Legendre polynomials are:

$$
\begin{aligned}
L_0(x) &= 1 \\
L_1(x) &= x \\
L_2(x) &= \frac{1}{3}\left(3x^2 - 1\right) \\
L_3(x) &= \frac{1}{2}\left(5x^3 - 3x\right) \\
L_4(x) &= \frac{1}{8}\left(35x^4 - 30x^2 + 3\right) \\
L_5(x) &= \frac{1}{8}\left(63x^5 - 70x^3 + 15x\right)
\end{aligned}
$$

In the figure below the first 6 Legendre polynomials are plotted:

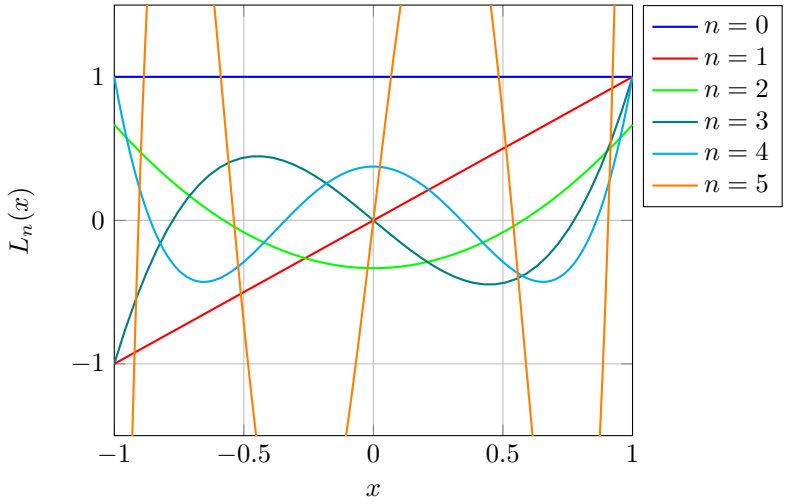

Fig. B.2: Representation of the first 6 Legendre Polynomials.

B.3 Laguerre polynomials

Laguerre polynomials are an orthogonal basis of $L^2_w[0;+\infty]$ with respect to the weight function $w(x) = \exp(-x)$. The Laguerre polynomials satisfy the following recurrence relation[1]:

$$
La_n(x) = \frac{1}{n}\left[(2n - 1 - x)\, La_{n-1}(x) - (n-1)\, La_{n-2}(x)\right], \quad \text{with} \quad La_0 = 1 \tag{B.10}
$$

Once the recurrence relation has been written the square norm for the Laguerre polynomials can be evaluated:

$$
\langle La_n(x), La_n(x)\rangle = \int_0^{+\infty} La_n^2(x)\exp(-x)dx = 1 \tag{B.11}
$$

Using (B.10) the first 6 Laguerre polynomials are:

$$
\begin{aligned}
La_0(x) &= 1 \\
La_1(x) &= -x + 1 \\
La_2(x) &= \frac{1}{2}\left(x^2 - 4x + 2\right) \\
La_3 &= \frac{1}{6}\left(-x^3 + 9x^2 - 18x + 6\right) \\
La_4 &= \frac{1}{24}\left(x^4 - 16x^3 + 72x^2 - 96x + 24\right) \\
La_5 &= \frac{1}{120}\left(-x^5 + 25x^4 - 200x^3 + 600x^2 - 600x + 120\right)
\end{aligned}
$$

In the figure below the first 6 Laguerre polynomials are plotted:

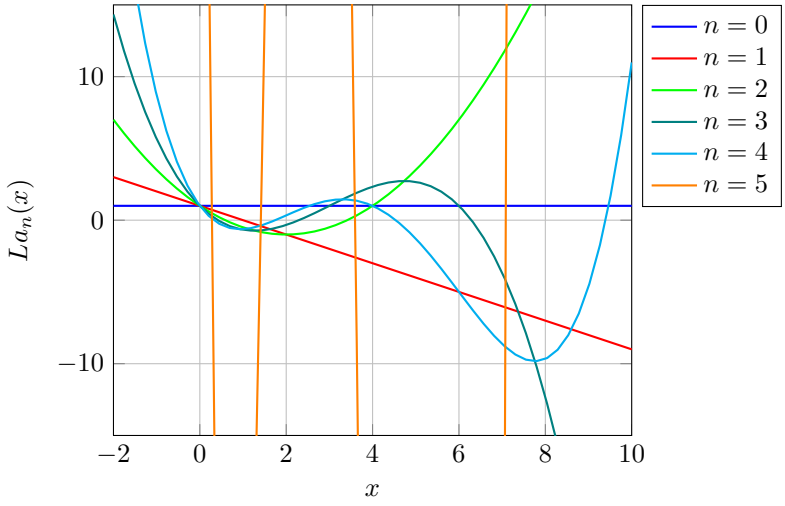

Fig. B.3: Representation of the first 6 Laguerre Polynomials.

Bibliography

[1] Milton Abramowitz, Irene A Stegun, et al. *Handbook of mathematical functions*, volume 1. Dover New York, 1972.

[2] Ronald J Adrian and Jerry Westerweel. *Particle image velocimetry*, volume 30. Cambridge University Press, 2011.

[3] A Badillo, R Kapulla, and B Niceno. Uncertainty quantification in cfd simulations of isokinetic turbulent mixing layers. 2013.

[4] A Badillo, B Ničeno, J Fokken, R Kapulla, J Ko, and J Galpin. Uncertainty quantification of the effect of random inputs on computational fluid dynamics simulations of the gemix experiment using metamodels.

[5] Frederick W Byron and Robert W Fuller. *Mathematics of classical and quantum physics*. Courier Corporation, 2012.

[6] Ismail B Celik. Introductory turbulence modeling. *Western Virginia University Class Notes*, 1999.

[7] Hyeong Do Kweon, Jong Sung Kim, and Kang Yong Lee. Fatigue design of nuclear class 1 piping considering thermal stratification. *Nuclear Engineering and Design*, 238(6):1265–1274, 2008.

[8] Matthew C Dunn, Babak Shotorban, and Abdelkader Frendi. Uncertainty quantification of turbulence model coefficients via latin hypercube sampling method. *Journal of Fluids Engineering*, 133(4):041402, 2011.

[9] E Eggertson, R Kapulla, J Fokken, and H Prasser. Turbulent mixing and its effects on thermal fatigue in nuclear reactors. *World Academy of Science, Engineering and Technology*, 52(1):206–213, 2011.

[10] Ansys Fluent. 14.0: Theory guide, ansys. *Inc., Canonsburg, PA*, 2011.

[11] J Fokken, R Kapulla, G Galgani, O Schib, K Pawa, and HM Prasser. Lif measurements and self-similarity considerations in a stably stratified isokinetic turbulent mixing layer. *Lasermethoden in der Strmungsmesstechnik*, 2010.

[12] C Gourdin, S Chapuliot, JP Magnaud, and T Payen. A hydro-thermo-mechanics analyze of the thermal fatigue in the mixing tee junction. 2003.

[13] Charles Hirsch, editor. *General introduction to Uncertainty Management and Risk Analysis*.

[14] John Kim, Parviz Moin, and Robert Moser. Turbulence statistics in fully developed channel flow at low reynolds number. *Journal of fluid mechanics*, 177:133–166, 1987.

[15] Andrey Nikolaevich Kolmogorov. The local structure of turbulence in incompressible viscous fluid for very large reynolds numbers. In *Dokl. Akad. Nauk SSSR*, volume 30, pages 299–303, 1941.

[16] Simon Kuhn, Olivier Braillard, Bojan Ničeno, and Horst-Michael Prasser. Computational study of conjugate heat transfer in t-junctions. *Nuclear Engineering and Design*, 240(6):1548–1557, 2010.

[17] BE Launder and DB Spalding. Lectures in mathematical models of turbulence. 1972.

[18] Brian Edward Launder and DB Spalding. The numerical computation of turbulent flows. *Computer methods in applied mechanics and engineering*, 3(2):269–289, 1974.

[19] Brian Edward Launder and Dudley Brian Spalding. Lectures in mathematical models of turbulence. 1972.

[20] K-J Metzner and U Wilke. European therfat projectthermal fatigue evaluation of piping system teeconnections. *Nuclear Engineering and Design*, 235(2):473–484, 2005.

[21] Habib N Najm. Uncertainty quantification and polynomial chaos techniques in computational fluid dynamics. *Annual Review of Fluid Mechanics*, 41:35–52, 2009.

[22] Stephen B Pope. *Turbulent flows*. Cambridge university press, 2000.

[23] H-M Prasser, A Böttger, and J Zschau. A new electrode-mesh tomograph for gas–liquid flows. *Flow measurement and instrumentation*, 9(2):111–119, 1998.

[24] Lewis Fry Richardson. *Weather prediction by numerical process*. Cambridge University Press, 1922.

[25] Wolfgang Rodi. Turbulent models and their application in hydraulics a state of the art review. *International Association for Hydraulics Research, Delft*, 1980.

[26] Ralph C Smith. *Uncertainty Quantification: Theory, Implementation, and Applications*, volume 12. SIAM, 2013.

[27] Ilya M Sobol. Global sensitivity indices for nonlinear mathematical models and their monte carlo estimates. *Mathematics and computers in simulation*, 55(1):271–280, 2001.

[28] Il'ya Meerovich Sobol'. On sensitivity estimation for nonlinear mathematical models. *Matematicheskoe Modelirovanie*, 2(1):112–118, 1990.

[29] Henk Kaarle Versteeg and Weeratunge Malalasekera. *An introduction to computational fluid dynamics: the finite volume method*. Pearson Education, 2007.

[30] La Vision. *Flow Master, Product Manual*.

[31] La Vision. *LIF in Liquid Fluids, Product Manual*.

[32] Th Von Karman. Mechanical similitude and turbulence. 1931.

[33] C Walker, M Simiano, R Zboray, and H-M Prasser. Investigations on mixing phenomena in single-phase flow in a t-junction geometry. *Nuclear Engineering and Design*, 239(1):116–126, 2009.

[34] David C Wilcox et al. *Turbulence modeling for CFD*, volume 2. DCW industries La Canada, CA, 1998.